Fall 2021

Mechanical Properties of Nanomodified Hybrid GFRP Composite Materials

Micah Rop Kimutai

MECHANICAL PROPERTIES OF NANOMODIFIED HYBRID GFRP COMPOSITE MATERIALS

by

MICAH KIMUTAI

(Under the Direction of Ermias Koricho)

ABSTRACT

The mechanical behavior of the nanomodified hybrid epoxy matrix was investigated in glass fiber reinforced plastics (GFRP). In this study, five nanocomposite configurations were modified with as received halloysite, nanomer I.28E, HNT-APTES, and the hybrid combinations of the two HNTs with the nanomer I.28E. To evaluate the effects and morphological characteristics of the individual fillers and the hybrid configurations on the epoxy resin matrix, TGA, DSC, and DMA were analyzed. To understand the effect of the five configurations on the neat GFRP laminate, mode I interlaminar fracture toughness, tensile, and vibration properties were investigated. Electron microscopy testing techniques were used to support the results and conclusions. The addition of the filler material showed significant improvement in the GFRP materials' properties, with the hybrid configuration showing exceptional results. Overall, the work demonstrated the ability to tailor GFRP composite properties using hybrid modified fillers. The data suggest that toughening epoxy with nanomodified filler materials is instrumental to various applications by improving and maintaining the overall integrity of structures, such as in the automotive and aerospace industries.

INDEX WORDS: GFRP composites, Nanomodified, Epoxy resin, Interfacial relationship, Morphological characteristics, Mechanical properties

MECHANICAL PROPERTIES OF NANOMODIFIED HYBRID GFRP COMPOSITE MATERIALS

by

MICAH ROP KIMUTAI

B. Eng., Moi University, Kenya, 2013

A Thesis Submitted to the Graduate Faculty of Georgia Southern University

in Partial Fulfillment of the Requirements for the Degree

MASTER OF SCIENCE

MECHANICAL PROPERTIES OF NANOMODIFIED HYBRID GFRP COMPOSITE MATERIALS

by

MICAH ROP KIMUTAI

Major Professor:	Ermias Koricho
Committee:	Shainaz Landge
	Hossein Taheri

Electronic Version Approved:
December 2021

DEDICATION

I am pleased to dedicate this fulfillment to my mother, Priscah Jemosbei, for the motivation and always being there and inspiring me towards excellence.

This achievement would not have been possible without the tremendous support of Mr. Mathew Rutto's family at large for their undying support and mentoring.

ACKNOWLEDGMENTS

It has been my greatest honor to work with my advisor, Dr. Ermias G. Koricho. My immense thanks to Dr. Koricho for his dedication and guidance in finishing this work. Many thanks to Dr. Shainaz M. Landge, who helped me on numerous occasions and allowed me to do part of my work in her lab. I want to thank my other committee member, Dr. Hossein Taheri, for the excellent guidance throughout my master's degree.

The present work wouldn't be successful without Dr. Rafael Quirino for his selfless guidance and interpretation of TGA, DSC, and DMA work. Dr. Jinki Kim, your tremendous support is highly appreciated. Special appreciation to Dr. Shaowen Xu, Dr. Kamran Kardel, and Mr. Andrew Diamanduros for always being there for me whenever I needed them.

The task would not be finished without the help from all of my fellow undergraduate and graduate students. I appreciate Mohammad Fuad Hassan for his support in manufacturing and testing the composite materials and Dziwodo Abotsi for his help during the preparation processes. Malachi Kent, John Johnson, and Miles San Soucie, your help during the preliminary experimental works and functionalization processes are highly appreciated. Thanks to Mathew Sands and Ibrahim Inusah for the dedication and excellent support that enabled me to finalize the tasks presented in this study.

I am humbled by the excellent knowledge I acquired from Thomas Mockler and Alexandra Grantham that enabled me to complete my study successfully. Special thanks to Mr. Andrew Michaud for his help during the composite materials testing preparation processes.

Last but not least, I would like to thank my entire family and friends for their support and understanding.

TABLE OF CONTENTS

LIST OF TABLES

LIST OF FIGURES

ABBREVIATIONS

GNPs: Graphene Platelets

CNTs: Carbon Nanotubes

BNNs: Hexagonal boron nitride nanosheets

BNNTs: Boron nitride nanotubes

SiC: Silicon carbide

Al_2O_3:Aluminum oxide

MWCNT: Multiwalled carbon nanotube

SWCNT: Single-walled Carbon Nanotube

SiO_2: Silicon Dioxide (Silica)

S-MWCNT-COOH: COOH-functionalized short multi-walled carbon nanotubes

LHT-COOH: Carboxylic acid group functionalized stacked-cup carbon nanofibers

GO: Graphene oxide

MLG: Multilayer Graphene

TiO_2: Titanium Dioxide

CNF: Carbon nanofibers

SDS: Sodium dodecyl sulfate

PVA: Poly(vinyl alcohol)

ZnO: Zinc Oxide

GrNPs: Graphite nanoparticles

CNC: Cellulose nanocrystals

CFG: Carboxylic Functionalized Graphene

HNT: Halloysite

FRP: Fiberglass Reinforced Plastic

CFG: Cemented Fiber Glass

FRC: Fiber Reinforced Composite

GRE: Glass Reinforced Epoxy

GFRP: Glass Fiber Reinforced Plastic

MMT: Montmorillonite

APTES: 3-Aminopropyl)triethoxysilane

RGO: Reduced Graphene Oxide

HRGO: Halloysite Nanotubes-Reduced Graphene Oxide Hybrids

CHAPTER 1

1. INTRODUCTION

1.1 Purpose of Study

This study seeks to understand the mechanical properties of hybrid nanomodified glass fiber reinforced plastic (GFRP) composite materials. Studies have shown that GFRP composite materials have superior properties to replace conventional materials such as steel, aluminum, etc. (Chavhan and Wankhade 2020). In general, fiber-reinforced polymer materials offer better properties in some aspects compared to other materials, such as corrosion resistance, high strength and stiffness to weight ratio, and the ability to be tailored to various configurations (Eslami, Taheri-Behrooz, and Taheri 2012). Several studies have proven the need for the functionalization of nanoparticles. Functionalization enhances the properties of particles through surface modification without altering their shape.

1.2 How this Study is Original

Most experiments have shown that Glass Fiber Reinforced Plastic (GFRP) composite materials have superior properties. Still, the effect on the mechanical properties of hybrid nanomodified GFRPs has not been thoroughly studied. Flexural strength and stiffness are not basic material properties for fiber-reinforced composites. Application of GFRP composites in aerospace, civil, automotive, and military are continually subjected to stresses in different directions. Hence, it is important to study the materials' thermal stability, storage modulus, fracture toughness, tensile properties, and vibration properties.

1.3 Hypothesis

"If nanomodified hybrid fillers are incorporated in GFRP reinforcement-matrix, the materials' mechanical properties will be greatly improved as compared to neat GFRP composites."

CHAPTER 2

2. LITERATURE REVIEW

2.1 What is a Composite Material?

A typical composite material comprises two or more materials different in composition mixed and bonded together on a very small scale, with the new combined material exhibiting better properties than would each material individually (Nagavally 2017; Enamul Hossain 2011). Generally, a composite material comprises reinforcement such as fibers, particles, flakes, and fillers embedded in a matrix, i.e., polymers, metals, ceramics, etc., (Nagavally 2017). The matrix holds the reinforcement to form the desired shape, while the reinforcement improves the overall properties of the matrix (Nagavally 2017). Composite materials are typically classified as Fiberglass Reinforced Plastic (FRP or GRP), Cemented Fiber Glass (CFG), Fiber Reinforced Composite (FRC), and Glass Reinforced Epoxy (GRE).

2.2 Fiber Reinforced Plastics (FRPs)

The growing need for efficient, low-cost, reliable but lightweight components due to economic, ecological, and social conditions, which are an integral part of today's product development, has resulted in fiber-reinforced polymers (FRPs) in numerous applications (Fleischer et al. 2018; Marichelvam 2020). FRPs tend to have high specific strength and stiffness, low thermal expansion, and corrosion resistance. In general, FRP consists of two or more essential components. The goal of creating composites is to achieve improved properties by exploiting the advantages of each component. Although the material properties of glass fiber-reinforced polymers (GFRPs), including the modulus of elasticity, ultimate strength, and durability, are not comparable to those of carbon fiber-reinforced polymers (CFRPs) and basalt fiber-reinforced polymers (BFRPs). In contrast, the GFRP has the following advantages: (1) relatively low price, (2) excellent ductility of reinforced components, and (3) suitability for a large-area application (Wei, Sun, and Zhu 2020).

2.3 Review of Composites Materials Properties

2.3.1 Review of GFRP Materials Properties

GFRP consists of a polymer matrix and glass fibers. The polymer matrix is usually an epoxy resin, polyester thermosetting resin, or vinyl ester. Table 2.1 shows the fiberglass properties.

Table 2.1: Fiber Glass Properties

Glass	Application	Specific Gravity (g/cm^3)	Young's Modulus (GPa)
E-Glass	Abrasion & Vibration Resistance	2.56-2.62	78-79
E-CR Glass	Electrical & Corrosion	~2.62	~82
C-Glass	Low Ph Corrosion	~2.39	~68
H-Glass	High Modulus	~2.60	~87.5
AR-Glass	Alkali Resistant	~2.63	~77.5
S-Glass	High Strength	~2.43	~88

Due to outstanding properties such as excellent thermal and mechanical properties, compatibility with most fibers, good chemical and wear resistance, low compression shrinkage, significant adhesion resistance, good dielectric properties, and thermal properties, and low cost, epoxy polymer/resin has found wide application in areas such as structural material and matrix of composites (Mishra et al. 2020; Vardhan, Ramesh, and Reddy 2020). Despite these properties associated with epoxy resins, they tend to be brittle, resulting in low resistance to crack propagation and hence the need for modification to enhance the properties (Truong and Choi 2020). Considering the low cost and excellent properties associated with GFRP composites, GFRPs have found application in many areas such as the aerospace industry, automotive industry, chemical industry, marine applications, machine components, domestic applications, etc. It is good to note that the most crucial aspect in manufacturing GFRP composites is finding the best interaction between the fiber and the matrix. Studies have shown that GFRP composites are susceptible to delamination, hence the need to overcome such challenges.

Chawla, Ray-Chaudhuri, and Kitey (2019) have studied the influence of short fibers on interlaminar fracture toughness. Two different epoxy systems were used to manufacture the laminates, (1) neat epoxy and (2) epoxy system reinforced with 2% (volume fraction) short fibers. A double cantilever beam test showed increased resistance to interlaminar crack growth of GFRP laminates with short fibers.

Research has shown that GFRP composite materials can replace conventional materials traditionally used in moving parts in the automotive industry. Marichelvam (2020) have investigated the mechanical properties of automobile struts made by GFRP composites. The study showed significant specific strength improvement of the GFRP strut compared to the conventional steel strut.

2.3.2 Effect of Filler Materials on Composites

The ever-growing industrial sectors such as automotive and aerospace have increased the demand for composite materials to shift from plain composite to a hybrid of two or more fibers or filler particles added into composites (Chavhan and Wankhade 2020). Although the laminates have excellent in-plane properties, a dangerous phenomenon for laminates is delamination. Delamination tends to grow inside the material slowly, and with time the material can lose up to 60% of its strength and stiffness (Chawla, Ray-Chaudhuri, and Kitey 2019; Garcia et al. 2017). Studies have shown that the inclusion of fillers in composite materials tends to enhance their mechanical properties such as delamination, tensile stress, flexural stress, good thermal, chemical resistance, etc., (Ruban Rajasekar et al. 2018; Fereidoon, Memarian, and Ehsani 2013). To enhance the reliability of laminated structures, the damage tolerance of a composite can be improved by incorporating toughened delamination-resistant resin (Sela and Ishai 1989). Studies have shown that effective dispersion and improved interfacial properties can be achieved by incorporating two-component hybrid nanofillers into the polymer matrix (Domun et al. 2019). Generally, nanofillers are classified as metals (e.g., Al, Fe, etc.), metal oxides (e.g., Al_2O_3, TiO_2, ZnO, etc.), organic fillers (e.g., CNT, SWCNT, MWCNT, graphene, etc.), inorganic fillers (e.g., SiC, SiO_2, etc.) and others such as nano clays (Nayak et al. 2019).

Venkatesan, Palanikumar, and Rajendra Boopathy (2018) have investigated glass fiber composite materials' wear behavior. In their study, the composite materials were incorporated with CNT particles. The experimental results showed that the wear rate decreased as the CNT filler percentage increased. Withers et al. (2015) have studied the mechanical strength, stiffness, ductility, and fatigue life of glass fiber composites nanomodified with Cloisite 30B filler material. The results showed that nanomodified composites had improved mechanical properties than the neat glass fiber composite material.

Mishra et al. (2020) have investigated the effect of graphene addition on glass/epoxy nanocomposite laminates with two different lay-ups, i.e., [(0/90)12s and (0/90/±45)6s]. The study showed improved tensile, flexural, and impact properties for both the laminates with graphene reinforcement compared to neat material without graphene content. Kostagiannakopoulou et al. (2015) studied the mode-I fracture toughness on CFRPs nanomodified with graphene nano-platelets and graphene oxide. The study showed a significant increase in the interlaminar toughness for composites impregnated with the case of graphene nano-platelets. Bourchak et al. (2018) have studied the fatigue behavior of GFRP laminates impregnated with 0.1 wt% of single-walled carbon nanotubes (SWCNTs) and 0.1 wt% of GNPs. The results showed that incorporating 0.1 wt% of SWCNTs increased the fatigue strength coefficient (FSC) and the fatigue strength exponent (FSE) by 51% and 24%, respectively. Incorporating similar wt.% of GNPs to the GFRP laminates enhanced the FSC and FSE by 33% and 25%, respectively.

Mourad et al. (2020) have extensively assessed the impact behavior on Kevlar/epoxy laminates by incorporating silicon carbide (SiC), aluminum oxide (Al_2O_3), and multi-walled MWCNT as the filler materials. The study showed that the addition of small amounts of nanofillers effectively improved the damage propagation resistance and interlaminar shear strength of the fabricated composites. Among all the examined samples, the lowest number of damaged layers with the least damaged area was obtained with the addition of 0.5 wt% MWCNT. Kara et al. (2018) studied the impact behavior of CFRP nanomodified with MWCNT nanotubes at different temperatures (23 °C, 0 °C, −50 °C, −100 °C, −196 °C). The results showed that the addition of nanoparticles to the specimens resulted in higher contact force values for the

same temperature and minor damage in the sample sections. Sravanthi et al. (2020) performed an experimental investigation of impact responses of GFRP nanomodified with Micro carbon (5, 10, 15 wt%) and MWCNT (2, 4, 6 wt%). Their study showed that the impact properties of composite material improved with the addition of the filler to the epoxy matrix, i.e., up to 5 wt% μ-carbon and 4 wt% MWCNT.

Panchagnula and Kuppan (2019) investigated the tensile, flexural, and hardness properties of GFRPs filled with 0.1%, 0.2%, 0.3%, and 0.4% MWCNTs by weight. The results showed an overall improvement in the mechanical properties of nanomodified Composites compared to neat GFRP composite material. Guru Mahesh and Jayakrishna (2019) studied the tensile, compression, and flexural properties of composite materials nanomodified with Al_2O_3. In general, the results showed that an increase in the percentage weight of nano aluminum oxide improved the mechanical properties of the composite material.

Koricho et al. (2015) have performed the impact behavior of pristine and nano micro-modified GFRP for possible lightweight materials for vehicle applications. The hybrid nano micro-fillers chosen were Cloisite 30B nanoclay and Glass Bubbles Im16K. The experimental results showed that the hybrid laminate exhibited more absorbed energy with peak reaction force sustained longer than neat GFRP. Domun et al. (2019) have investigated the impact response of GFRP composite materials nanomodified with graphene platelets (GNPs), carbon nanotubes (CNTs), boron nitride nanosheets (BNNS)/CNT hybrid, and BNNTs/GNPs hybrid nanoparticles. Their study observed the highest absorbed energy for the GFRP composite nanomodified with BNNT/GNP hybrid epoxy matrix.

Kostagiannakopoulou et al. (2017) studied the synergistic effect of incorporating hybrid nanofillers of Graphene Nano-Platelets (GNPs) and Multi-Walled Carbon Nanotubes (MWCNTs) on CFRPs composites, i.e.,, (case 1: 0.5%wt. GNPs and 0.5%wt. MWCNTs, case 2: 0.5%wt. GNPs and 1%wt. MWCNTs). The inclusion of hybrid nanofillers to the matrix showed improved Mode-I (G_{IC}) and Mode-II (G_{IIC}) fracture toughness compared to the neat CFRP composite material. Mode I G_{IC} was enhanced up to 45% in the second hybrid, whereas composites with GNPs or MWCNTs at equal amounts exhibited 27%

and 31% increase, respectively. Mode II results showed the second hybrid with the highest increase of G_{IIC} up to 25%, while the individual nanofillers with the same contents achieved 18% and 13% increase.

Das et al. (2020) have investigated the mechanical properties of GFRP laminates incorporated with salinized milled graphite nanoparticles (GrNPs). The results that the SGrNPs (0.5 wt%) reinforced GRFP laminated composites reveal the enhancement in the mechanical properties such as tensile strength (~33%), tensile modulus (~21%), toughness (~35%), flexural strength (~42.6%), work of fracture (~57%), and short beam strength (~23%), respectively. Vishal Kumar Rao et al. (2021) have studied the mechanical properties of Carboxylic Functionalized Graphene (CFG) and Graphene Oxide (GO) on E-glass fiber composite materials. Nanocomposites were prepared by varying the weight percentage of each nanomaterial, i.e., 0.4%, 0.6%, and 0.8%. Results showed that 0.6 wt% of CFG on the E-glass fabric reinforced composite improved the flexural strength, tensile strength, impact strength, heat deflection, and hardness of 30%, 39%, 22%, 12%, and 20%, respectively. The results generally showed improved properties of composite materials incorporated with CFG compared to pure and GO composite material configurations. Truong and Choi (2020) studied the mode I fracture toughness of CFRP composites modified with COOH-functionalized short multi-walled carbon nanotubes (S-MWCNT-COOH) by varying filler percentage, i.e., 0.5, 1, and 1.5 wt%. The study showed that the toughness of the CFRP composites incorporated with S-MWCNT-COOH significantly improved compared to pure CFRP. Krishnaiah et al. (2021) have investigated the mechanical, dynamic-mechanical, and thermal performance of polypropylene (PP) polymer nanomodified with HNT-APTES. Results showed that incorporating 6 wt% of the HNT-APTES to the polymer improved the tensile strength, modulus, and impact properties by 28%, 45%, and 60%, respectively. Thermal stability, crystallinity, and dynamic modulus improved by 18 °C, 22%, and 28%, respectively.

Studies have shown that proper selection and well dispersion of filler materials can improve polymer matrix properties such as thermal stability, storage modulus, moisture absorption resistance, glass transition temperature, etc.

Summary of filler materials that have been utilized to improve the mechanical properties of different kinds of composite materials is shown in Tables 2.2 and 2.3.

Table 2.2: Individual Non-Functionalized Fillers on Composite Materials

	Impact	**Tensile**	**Fracture**	**Flexural**	**Fatigue**	**Compression**	**Hardness**
GNPs	(Domun et al. 2019), (Mishra et al. 2020)	(Mishra et al. 2020)	(Kostagiannakopoulou et al. 2015), (Kostagiannakopoulou et al. 2017)	(Mishra et al. 2020)	(Bourchak et al. 2018)		
CNTs	(Domun et al. 2019)						
MWCNTs	(Mourad et al. 2020), (Viets, Kaysser, and Schulte 2014), (Kara et al. 2018), (Sravanthi et al. 2020)	(Behera, Rawat, and Singh 2018), (Panchagnula and Kuppan 2019)	(Kostagiannakopoulou et al. 2017), (Behera et al. 2019), (Saurabh et al. 2020)	(Panchagnula and Kuppan 2019)	(Gaurav and Singh 2019)		(Panchagnula and Kuppan 2019)
SWCNTs					(Bourchak et al. 2018)		
TiO_2				(Vardhan, Ramesh, and Reddy 2020)			
Al_2O_3	(Mourad et al. 2020)	(Mahato et al. 2020), (Guru Mahesh and Jayakrishna 2019)		(Vardhan, Ramesh, and Reddy 2020), (Mahato, Dutta, and Chandra Ray 2019), (Guru Mahesh and Jayakrishna 2019)		(Guru Mahesh and Jayakrishna 2019)	

Cont. Table 2.2: Individual Non-Functionalized Fillers on Composite Materials

	Impact	**Tensile**	**Fracture**	**Flexural**	**Fatigue**	**Compression**	**Hardness**
MLG			(Saurabh et al. 2020)				
SiO_2	(Mohammady and Khairou 2021)		(Maharana, Pandit, and Pradhan 2021)				
GO			(Kostagiannakopoulou et al. 2015), (Ning et al. 2015)				
ZnO	(Jagadish Chandra Bose et al. 2019)						
Cloisite 15A	(Binu, George, and Vinodkumar 2016)	(Binu, George, and Vinodkumar 2016)					
Cloisite 30B	(Nayak et al. 2019)			(Nayak et al. 2019)			(Nayak et al. 2019)
CNC	(Sundareswaran, Rajendran, and Dinesh Kumar 2021)	(Sundareswaran, Rajendran, and Dinesh Kumar 2021), (Kumar et al. 2020)	(Sundareswaran, Rajendran, and Dinesh Kumar 2021)	(Sundareswaran, Rajendran, and Dinesh Kumar 2021), (Kumar et al. 2020)			
HNT		(Kim et al. 2015)					
SiC	(Mourad et al. 2020)			(Vardhan, Ramesh, and Reddy 2020)			
µ-carbon	(Sravanthi et al. 2020)						

Table 2.3: Hybrid and Surface Modified Fillers on Composite Materials

	Impact	**Tensile**	**Fracture**	**Flexural**	**Thermal**	**Hardness**
Silanized GrNPs		(Das et al. 2020)	(Das et al. 2020)	(Das et al. 2020)		
CFG	(Vishal Kumar Rao et al. 2021)	(Vishal Kumar Rao et al. 2021)		(Vishal Kumar Rao et al. 2021)	(Vishal Kumar Rao et al. 2021)	(Vishal Kumar Rao et al. 2021)
BNNS/CNT	(Domun et al. 2019)					
(BNNTs)/GNPs	(Domun et al. 2019)					
30B nanoclay and 3MTM Bubbles Im16k	(Koricho et al. 2015)					
S-MWCNT-COOH			(Truong and Choi 2020)			
Functionalized Carbon Nanofiber			(Wang et al. 2015)			
Functionalized Fumed Silica			(Battistella et al. 2008)			
MWCNT/MLG			(Saurabh et al. 2020)			
GNP/MWCNTs			(Kostagiannakopoulou et al. 2017)			
HNT-APTES	(Vahedi and Pasbakhsh 2014), (Krishnaiah et al. 2021)	(Krishnaiah et al. 2021)	(Chen et al. 2021)			
HRGO		(Mia et al. 2019)	(Mia et al. 2019)			

2.4 Factors that Determine Composite Materials' Properties

When selecting the constituents of the composite for a particular function, it is vital to note that not only their individual properties are essential but also factors such as concentration (fillers), configuration and thickness (fibers), void content, and environmental conditions need to be taken into consideration.

2.4.1 Concentration of Fillers

Though filler materials can modify polymers' properties, such as the modulus and strength, high filler loadings may impact the processability, ductility, and strength of the final composite material (Leong et al. 2004). Studies have shown that appreciable morphological properties of the nanocomposite can be observed at a low percentage of the filler material, i.e., before the matrix reaches agglomeration (Gaaz et al. 2017; Senthil Kumar et al. 2018; Sharma et al. 2012). Examples of typical shapes of filler materials that have been extensively utilized to improve the mechanical properties of composites are shown in Figure 2.1.

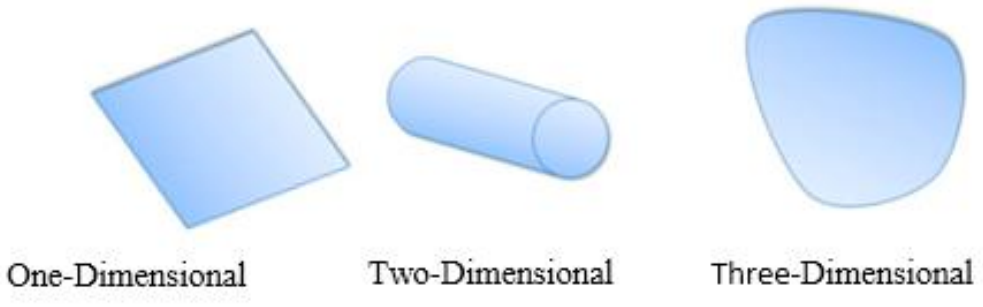

Figure 2.1: Examples of Nanofillers

Gaaz et al. (2017) have studied the impact of halloysite on the thermo-mechanical properties of polymer composites. The study showed that though halloysite nanotubes exhibited enhanced strength compared to neat polymer properties, the tensile strength of the polymer increased directly with the increase in the content of HNTs up to the build-up stage, then declined.

Senthil Kumar et al. (2018) have investigated the influence of Cloisite 25A nanoclay on GFRP composite laminates. The materials' properties analyzed are the tensile, flexural, compression, and thermal analysis. The study observed that the low clay content filled GFRP laminates showed better performance than high clay content filled nanocomposites. It is important to note that though Sravanthi et al. (2020) studies showed improved impact properties with the addition of micro carbon and MWCNT, the optimum build-up stage was reached at 5 wt% for micro carbon and 4 wt% for MWCNT.

Nayak et al. (2019) studied the effect of Cloisite 30B MMT nanoclay of varying weight (0%, 1%, 3%, 5%, and 7%) on fiber-reinforced composite. Results showed 5% loading of nanoclay being the optimum amount at which the hardness, impact strength, flexural strength, and specific wear rate properties significantly improved. Srivastava and Pandey (2019) investigated the mechanical behavior and thermal stability of HNT (1 wt%, 2 wt%, 3 wt%, 4 wt%, and 5 wt%) on epoxy resin nanocomposites. In their study, 3 wt% loading of HNTs in epoxy resin depicted remarkable improvement. In summary, 3 wt% loadings showed about 55.4%, 25.9%, 110.9%, 2.8%, and 30.7% improvement in the tensile strength, flexural strength, impact strength, hardness, and thermal stability properties, respectively.

2.4.2 Configuration and Thickness Of Fibers

Selected thickness and fibers orientation affect the material behavior (Bazli, Ashrafi, Jafari, Zhao, Singh Raman, et al. 2019; Bazli, Ashrafi, Jafari, Zhao, Gholipour, et al. 2019; Jafari et al. 2019). The fiber configuration such as continuous unidirectional, continuous woven, and chopped will result in different properties with the same matrix.

At elevated temperatures, the flexural and impact behavior studied by Bazli, Ashrafi, Jafari, Zhao, Gholipour, et al. (2019) showed that laminates with unidirectional fibers had the best performance, and randomly distributed fibers were the most vulnerable. In contrast, woven fibers were almost between the two material configurations.

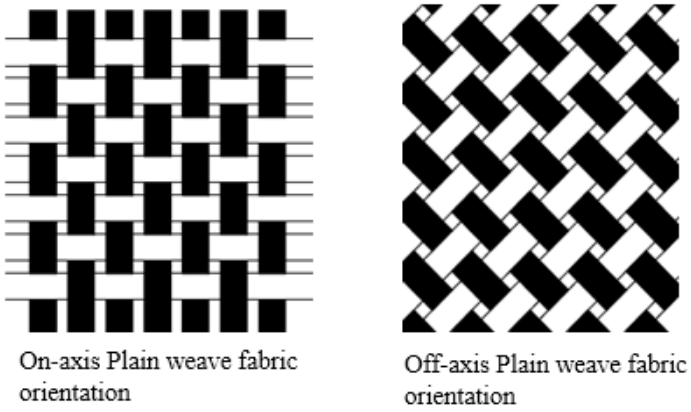

Figure 2.2: Unidirectional Plain Weave Fiber with Different Orientations

2.4.3 Void Content

Kosmann et al. (2015) have studied the effect of voids in composite materials. The authors noted that voids within fiber bundles usually have small dimensions and often have spherical shapes that reduce the bonding strength between fiber and matrix. This behavior leads to stress concentrations and high shear stresses between fiber and matrix, and hence the matrix and inter-fiber ruptures. The authors noted that to ensure a component's service over a long period, knowing precisely the material-specific behavior, including the effect of voids, is critical.

2.5 Selected Nanomodification Materials

The use of nanomer I.28E and halloysite fillers on GFRP composites is increasing owing to their structure and composition. They are readily available and much cheap than other nanoparticles such as CNTs.

2.5.1 Nanomer I.28E Nanoparticles

Nanomer I.28E is a Montmorillonite Clay with a platelet-like structure. Montmorillonite Clay General formula is $R_{0.33}Al_2Si_4O_{10}(OH)_2 + nH_2O$, where R represents one or more of the cations Na^+, Ka^+, Mg^{2+}, Ca^{2+}. Nanomer I.28E is surface modified with 25-30 wt. % trimethyl stearyl ammonium ($C_{21}H_{46}N+$). Nanomer I.28E is known to improve modulus and rheology control and enhance chemical resistance.

Tcherbi-Narteh et al. (2013) have evaluated the effects of different montmorillonite nanoclays (MMT) on the thermal stability and degradation of epoxy composites exposed to UV radiation and elevated temperatures. In their study, diglycidyl ether of bisphenol A (DGEBA) epoxy resin, SC-15, was reinforced with three different 2 wt. % montmorillonite nanoclays namely nanomer I.28E, Cloisite 10A and Cloisite 30B. High-resolution TEM micrographs in conjunction with XRD studies showed nanomer I.28E seemed to be well dispersed relative to the others. Overall, DMA results showed an increase in storage modulus with the organo nanoclays into the epoxy resin. The Cloisite 30B configuration showed an increase of about 13% in storage modulus. In contrast, nanomer I.28E and Cloisite 10A both showed a modest increase of about 5% at 30^0C. Glass transition temperatures, on the other hand, showed there was a modest increase of about 6 and 5% for nanomer I.28E and Cloisite 30B systems, respectively, and a decrease of about 4% for that of Cloisite 10A compared to the neat SC-15 epoxy resin. TGA analyses were performed to understand the clays' decomposition profile. TGA decomposition started at a relatively lower temperature for samples with Cloisite 30B and higher for both unmodified and nanomer I.28E modified samples. At the end of the TGA ran, unmodified SC15 had the least residue, followed by Cloisite 30B, nanomer I.28E, and finally Cloisite 10A with the most residue. In general, as per their study, the addition of nanoclays showed improved thermal properties compared to the neat composite and better retention of material properties after exposure to UV radiation.

2.5.2 Halloysite Nanotubes

Halloysite ($Al_2(OH)_4Si_2O_5.2H_2O$) natural clay mineral that has tubular and a porous structure, chemically like kaolinite, dickite, or nacrite, differing mainly in the morphology of the crystal (Zhang et al. 2020; Tang et al. 2011). The outer surface of HNTs has SiO_2 bonds and Al_2O_3 bonds in the inner lumen of the nanotubes (Krishnaiah et al. 2021). Owing to HNTs nanosized tubular morphology and the porous structure and higher specific area, HNTs tend to exhibit higher pozzolanic reactivity favoring the geo-polymerization of the particles (Zhang et al. 2020). Studies have shown that incorporating HNTs to epoxy improves toughening mechanisms such as crack deflection, crack pinning, and crack bridging, water

absorption resistance without compromising thermal properties such as the polymer's glass transition temperature (Ulus et al. 2020).

Mia et al. (2019) have studied the thermal and mechanical properties of HNT nanotubes-reduced graphene oxide hybrids (HRGO) in epoxy resin. The results showed that epoxy nanocomposites with the addition of HRGO exhibited significant improvement of the tensile strength, storage modulus, and fracture toughness. The improvement in fracture toughness was attributed to crack deflection and crack pinning mechanisms.

Morphological characteristics of halloysite have enabled hybrid nanocomposites that incorporate HNTs with other filler materials.

2.5.3 (3-Aminopropyl)Triethoxysilane (APTES)

Several studies have shown improved properties of polymer nanocomposites in the cases where clays have been modified with APTES (Daitx et al. 2015). Vahedi and Pasbakhsh (2014) have studied the impact and fracture behavior of epoxy incorporated with surface modified HNTs by APTES. Modification of HNTs improved their dispersion in the epoxy matrix at lower concentrations of HNTs. In general, modification HNTs by APTES showed considerably enhanced impact toughness of epoxy/HNTs nanocomposites than unmodified HNTs.

2.6 Mechanical Properties of Materials

To establish the usefulness and the expected service life of the material, various mechanical properties need to be analyzed. Mechanical properties help classify, identify, and compare various materials.

2.6.1 Fracture Toughness

Delamination is one of the significant phenomena that leads to composite laminate failure. It continually grows internally, hence the need to be mitigated to increase the materials service life. In general terms, the fracture toughness of a material is the amount of energy it will absorb with a preexisting flaw or crack before it fails or breaks.

The critical strain energy release rate (G_{IC}) is calculated from the fracture data of composite DCB specimens as per equation 2.1 (Ruban Rajasekar et al. 2018).

$$G_{IC} = \frac{1}{N}\sum_{i=1}^{N}\left(\frac{P_{cr}^2\, a^2}{3BEI} + \frac{P_{cr}\,\delta_{cr}}{Ba}\right) \quad \text{.....2.1}$$

Where P_{cr} is critical load, a is crack length, B is the breadth, E is Young's Modulus, I is the moment of inertia, δ_{cr} is critical deflection, and N is the number of fracture data.

The critical load (P_{cr}) is evaluated from equation 2.2 (Ruban Rajasekar et al. 2018).

$$P_{cr} = \sqrt{G_{IC}\left\{\frac{a^2}{BEI} + \frac{2a}{BK}\right\}^{-1}} \quad \text{.....2.2}$$

Where K is the rotational spring constant.

Equation 2.3 gives the maximum load expected during a DCB test of a material with a known modulus and G_{IC} (Ruban Rajasekar et al. 2018).

$$P_{max} = \frac{B}{a}\sqrt{\frac{G_{IC}(2h)^3 E_{11}}{96}} \quad \text{.....2.3}$$

2.6.2 Tensile Testing

When a pulling force is applied to the material, the specimen's response to the stress is a measure of tensile test.

Davis (2004) has outlined the basics for tensile testing whereby engineering stress, or nominal stress, *s*, is defined in equation 2.4, whereas engineering strain, or nominal strain, *e*, is defined in equation 2.5.

$$s = \frac{F}{A_0} \quad \text{.....2.4}$$

Where F is the tensile force, and A_0 is the initial cross-sectional area of the gage section.

$$e = \frac{\Delta L}{L_0} \quad \text{.....2.5}$$

Where L_0 is the initial gage length, and ΔL is the change in gage length (L - L_0).

2.6.2.1 Elastic Deformation

Elastic deformation refers to reversible deformation when small stresses are applied to the material and removed (Davis 2004).

The initial portion of the curve is usually a linear slope referred to as the elastic modulus or young's modulus denoted by equation 2.6 (Davis 2004).

$E = s/e$……..…..…….2.6

In the elastic range, the ratio, ν, of the magnitude of the lateral contraction strain to the axial strain is called Poisson's ratio, as expressed in equation 2.7 (Davis 2004).

$\nu = -e_y/e_x$ (in an *x*-direction tensile test) ……..…2.7

2.6.2.2 Tensile Strength

Tensile strength is defined as the highest value of engineering stress and is sometimes referred to as ultimate tensile strength (Davis 2004).

$F^{tu} = Pmax/A$ ……...……...…2.8

Where:

F^{tu} = ultimate tensile strength, Mpa

$Pmax$ = maximum force before failure, N

A = average cross-sectional area of the specimen

2.6.2.3 Ductility

The ability of a material to sustain a substantial deformation before fracture under tensile stresses is referred to as ductility.

Percent elongation can be defined in equation 2.9 (Davis 2004).

$\%El = \left[\left(L_f - L_O\right)L_0\right] * 100$……..……..…...…2.9

where L_0 is the initial gage length, and L_f is the length of the gage section at fracture.

2.6.3 Vibration Analysis

Most components, such as aircraft, vehicles, etc., are constantly subjected to vibration and fail due to large-amplitude vibrations. Through vibration analysis, a high damping ratio shows that the material will respond quickly to unwanted disturbances compared to material with a low damping ratio. In that regard, one of the methods of reducing vibration is to increase the damping of the composite material by incorporating nanofiller materials into the matrix. Free decay vibration analysis helps to characterize the dynamical behavior of the materials.

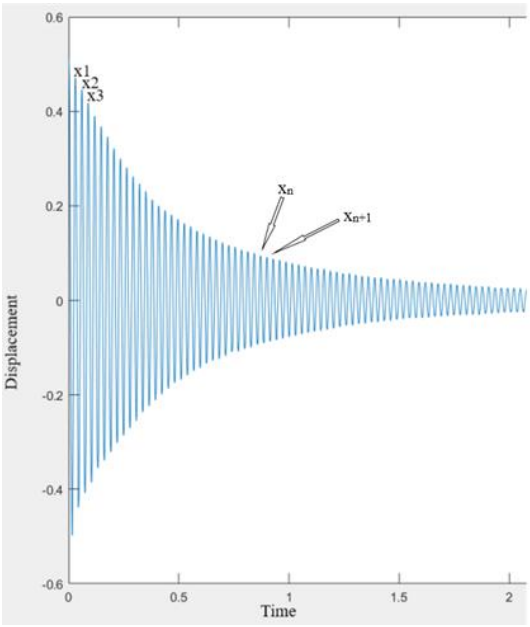

Figure 2.3: Displacement versus Time Oscillation

From vibration analysis; Displacement versus time Oscillation

$$\delta = ln\frac{x1}{x2}, \quad \text{……..…….....….....…2.10}$$

whereby for more precise results:

$$\delta = \frac{1}{n} ln\frac{x1}{xn+1} \quad \text{…….……...……2.11}$$

where xn is the n^{th} amplitude of the oscillation.

The damping ratio is hence calculated as follows:

$$\zeta = \frac{\delta}{\sqrt{(4\pi^2+\delta^2)}} \quad \text{……..…....2.12}$$

CHAPTER 3

3. METHODOLOGY

3.1 Manufacture of the Materials

Twelve on-axis [0/90] E-glass plain weave fabric with a weight of 280 g/m^2 reinforcement was used in this study. The matrix resin used was a two-part toughened epoxy, namely SC-15, obtained from Kaneka Aerospace LLC.

In this study, three main nanofillers were used, namely;

i. As received pure non-surfaced modified halloysite.

ii. As received, surfaced modified nanomer I.28E.

iii. Halloysite surface modified with (3-Aminopropyl) triethoxysilane/APTES-$H_2N(CH_2)_3Si(OC_2H_5)_3$.

Pure halloysite, nanomer I.28E, and APTES were all purchased from Sigma Aldrich. Six GFRP composite materials were manufactured that included pristine and two-hybrid GFRPs comprising at least two filler materials, as shown in Figures 3.1 and 3.2. Epoxy resin samples were also manufactured for TGA, DSC, and DMA analysis. Since higher filler loadings may adversely affect composites' processability, ductility, and strength, 1% filler concentration was chosen for this study.

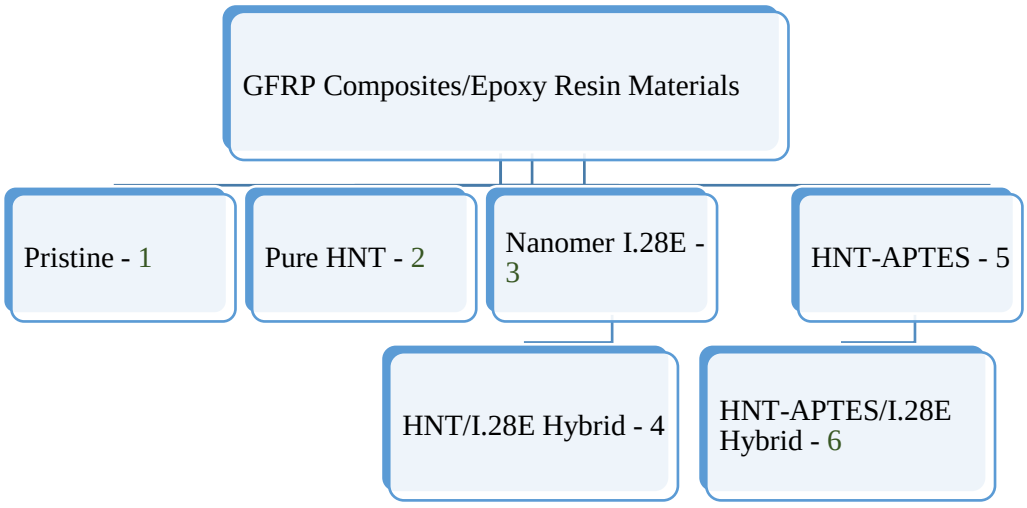

Figure 3.1: Manufactured GFRP Composites/Epoxy Resin Samples Design

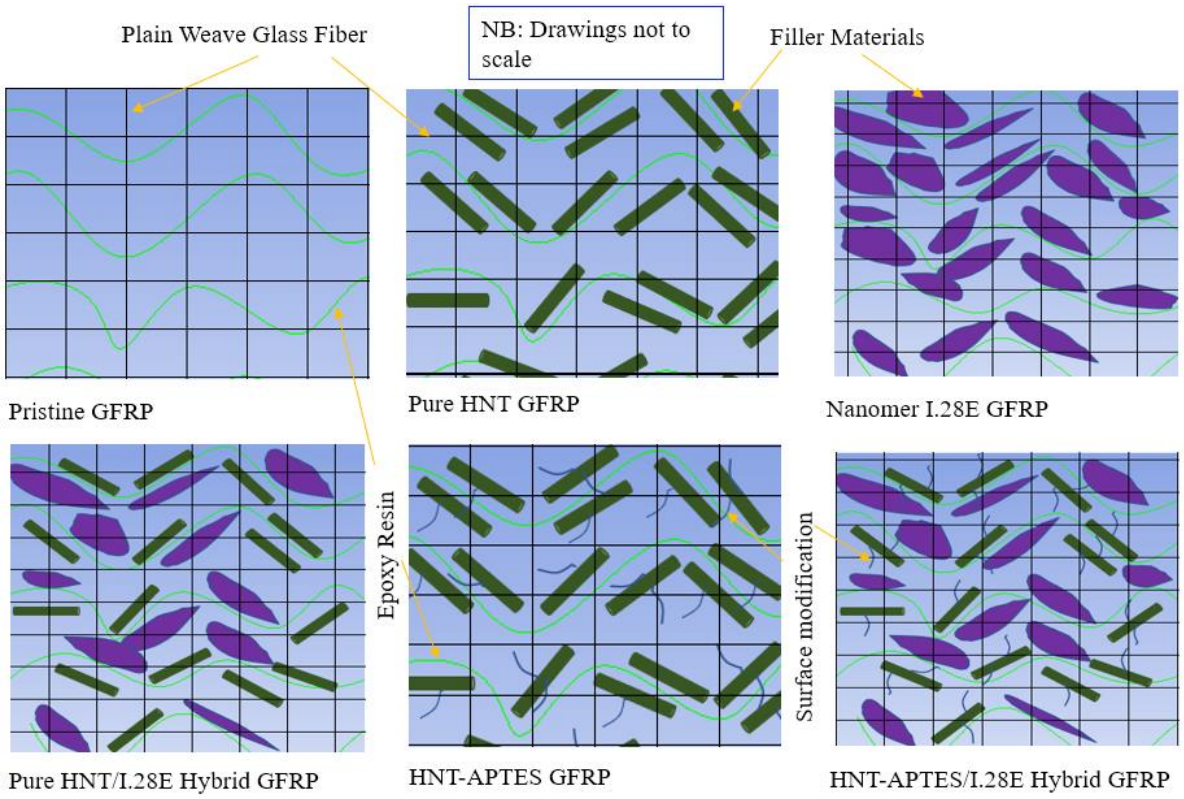

Figure 3.2: Manufactured GFRP Composites Design

The properties of the selected additives are shown in Table 3.1.

Table 3.1: Properties of the Selected Nanofillers

Material	**Halloysite Nanoclay**	**Nanomer I.28E**
Clay type	Aluminosilicate Clay	Montmorillonite Clay
Formula	• $Al_2Si_2O_5(OH)_4 \cdot 2H_2O$	• $R_{0.33}Al_2Si_4O_{10}(OH)_2 + nH_2O$, R represents one or more of the cations Na^+, Ka^+, Mg^{2+}, Ca^{2+}
Shape	• Tubular	• Plate-like nanoparticles
Size	• Diameter: 30-70 Nanometers • Length:1-3 microns	• Particle size < 20 microns
Surface modification as received	• NO	• Yes: According to the supplier's website (Sigma Aldrich), the material is modified with - 25-30 wt. % trimethyl stearyl ammonium
Properties	• Low electrical, thermal conductivity, and strong hydrogen interactions	•

3.1.1 Halloysite Surface Modification

During silane modification, 20g as-received HNTs were dispersed in toluene and 100 ml APTES added dropwise, sonicated for 30 minutes, and after that refluxed while magnetically stirring for 24 h at 110 °C. The silane-modified HNTs were obtained by centrifugation (3,000 rpm) and rinsed several times with toluene to eliminate the remaining organosilanes. The filtered residuals were then dried for 24 h at 70 °C temperature, and silane-modified HNT was abbreviated as "HNT-NH_2" (HNT-APTES)/HNT Amine. Possible functionalized HNT is shown in Figure 3.3.

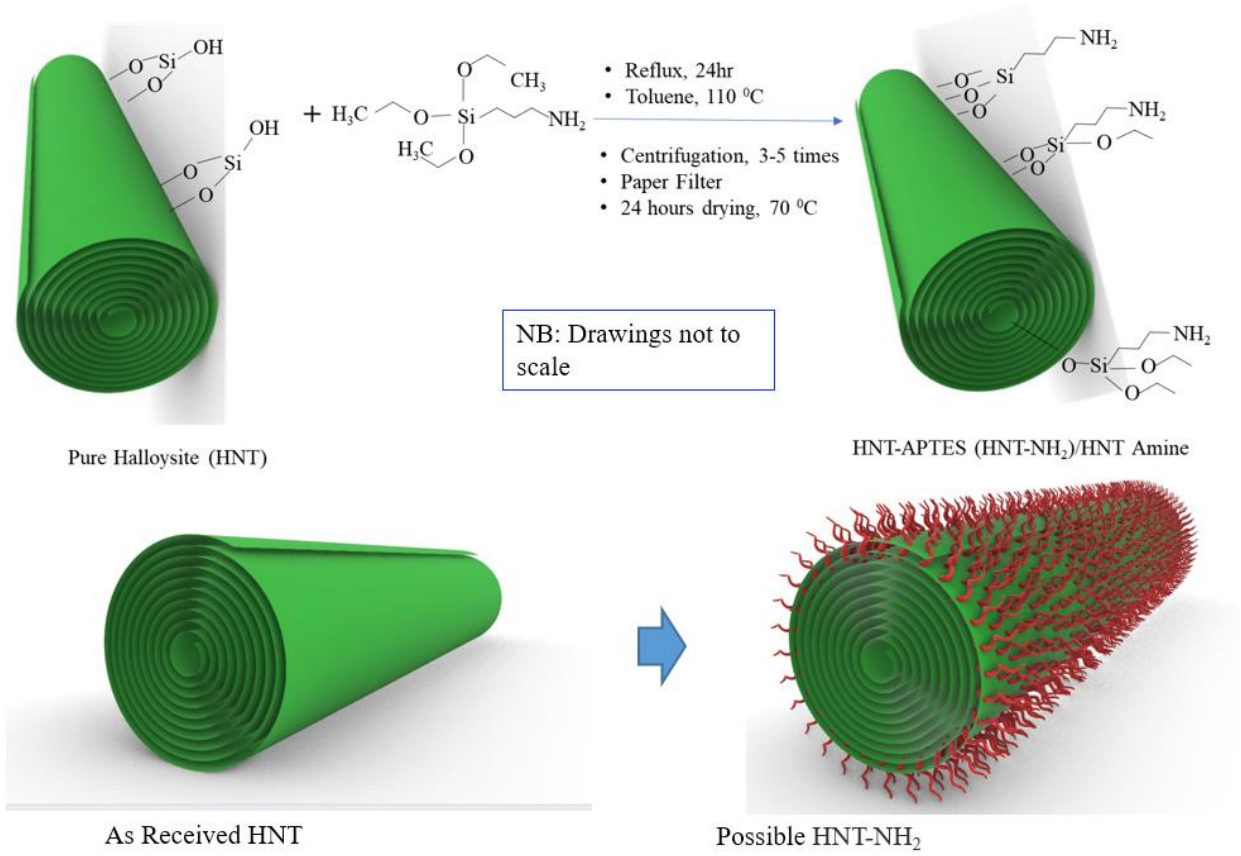

Figure 3.3: Schematic Halloysite-APTES Functionalization

3.1.2 Epoxy Resin and as Received Filler Materials Preparation

Part A of SC-15 epoxy was mixed thoroughly with the desired concentration for each material configuration (1% HNT, 1% I.28E and 1% Hybrid fillers). The resulting material was then mixed using a magnetic stirrer, followed by ultrasonication for 30 minutes, whereby intermittent sonicating energy (10s energy, 5s pause) was applied to control the rise in temperature of the compound. Before degassing, Part A and Part B of SC-15 were mixed thoroughly. Figure 3.4 shows the typical resin preparation set-up used.

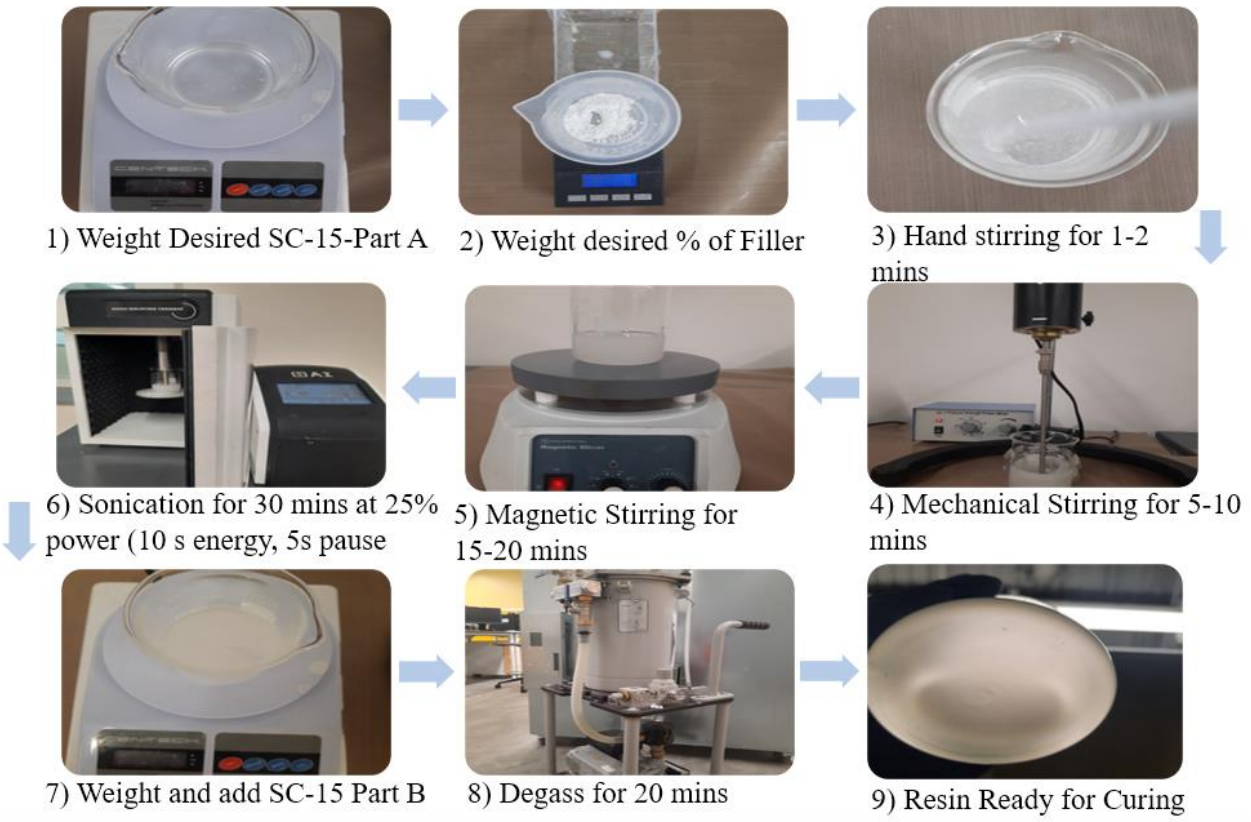

Figure 3.4: Typical Epoxy-Resin Preparation Setup

3.1.3 Epoxy Resin and Functionalized Filler Materials Preparation

Functionalized filler materials did show agglomeration even after all the resin preparation processes had been optimized. Homogenization was the method used to mitigate the problem. Homogenization was done at the lowest speeds possible to reduce the particles sizes at 2 minute intervals since high speeds could rupture the cell membrane. Once no feasible particles were present, processes 5-9 in Figure 3.4 followed. Figure 3.5 shows the agglomeration photos and homogenization setup.

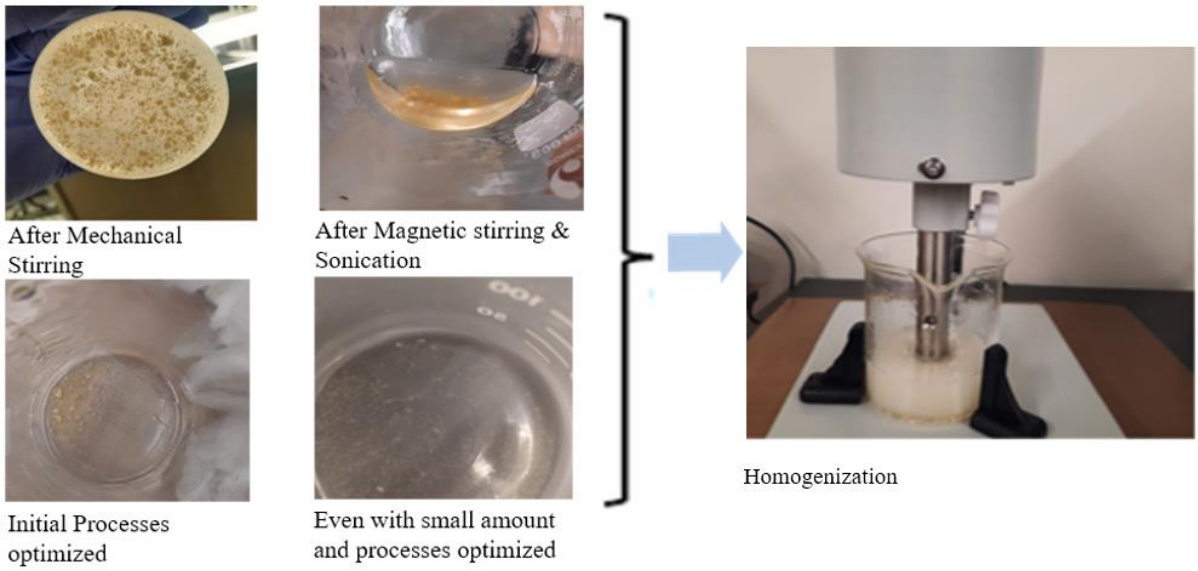

Figure 3.5: Agglomeration Photos and Homogenization Setup

3.2 Composite Materials Manufacturing

GFRP composite samples were manufactured using a liquid molding process. Twelve on-axis [0/90] reinforcements were prepared whereby an aluminum mold with the dimension of 600 mm x 850 was used to fabricate 400 mm x 550 mm plates, as shown in Figure 3.6. To obtain mode-I specimens for interlaminar fracture toughness (double cantilever) testing, a 50 mm width Teflon sheet was placed on one end between the sixth and seventh pliers (in the middle of the laminate). After a hand layup process, the mold was sealed using a vacuum bag and sealant tape at vacuum (29 in-Hg). The laminate was then cured in a convection oven at 60 °C for 2 h and post-cured at 94 °C for 4h. A detailed summary of hand-layup in-cooperation of the liquid molding process is shown in Figures 3.7-3.9. The thickness of the cured laminate was found to be varied between 2.90 mm and 3.10 mm. The laminate coupons were cut by a water-jet machine to achieve the final dimensions for the vibration analysis, tensile strength, and mode I fracture toughness per the ASTM standards. For TGA, DSC, and DMA analysis, thoroughly degassed epoxy resin mixture without reinforcement were poured into pre-pared silicone molds and cured in a convection oven at 60 °C for 2 h and post-cured at 94 °C for 4h.

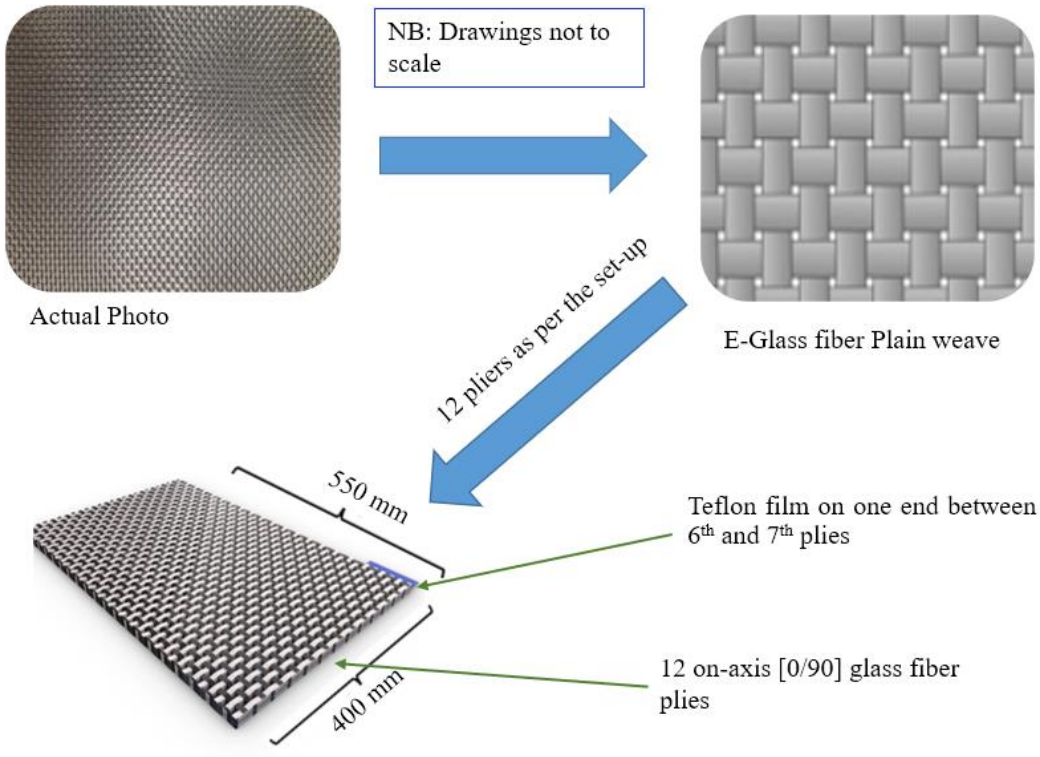

Figure 3.6: Twelve on-axis [0/90] Reinforcement Setup

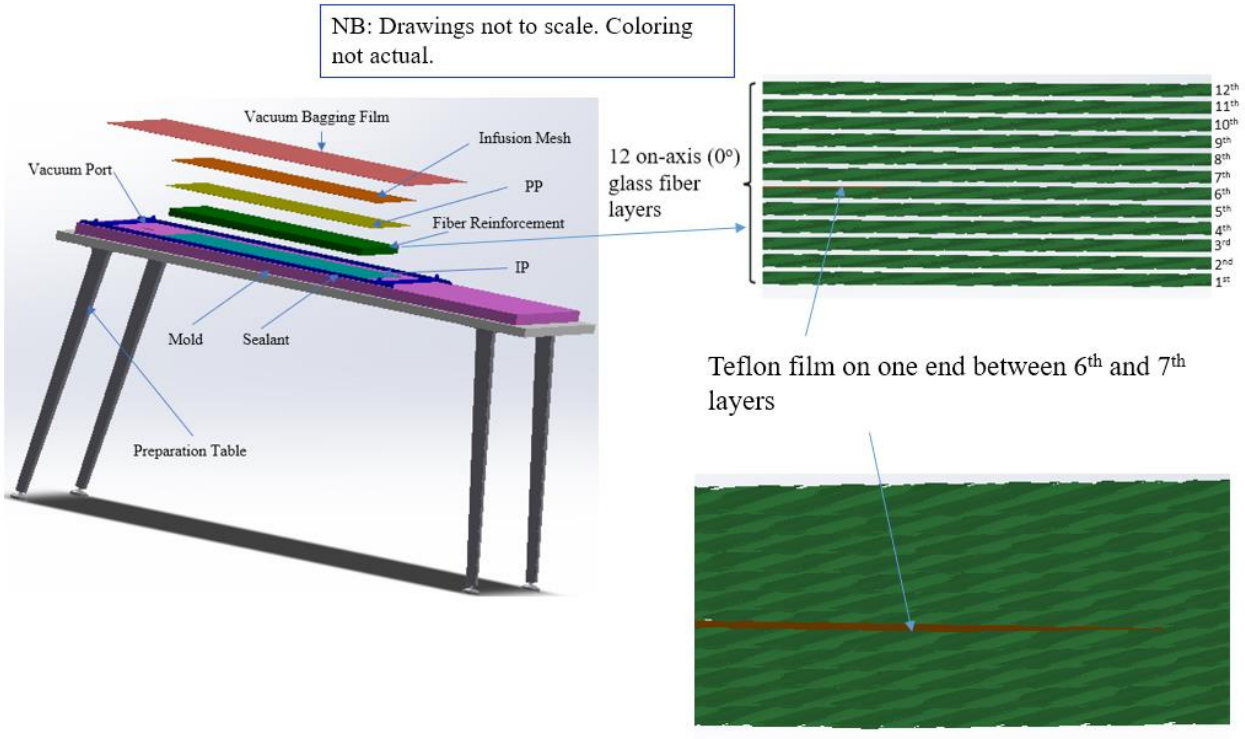

Figure 3.7: GFRP Hand Lay-Up Setup

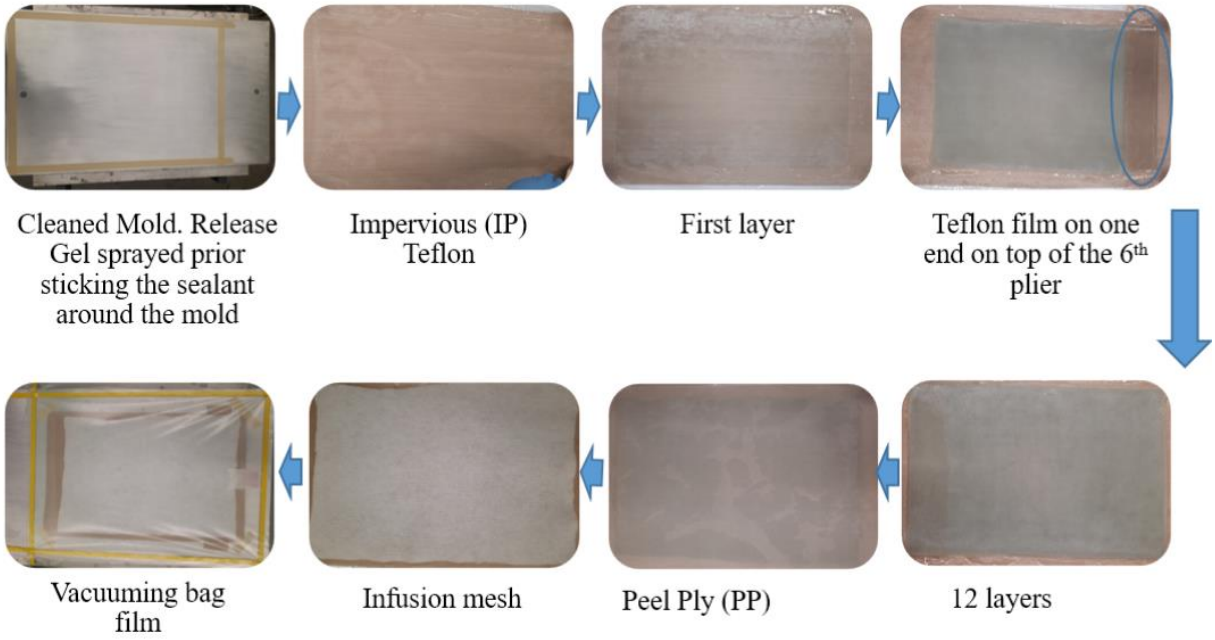

Figure 3.8: GFRP Materials Hand Laying Processes

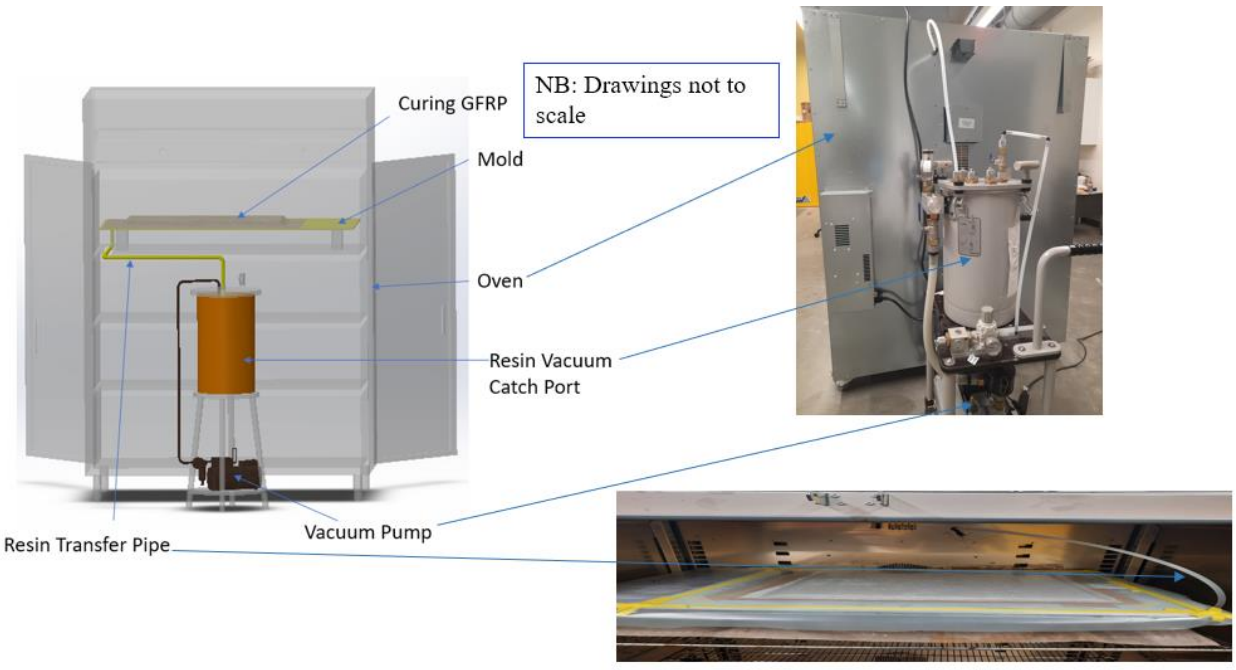

Figure 3.9: GFRP Laminate Curing Setup

3.3 Experimental Set-Up

In this study, to fully understand the effect of the mechanical properties of the GFRP composites impregnated with nanomodified and hybrid fillers, fracture toughness, tensile and vibration properties of the materials were done, and the results compared with the neat GFRP materials. TGA, DSC, and DMA analysis of the selected fillers were analyzed to determine their thermal stability, purity, and interfacial interactions between the epoxy resins.

3.3.1 Thermogravimetric Analysis - TGA

In TGA, a small sample mass is analyzed as a function of time in each temperature range. TGA is mostly used to determine the thermal stability of polymers and the composition of sample constituents (Ng et al. 2018). Generally, the material is considered thermally stable if the change in mass is not observed (Ng et al. 2018; Al Hassan et al. 2021). In the present study, TGA was used to determine the amount of amine loading on the functionalized halloysite. The TGA analysis provided the thermal stability of the clays and epoxy resin samples. Research was done using TA instruments, TGA Q50 under a nitrogen atmosphere from room temperature to 700 °C at 10 °C/min. Approximately 10 mg of finely ground samples were heated in a platinum crucible. The nitrogen flows for both the balance and sample were maintained at 20.0 ml/min.

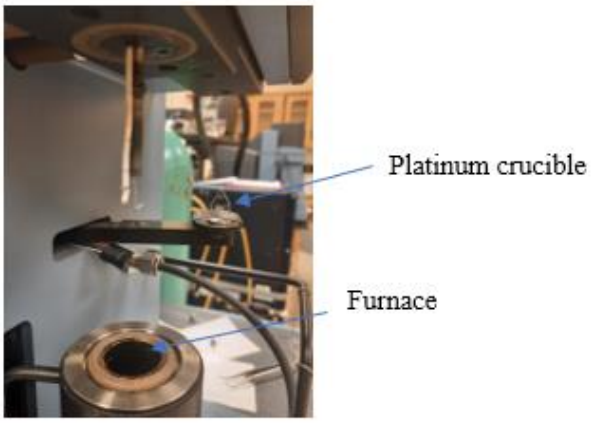

Figure 3.10: TGA Setup

3.3.2 Differential Scanning Calorimetry (DSC)

DSC is used to analyze the heat exchange differences between a sample and a reference such as air, whereby parameters such as enthalpies of reaction and glass transition temperature (T_g) can be analyzed (Al Hassan et al. 2021). In the present study, DSC was used to provide essential insights into the purity of the clay and epoxy resins samples. Enthalpies of reaction and glass transition temperature (T_g) of the epoxy resins were analyzed to determine the interfacial interactions between the epoxy polymer and the filler materials. Analysis was done using TA DSC250 differential scanning calorimeter in a nitrogen environment. Approximately 10mg samples were heated at 10 °C/min from -20 °C to 200 °C and cooled at the same rate.

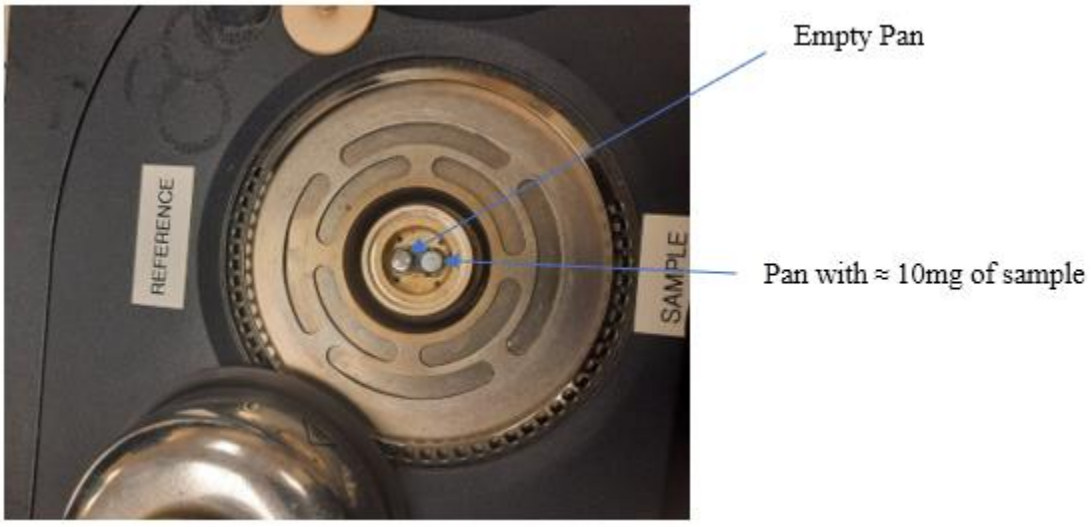

Figure 3.11: DSC Setup

3.3.3 Dynamic Mechanical Analysis (DMA)

DMA is a technique used to characterize polymers often by applying an oscillatory force on a sample at temperatures ranging well below and above their glass transition temperatures (T_g), and the material's response to this force is measured (McAninch et al. 2015; Bashir 2021). Interfacial interactions between the pure polymer matrix and the filled polymer are critical since they relate to bulk properties and service life (Bashir 2021).

This study carried out DMA on three samples for each epoxy resin configuration using TA Instruments DMA Q800. DMA was mainly used to provide essential insights into the interfacial interaction of epoxy resins. All specimens were cut in rectangular bars of nominal size 10.0 mm × 6.5 mm × 3.0 mm. The three-point clamp length had been standardized to 5mm hence input values into the software for DMA analysis were 5.0 mm × 6.5 mm × 3.0 mm. Data were collected from ambient temperature to 150 °C at a scanning rate of 3 °C/min.

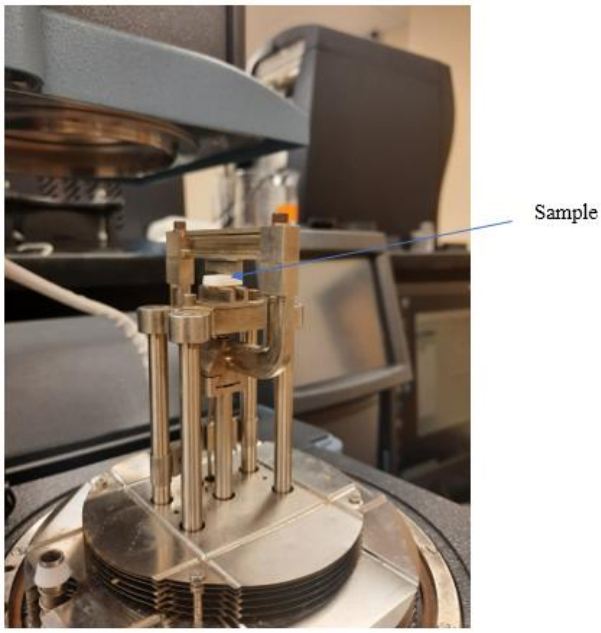

Figure 3.12: DMA Setup

3.3.4 Mode I Fracture Toughness Test for GFRP Specimens

Double Cantilever Beam (DCB) specimens were prepared as per ASTM D5528. Six samples for each GFRP configuration were tested using Mark 10- M5-300 universal testing machine. Two piano hinges were bonded on both sides (top and bottom) of each specimen using two parts T-88 adhesives. A paper ruler was bonded along one edge of a specimen to measure the crack propagation during the test. A loading speed of 5 mm/min was maintained, and force and opening displacement were measured using the MESUR software program. Figure 3.13 shows the DCB specimen setup. The delamination length, a, from the pre-delamination a_o was monitored during crack propagation.

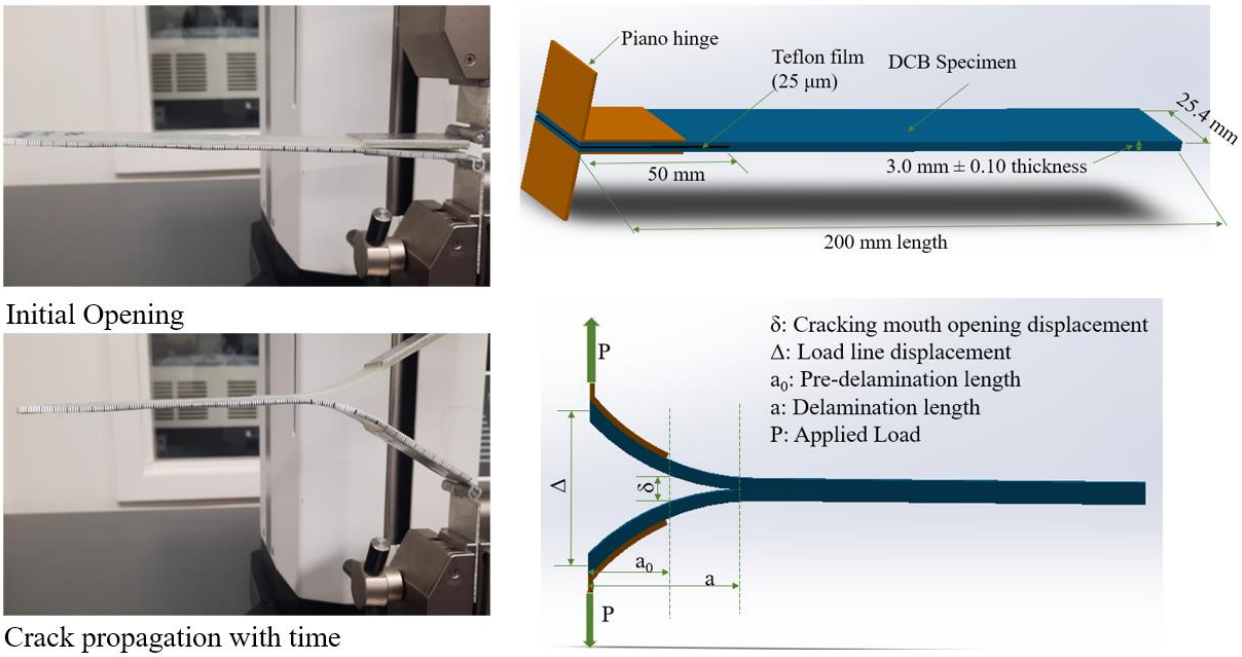

Figure 3.13: DCB Specimen Setup

3.3.5 Tensile Test for GFRP Specimens

Four specimens for each GFRPs were tested under tensile loading using MTS Criterion (Model 43) electromechanical universal testing machine with a capacity of 30 kN. Specimens were clamped using hydraulic wedge grips, as shown in Figure 3.15. According to ASTM D3039, samples were subjected to monotonic tensile loading with a 2 mm/min stroke rate.

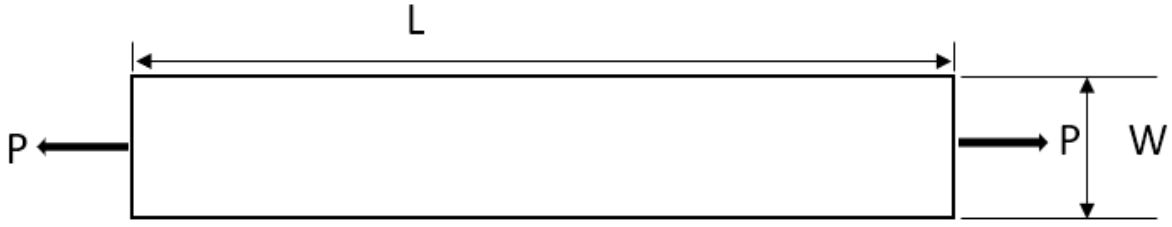

Figure 3.14: Tensile Specimen

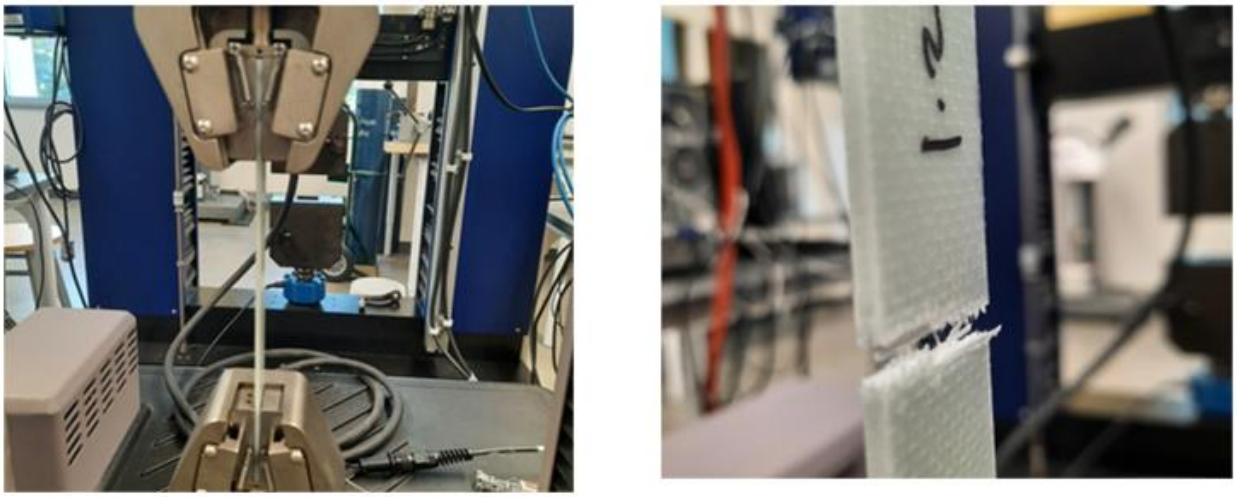

Initial Test set-up

After breakage of sample

Figure 3.15: Tensile Test Setup

3.3.6 Vibration Analysis

The characterization of the dynamic behavior for the GFRP composites was carried out through free decay vibration tests. 250 mm X 25.4 mm specimens were firmly clamped, and free vibration analysis were recorded using a portable optoNCDT 1420 laser with a measuring rate of 4kHz. The laser light was strategically placed at a fixed position on the unclamped end (but at the mid-width position), as shown in Figure 3.16. The clamped regions were 54 mm long; thus, the free span of the beams was 196mm. The test was done on the same test rig simultaneously to ensure the same boundary conditions and repeated at least three times for each sample to obtain multiple realizations. The signals were recorded during the vibration tests until an almost straight line was reached and sampled at 4000 Hz. MATLAB code was then used to generate the Fast Fourier Transform (FFT), whereby each sample's frequency (Hz) was determined. The damping coefficient for the samples was determined and averaged for each material.

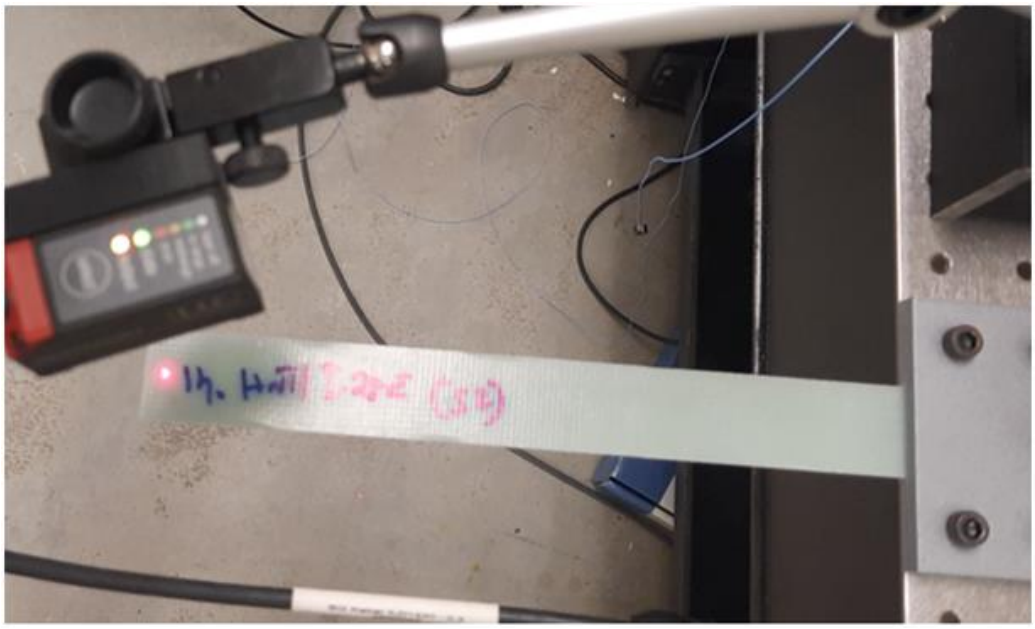

Figure 3.16: Vibration Analysis setup

3.3.7 Scanning Electron Microscope (SEM)

Clay and samples taken from mode-I and tensile fractured specimens were pre-coated with gold sputter coating to improve the conductivity. SEM on clay samples was done to confirm the clay shapes. SEM on Mode I and tensile fractured surfaces were performed to evaluate the state of dispersion and adhesion of the different clay configurations and the glass fiber epoxy resin matrix.

Sputter Equipment SEM Equipment

Figure 3.17: SEM Pre-Coating and Scanning Chamber Setup

CHAPTER 4

4. RESULTS

4.1 Thermogravimetric Analysis (TGA)

4.1.1 Clay Samples TGA Analysis

As earlier mentioned in this report, TGA was successfully used to determine the thermal stability of clay samples and provide an insight into the successful functionalization of the halloysite with APTES. Figures 4.1, 4.2, and 4.3 show TGA curves for HNT, HNT-APTES, and nanomer I.28E, respectively.

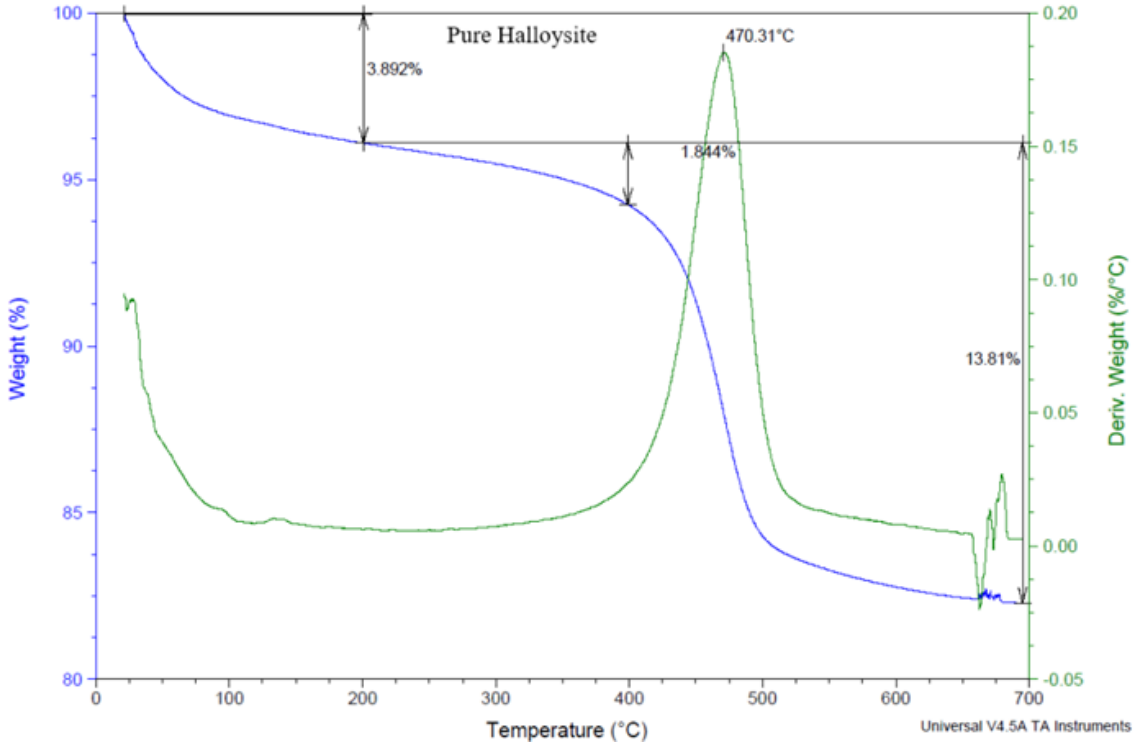

Figure 4.1: Pure Halloysite Clay TGA Curves

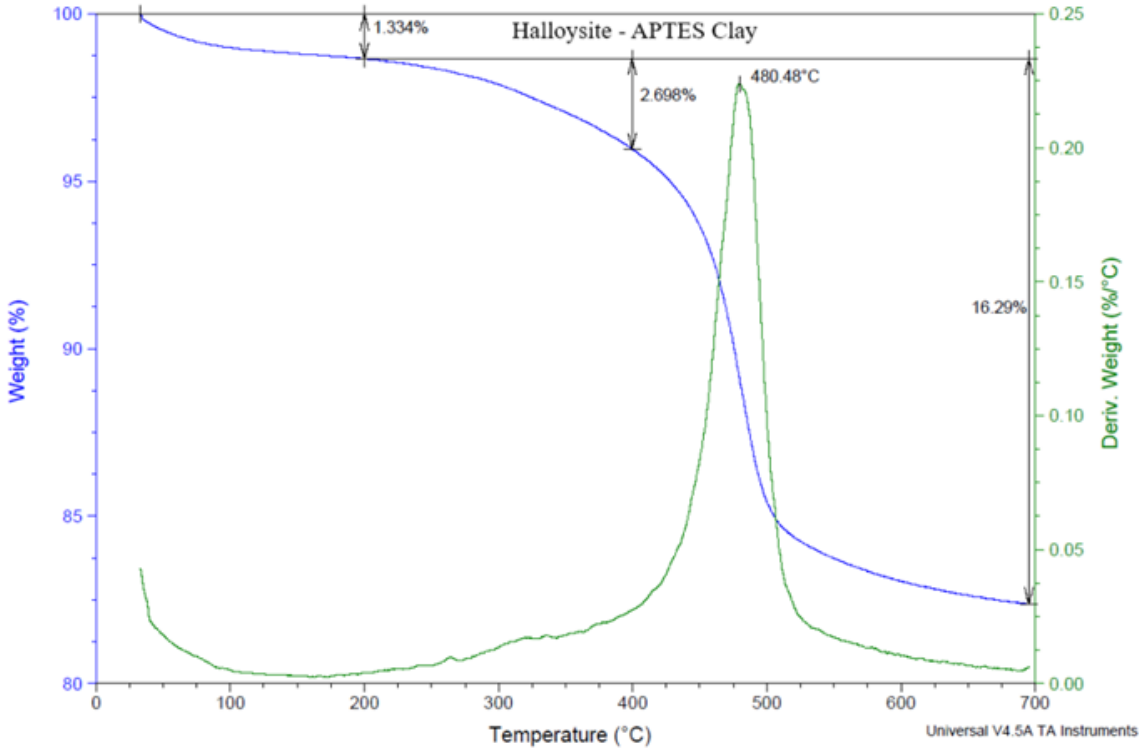

Figure 4.2: Halloysite-APTES Clay TGA Curves

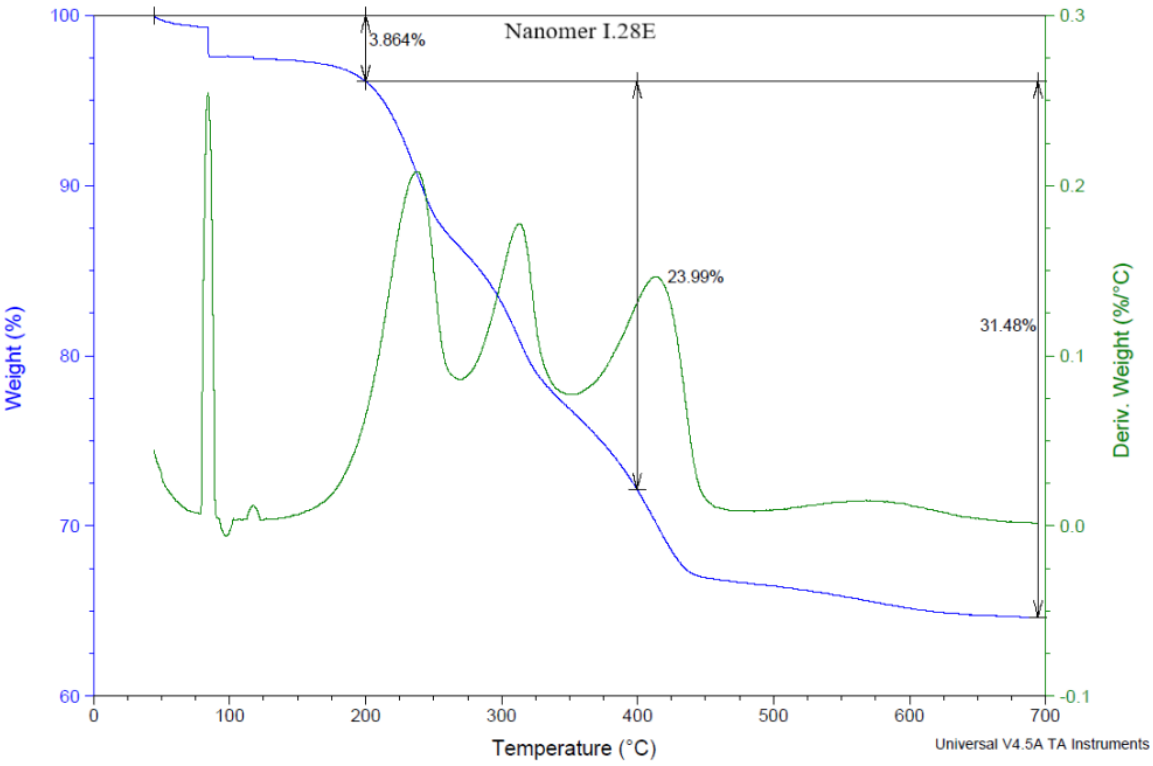

Figure 4.3: Nanomer I.28E Clay TGA Curves

Figures 4.1, 4.2, and 4.3 shows that the mass loss differences below 200 °C for HNT, HNT-APTES, and nanomer I.28E are ≈3.892%, ≈1.334%, and ≈3.864%, respectively. This mass loss is due to the residual solvents, moisture, and absorbed gasses (Murphy et al. 2020). HNT mass loss at temperatures less than 200 °C is higher than the functionalized HNT due to the utilization of the residual water during the functionalization. Results showed that HNT lost 1.844% of its weight within a range of 200 °C-400 °C, but the functionalized HNT-APTES lost 2.698%. The mass loss between 200 °C-400 °C is due to the decomposition of the organosilane and gradual interlayer water loss from the clay. A significant loss is noted in the temperature range from 400 to 700 °C.

The quantitative analysis (molar amount) of the grafted organosilane loading was determined using the adapted equation 4.1 (Murphy et al. 2020).

$$X = \frac{A-B}{100-(A-B)} \text{ X } \frac{1}{MW} \quad \text{.....4.1}$$

Where;

X - the molar amount of grafted organosilane per gram of clay,

A - mass % loss of a modified HNT from 200 to 700 °C ≈16.29%,

B - mass % loss of a pure HNT clay from 200 to 700 °C ≈13.81%,

and

MW is the molar mass of the hydrolyzed organosilane.

The effective molar mass of hydrolyzed and grafted APTES is 122g/mol (Yuan et al. 2008).

The molar mass for the functionalized halloysite was found to be 0.2084 mmol of silane/g of pure halloysite.

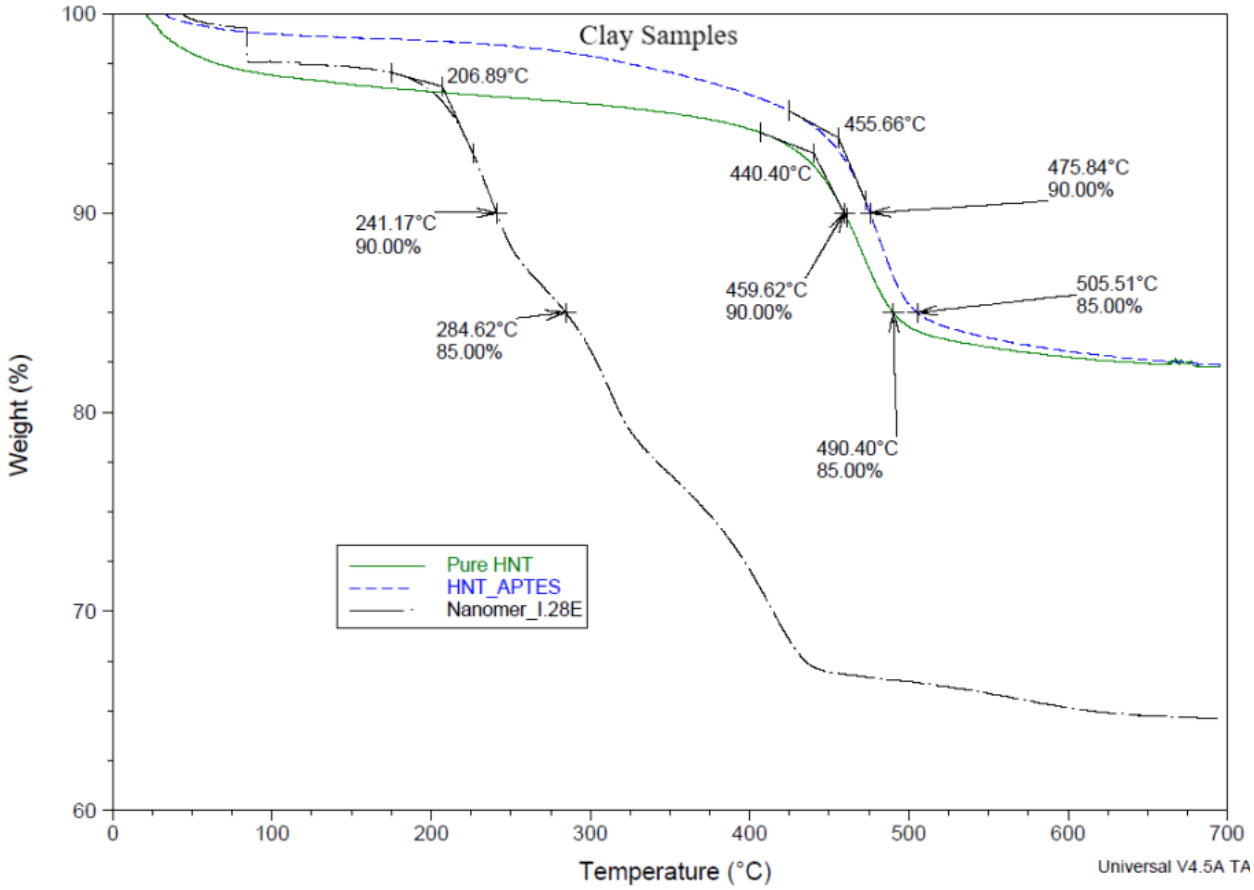

Figure 4.4: Illustrative Clay Samples T_{onset} and Analyzed Weight Percentage TGA Curves

Onset temperature (T_{onset}) is the point on the weight versus temperature curve where the deflection is first observed (i.e., the temperature at which noticeable mass loss begins). It relates to the beginning of material decomposition. From the analysis in Figure 4.4, the onset temperature for HNT-APTES was 455.66 °C and that of pure halloysite 440.40 °C. The onset temperature for the nanomer I.28E was much lower than the two halloysite clay samples. Temperatures to decompose I.28E, pure HNT, and HNT APTES clay samples to 90% weight are 241.17 °C, 459.62 °C, and 475.84 °C, respectively. At 85% weight decomposition, the same trend was observed, whereby the decomposition temperature was higher for HNT APTES followed by pure HNT and least for nanomer I.28E. The results show that HNT-APTES is more stable to thermal environment closely followed by pure halloysite clay and nanomer I.28E clay being the least stable.

4.1.2 Epoxy Resins TGA Analysis

TGA analysis on the epoxy resins provided an insight into the thermal stability of the samples. T_{onset} and temperatures at which 90, 80 & 50 weight % are remaining for each sample were analyzed. Figure 4.5 shows illustrative weight versus temperature curves for the samples, and Figure 4.6 shows, illustrative T_{onset} and selected weight % against temperature for the pure resin. Table 4.1 shows the analyzed T_{onset} data.

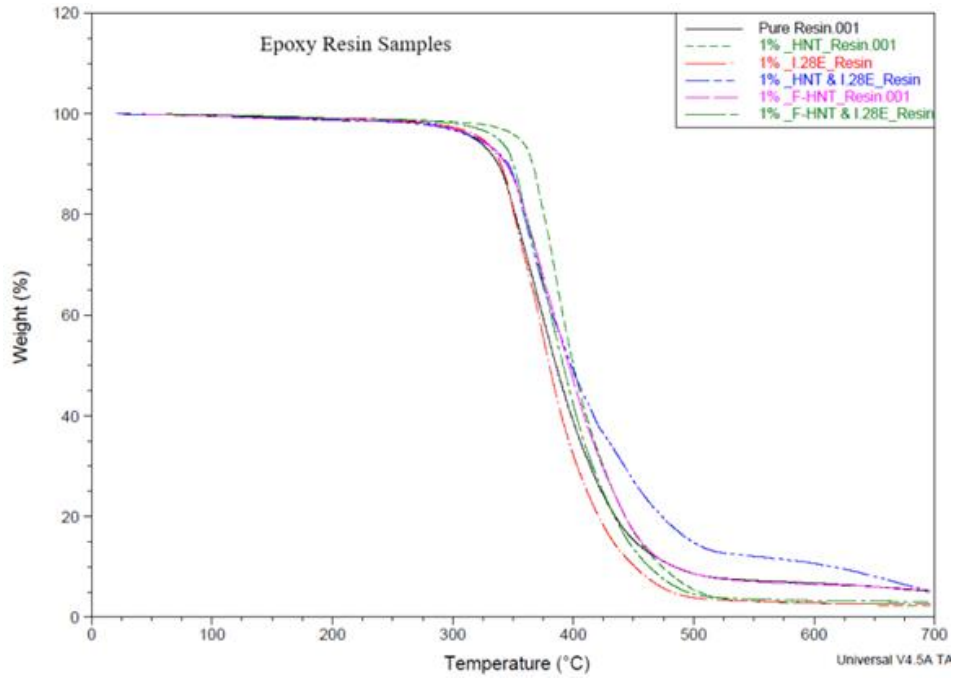

Figure 4.5: Epoxy Resins TGA Illustrative Weight versus Temperature Curves

As seen in Table 4.1, pure epoxy resin T_{onset} increased with the incorporation of filler materials to the polymer matrix. Though the increment compared to the pure resin could be seen as minimal, the thermal stability of the nanomodified polymers has been maintained. Table 4.2 and the corresponding Figure 4.7 shows temperatures needed to decompose the samples to different percentages by weight, i.e., 90%, 80% & 50%. For 90%, temperatures required to decompose the nanomodified polymer resins are higher than neat epoxy resins. Same trends are noted for 80% and 50% except for the epoxy resin nanomodified with nanomer I.28E.

Table 4.1: Epoxy Resins TGA T_{onset}

Material	T_{onset} (°C)
Pure SC-15 Resin	333.90
HNT SC-15 Resin	360.57
I.28E SC-15 Resin	335.84
HNT/I.28E SC-15 Resin	342.52
HNT-APTES SC-15 Resin	339.4
HNT-APTES/I.28E SC-15 Resin	344.7

Analyzed nanomer I.28E clay compared to the two halloysite clay samples showed the least stability. In that regard, comparing I.28E SC-15 resin to pure SC-15 resin could have resulted in the % difference of -0.26% for 80% weight and -1.44% for 50% weight.

$$\%\ Difference = \left(\frac{T\_\%W_{nano} - T\_\%W_{pristine}}{T\_\%W_{pristine}}\right) x100 \quad \text{.....4.2}$$

Where $T\_\%W_{nano}$ is the temperature for the selected %weight for nano enriched sample, and $T\_\%W_{pristine}$ is the temperature for the selected %weight for pure epoxy resin obtained from the TGA analysis.

Analyzed clay showed that functionalized halloysite showed better stability than pure halloysite sample. When the clays were incorporated into epoxy resin, opposite results were obtained. Since all the factors were kept constant, the minimal difference could be related to the samples' different particle size packaging densities, amount of samples, mode of preparation, and the surrounding atmosphere during testing of the samples. It is important to note that a small amount of the epoxy resins were cut from the cured samples and crushed accordingly to retrieve at least 10mg for TGA analysis. In general, the nano-filled epoxy resin samples' thermal stability compared to the neat epoxy resin is considered stable and within the range.

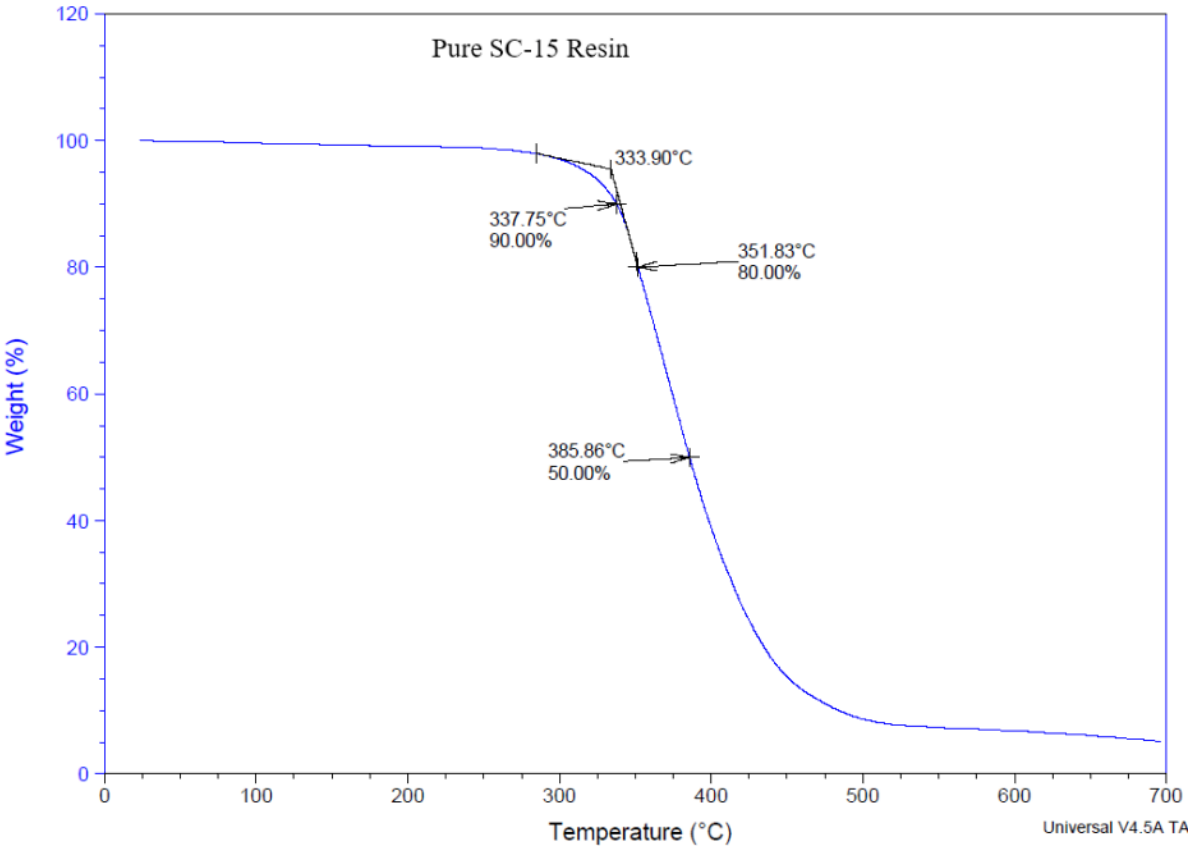

Figure 4.6: Illustrative Pure Resin TGA T_{onset} and Weight % versus Temperature Curves

Table 4.2: Epoxy Resins TGA Temperature (°C) at Different Weight %

Material	~W_{90}	~W_{80}	~W_{50}
Pure SC-15 Resin	337.75	351.83	385.86
HNT SC-15 Resin	366.43	375.67	400.24
I.28E SC-15 Resin	340.12	350.93	380.31
HNT/I.28E SC-15 Resin	346.26	359.06	398.47
HNT-APTES SC-15 Resin	344.13	360.77	396.48
HNT-APTES/I.28E SC-15 Resin	350.38	360.61	391.78

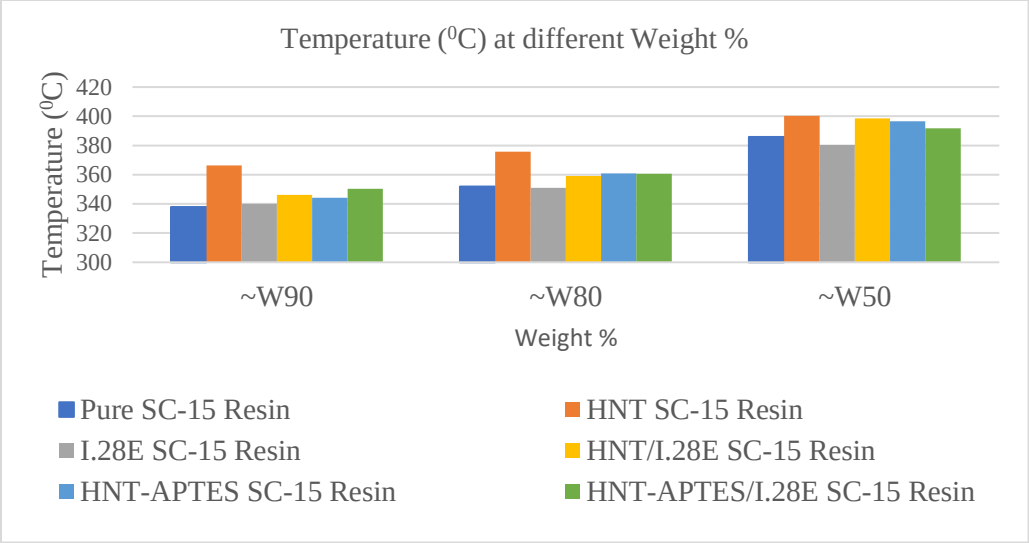

Figure 4.7: Epoxy Resins TGA Temperatures at Different Weight % Graphs

4.2 Differential Scanning Calorimetry (DSC)

4.2.1 Clay Samples DSC Analysis

Illustrative DSC Heat flow versus Temperature for pure halloysite is shown in Figure 4.8. The third phase (re-heating) proves that the peak shown in the first phase was due to the solvent being evaporated. The same scenarios were seen with the functionalized halloysite and nanomer I.28E clays. Figures 4.9 show the DSC curves for the three clay samples. There were no notable peaks during the cooling of the samples. DSC results proved that clay samples were pure.

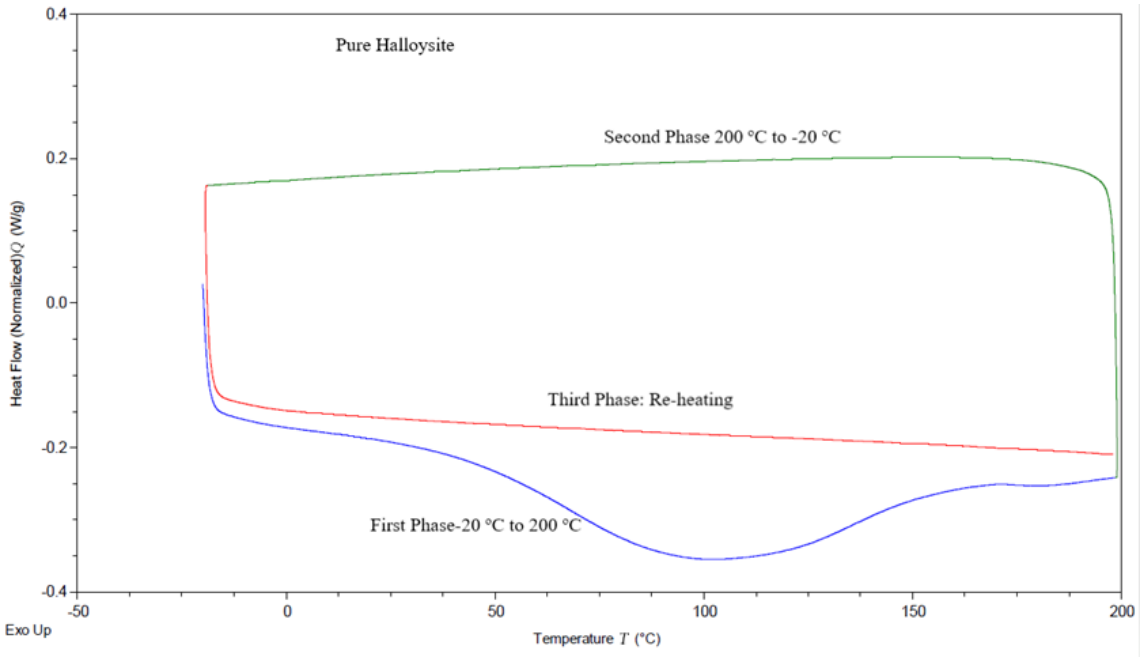

Figure 4.8: Illustrative DSC Heat flow versus Temperature for Pure Halloysite.

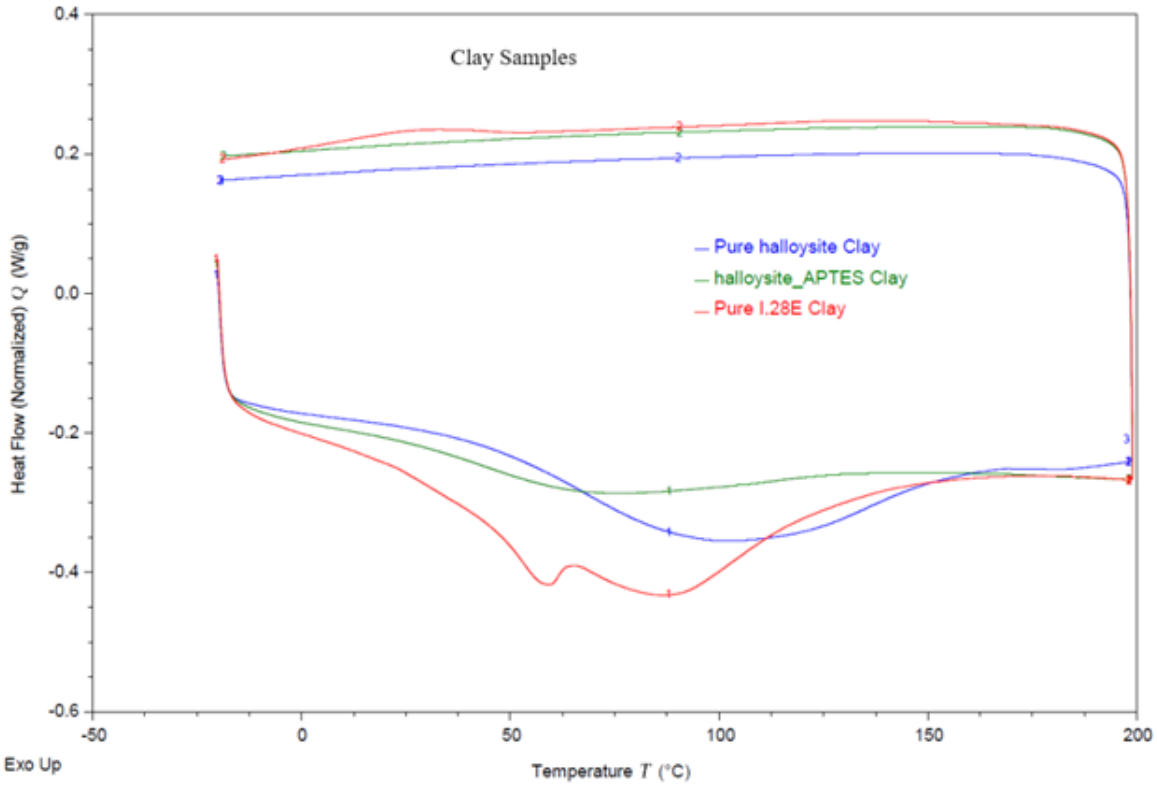

Figure 4.9: Clay Samples DSC Analysis

4.2.2 Epoxy Resin Samples DSC Analysis

Figure 4.10 shows the DSC curves for the epoxy resin samples. DSC results proved that samples were pure, and no chemical reaction occurred during the curing processes other than interfacial interaction of epoxy resins with the filler materials. The peaks for the epoxy resin samples are related to the glass transition temperatures (T_g), and the analyzed data are shown in Table 4.3 and the corresponding Figure 4.11.

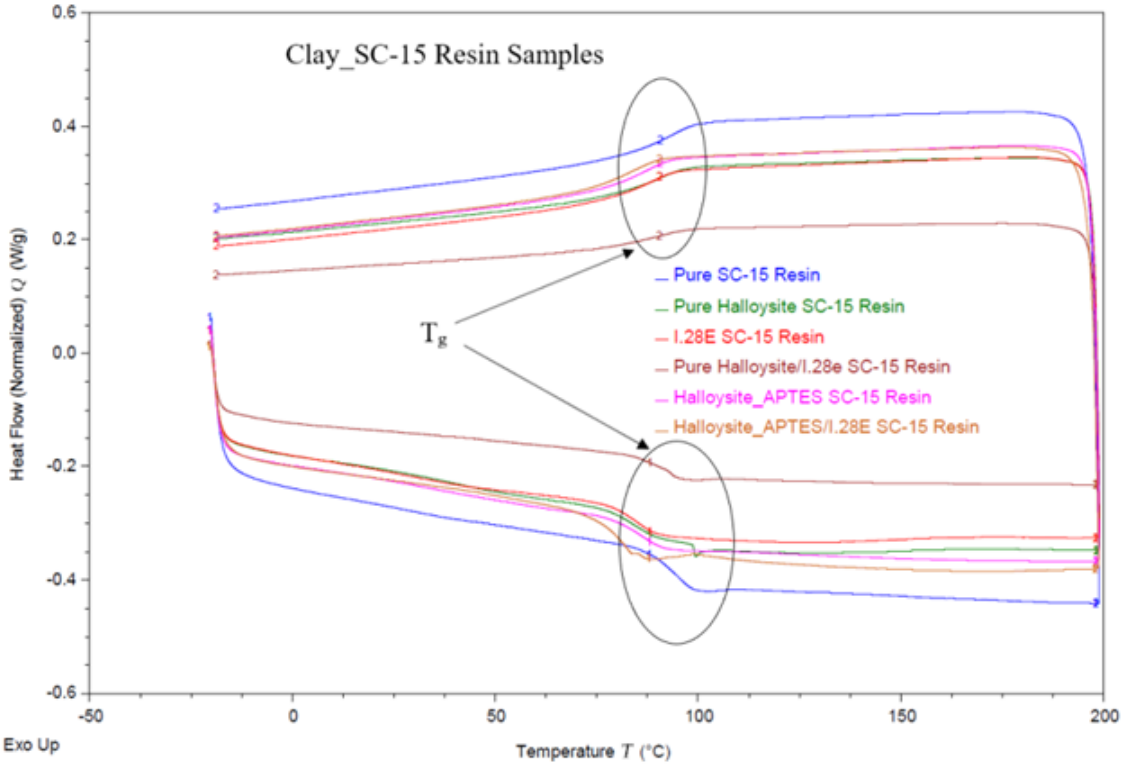

Figure 4.10: Epoxy Resin Samples DSC Analysis

Table 4.3: DSC Glass Transition Temperature

DSC Resin					
Epoxy Resin Materials	Glass Transition Temperature (T_g) (°C)		Standard Deviation	Average (T_g) (°C)	DSC_T_g % Difference
	-20 °C to 200 °C	200 °C to -20 °C			
Pure Resin	97.17	96.92	0.18	97.05	-
Pure HNT	90.40	93.04	1.87	91.72	-5.49%
I.28E	87.98	90.95	2.10	89.47	-7.81%
HNT/I.28E	94.03	97.57	2.50	95.80	-1.29%
HNT-APTES	89.59	90.93	0.95	90.26	-7.00%
HNT-APTES/I.28E	87.89	90.21	1.64	89.05	-8.24%

$$DSC\_T_g\ \%\ Difference = \left(\frac{DSC\_T_{g\_nano} - DSC\_T_{g\_pristine}}{DSC\_T_{g\_pristine}}\right) x100 \quad \text{.....4.3}$$

Where, $DSC\_T_{g\_nano}$ is the glass transition temperature for nano enriched sample, and $DSC\_T_{g\_pristine}$ is the glass transition temperature for pure epoxy resin obtained from the DSC analysis.

The T_g values in both phases (heating and cooling) showed minimal differences for each sample. The standard deviation for pure SC-15 resin and HNT-APTES SC-15 resin are 0.18 and 0.95, respectively. In general, the standard deviation was found to be <3.00. SC-15 pure resin had the highest average T_g value, and the surface nanomodified (HNT-APTES/I.28E) hybrid resin was the least. In comparison to the pure resin, the % differences for pure HNT, nanomer I.28E, HNT/I.28E hybrid, HNT-APTES, and HNT-APTES/I.28E hybrid epoxy resins were found to be -5.49%, -7.81%, -1.29%, -7.00%, and -8.24% respectively. The T_g values during heat treatment and cooling were found to be ranging from 80 °C to 110 °C, in which the enthalpies of the samples were analyzed as seen in Table 4.4 and the corresponding Figure 4.12.

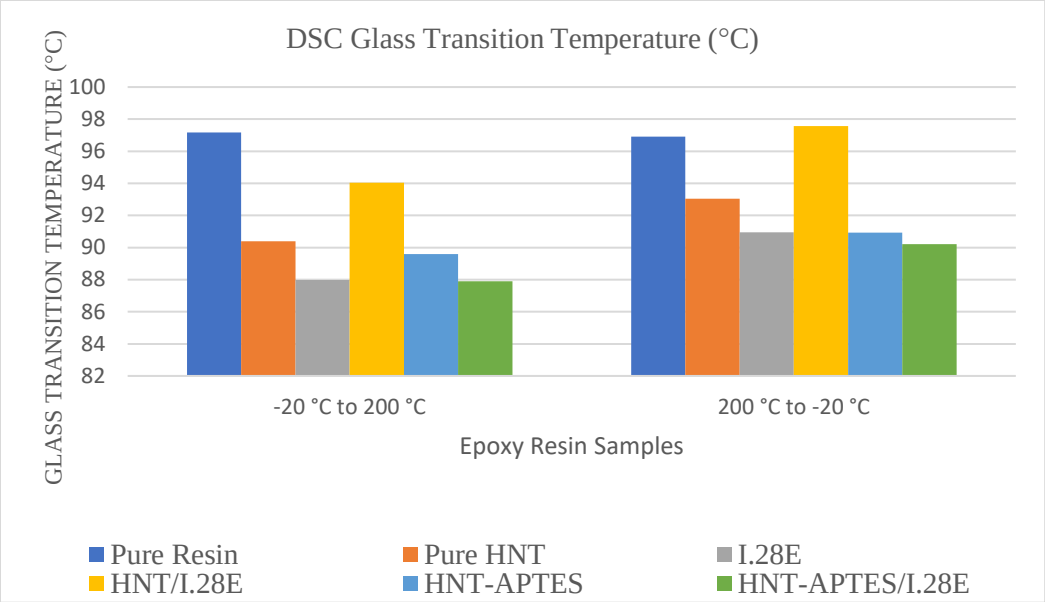

Figure 4.11: DSC Glass Transition Temperature Graphs

Table 4.4: DSC Enthalpy 80 °C to 110 °C

DSC - Resin Enthalpy-normalized (J/g) -Range analyzed (80 °C to 110 °C)		
Epoxy Resin Materials	Heating Phase (-20 °C to 200 °C)	$DSC_{enthalpy}$ % Difference
Pure Resin	1.7368	-
Pure HNT	2.4590	41.58%
I.28E	1.4862	-14.43%
HNT/I.28E	1.6501	-4.99%
HNT-APTES	2.7950	60.93%
HNT-APTES/I.28E Resin	2.2664	30.49%

$$DSC_{enthalpy}\ \%\ Difference = \left(\frac{DSC_{enthalpy\_nano} - DSC_{enthalpy\_pristine}}{DSC_{enthalpy\_pristine}}\right) x100 \ldots\ldots\ldots\ldots 4.4$$

Where, $DSC_{enthalpy\_nano}$ is the enthalpy for nano enriched sample, and $DSC_{enthalpy\_pristine}$ is the enthalpy for pure epoxy resin obtained from the DSC analysis.

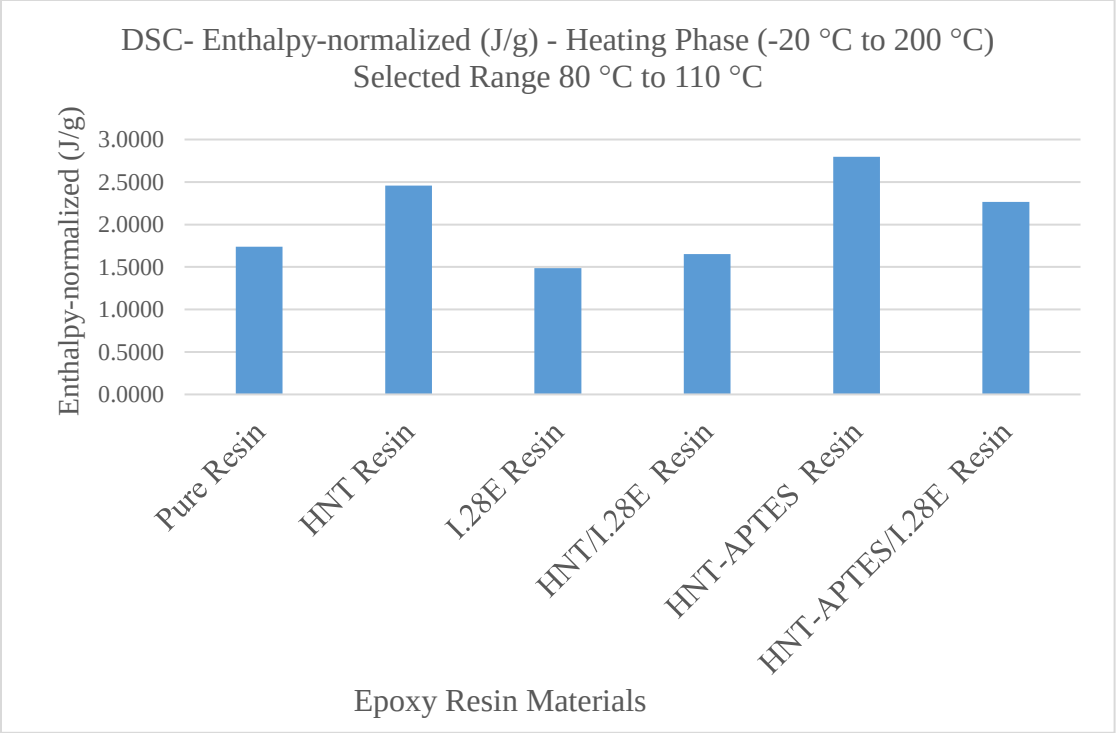

Figure 4.12: DSC Enthalpy from 80 °C to 110 °C graphs

Enthalpy analysis of the epoxy resins from 80 °C to 110 °C (epoxy resins samples T_g range) showed significant improvement on the pure resins modified with the two halloysite clays. The percentage difference for pure HNT, HNT-APTES, and HNT-APTES/I.28E hybrid resins were 41.58%, 60.93%, and 30.49%, respectively. Nanomer I.28E and HNT/I.28E hybrid resins showed a reduction in enthalpies (-14.43% and -4.99%, respectively) compared to the pure epoxy resin.

In general, the DSC_T_g % $Difference$ was found to be less than 10% for all the samples, whereas $DSC_{enthalpy}$ % $Difference$ for HNT, HNT-APTES, and HNT-APTES/I.28E hybrid showed improved enthalpy. This indicates good interfacial interactions between the pure epoxy and the three nano-filled resins. Comparing the enthalpy for the HNT/I.28E hybrid and I.28E epoxy resins, the HNT/I.28E hybrid showed higher enthalpy due to pure halloysite interfacial interactions with the polymer matrix.

4.3 Dynamic Mechanical Analysis (DMA)

Glass transition temperatures (T_g), storage modulus at selected temperatures, and tan delta (tan δ) results were analyzed using DMA for the Epoxy Resin Samples.

4.3.1 DMA Epoxy Resins Glass Transition Temperatures

As shown in Figure 4.13, at approximately 75 °C, a peak was observed on all the samples, which can be attributed to the resin used. Table 4.5 shows the glass transition temperature for the epoxy resin samples. The results show that the standard deviation for all the samples is less than 4. Comparing pure epoxy resin with resin incorporated with the different fillers shows that the % difference is less than 10%. As seen in Table 4.6, the same trend at which the T_g values compared to the neat epoxy resins has been maintained. The average DMA and DSC T_g values range from 95 °C to 110 °C and 85 °C to 100 °C, respectively. The DMA and DSC results showed the highest T_g values for pure resin while HNT-APTES/I.28E hybrid epoxy resin the least and the other nanomodified epoxy resin samples falling in between. Typically, a low concentration of nanoparticles leads to uniform dispersion inside the matrix with considerable distance between them, reducing T_g since the mobility of the loosely bound chains in the interfacial regions is not reduced (Bashir 2021). Though it is difficult to achieve the uniform dispersion at higher loadings, the distance between particles is reduced and may result in overlap of the interfacial layers hence the increase in the volume of the immobilized chains and consequently increase in the T_g values (Bashir 2021; Bindu and Thomas 2013). As mentioned in this report, this study was done using 1% weight filler concentration. The uniform dispersion of the nanoparticles could have resulted in large distances between them and hence the reduced T_g values compared to the pure epoxy resin. The nanomodified resin samples T_g % difference (in comparison to pure/unfilled epoxy resin) for both the DMA and DSC analysis were found to be less than 10%; nanocomposites are considered to be within the range of service life of composite materials. Though studies based on epoxy-clay configurations have shown increased T_g values while in some cases others have reported reduced T_g values, it is essential to note that the addition of clay affects the chemistry of the epoxy composition due to the interaction of the ions present on the surface of

the clay and epoxy molecules leading to various enhancements based on the polymer molecules (Tcherbi-Narteh et al. 2013).

Glass transition temperature by itself is not a determining factor of the usefulness of nano-modified polymer materials. Hence, DMA was further used to analyze tan delta and storage modulus in this study. As briefly discussed, DSC has been used to determine enthalpies of the epoxy resins apart from the glass transition temperatures, and TGA has been used to determine the thermal stability.

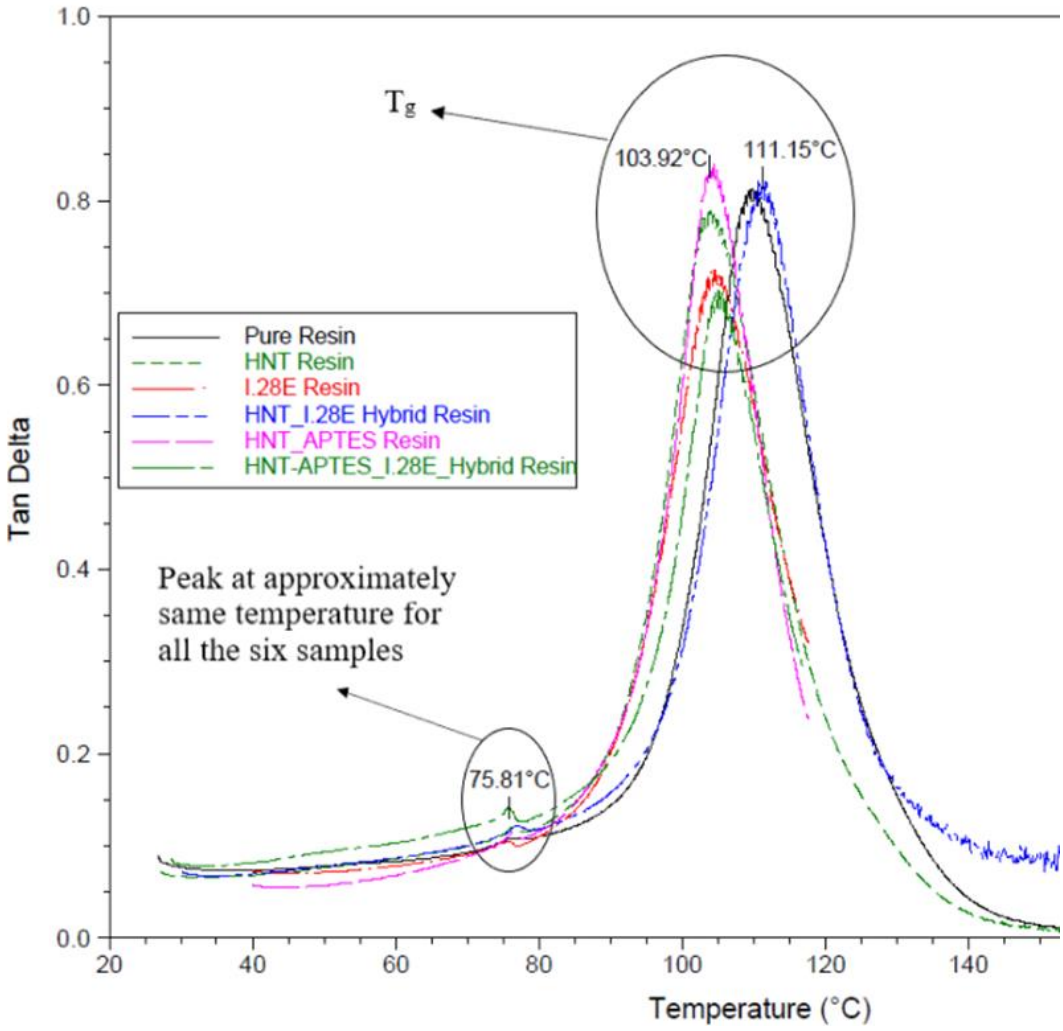

Figure 4.13: Illustrative DMA Epoxy Resins Curves

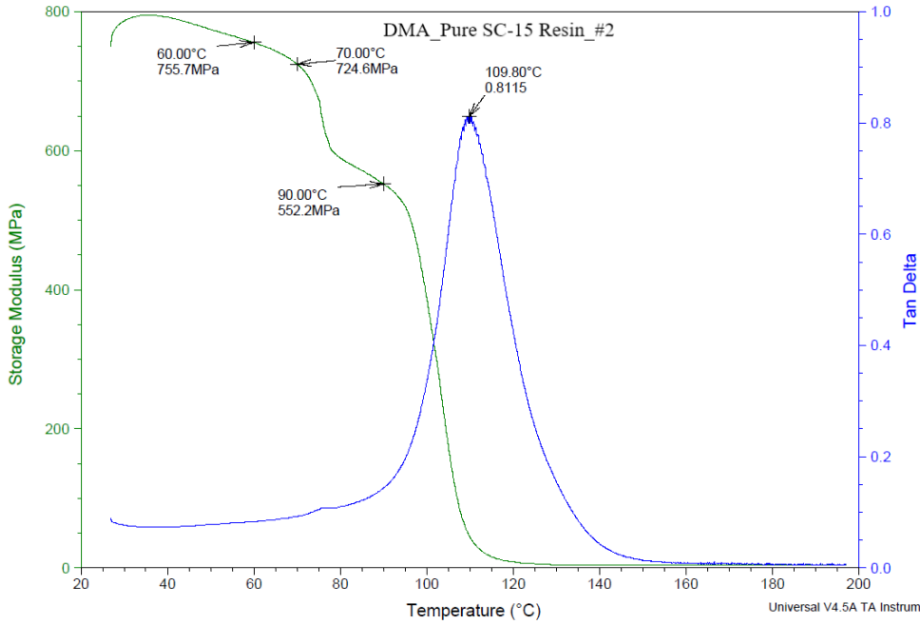

Figure 4.14: Illustrative DMA Epoxy Resin Storage Modulus and Tan Delta Versus Temperatures

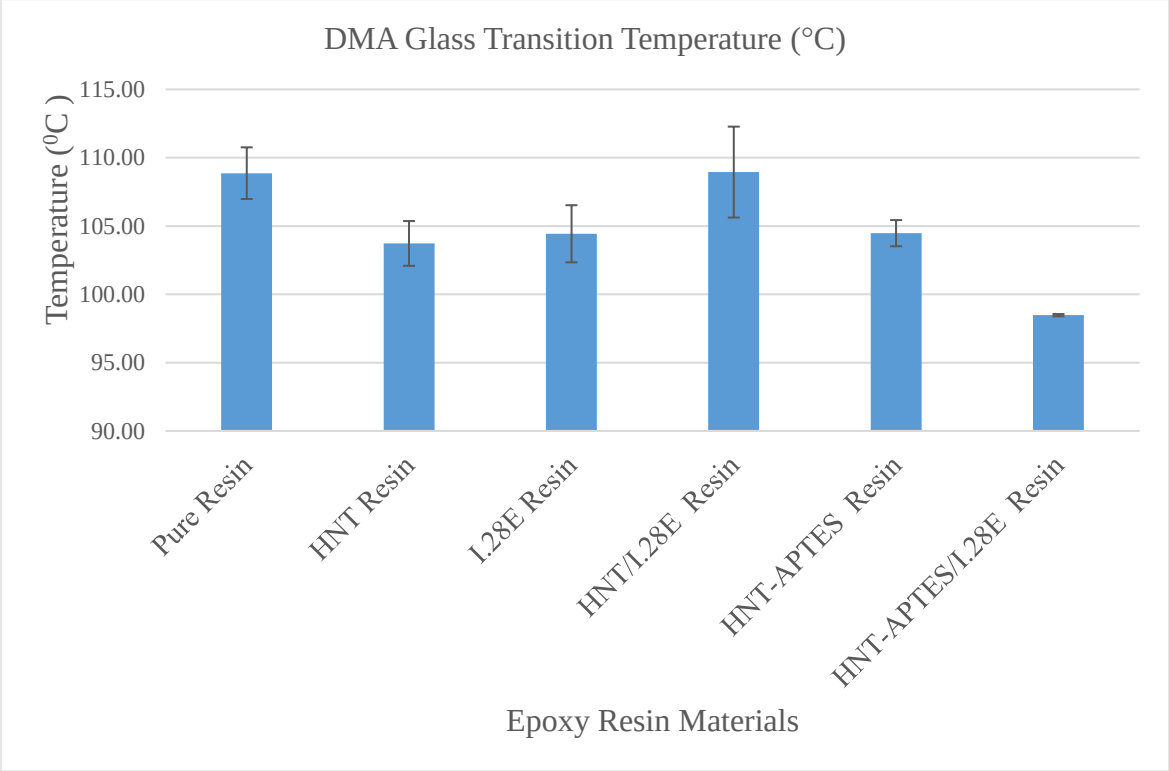

Figure 4.15: DMA Glass Transition Temperatures Graphs

Table 4.5: Epoxy resins DMA Glass Transition Temperature

	DMA Glass Transition Temperature (T_g) (°C)					
	Pure SC-15 Resin	HNT SC-15 Resin	I.28E SC-15 Resin	HNT/I.28E SC-15 Resin	HNT-APTES SC-15 Resin	HNT-APTES/I.28E SC-15 Resin
Sample 1	110.11	101.95	106.66	111.15	105.58	98.38
Sample 2	109.80	105.18	102.51	105.12	103.92	98.51
Sample 3	106.69	104.04	104.12	110.57	103.92	98.53
Average	108.87	103.72	104.43	108.95	104.47	98.47
Standard Deviation	1.89	1.64	2.09	3.33	0.96	0.08
DMA_T_g % Difference	-	-4.73%	-4.08%	0.07%	-4.04%	-9.55%

$$DMA\_T_g\ \%\ Difference = \left(\frac{DMA\_T_{g\_nano} - DMA\_T_{g\_pristine}}{DMA\_T_{g\_pristine}}\right) x100 \quad \text{.....4.5}$$

Where, $DMA\_T_{g\_nano}$ is the glass transition temperature for nano enriched sample, and $DMA\_T_{g\_pristine}$ is the glass transition temperature for pure epoxy resin obtained from the DMA analysis.

Table 4.6: DMA versus DSC Glass Transition Temperature

	Glass Transition Temperature (°C)					
	Pure SC-15 Resin	HNT SC-15 Resin	I.28E SC-15 Resin	HNT/I.28E SC-15 Resin	HNT-APTES SC-15 Resin	HNT-APTES/I.28E SC-15 Resin
DSC_T_g	97.05	91.72	89.47	95.80	90.26	89.05
DMA_T_g	108.87	103.72	104.43	108.95	104.47	98.47
DMA_T_g vs. DSC_T_g difference	11.82	12.00	14.96	13.15	14.21	9.42
DSC_T_g % Difference	-	-5.49%	-7.81%	-1.29%	-7.00%	-8.24%
DMA_T_g % Difference	-	-4.73%	-4.08%	0.07%	-4.04%	-9.55%

4.3.2 DMA Epoxy Resins Tan Delta

Tan delta, abbreviated as tan δ, is the ratio of loss modulus and storage modulus. It relates to the damping properties of viscoelastic materials such as polymers and nanocomposites. Table 4.7 and the corresponding Figures 4.16 and 4.17 show tan delta results from the DMA analysis. Studies have shown that with the understanding of the interfacial relationships of the nano-filled polymers, the peak value of tan δ is used to qualitatively indicate the internal friction of the polymer chain segments (Bashir 2021).

$$Tan\ \delta = E"/E' \quad \text{.....4.6}$$

Where $E"$ is the loss modulus (the ability of the sample to lose or dissipate energy), and E' is the elastic storage modulus (the ability of the sample to store or return energy).

DMA tan δ results for HNT-APTES, HNT-APTES/I.28E hybrid, and pure SC-15 were 0.9293, 0.8028, and 0.7987, respectively. The functionalized halloysite epoxy resin did show the highest tan δ value compared to the other filler materials, most probably due to more chain segments moving uniformly at that temperature within the matrix, increasing the internal friction, i.e., the loss modulus. The contributing factors are the uniform filler dispersion and the interfacial relationship between the HNT-APTES and the epoxy resin.

Table 4.7: DMA Tan Delta

Epoxy Resin Samples	DMA Tan Delta					
	Pure Resin	HNT Resin	I.28E Resin	HNT/I.28E Resin	HNT-APTES Resin	HNT-APTES/I.28E Resin
Sample 1	0.8344	0.7882	0.8030	0.8058	0.9464	0.8697
Sample 2	0.8115	0.7870	0.7082	0.7423	0.9395	0.7045
Sample 3	0.7503	0.6870	0.7187	0.7434	0.9021	0.8343
Average	0.7987	0.7541	0.7433	0.7638	0.9293	0.8028
Standard Deviation	0.0435	0.0581	0.0520	0.0363	0.0238	0.0870

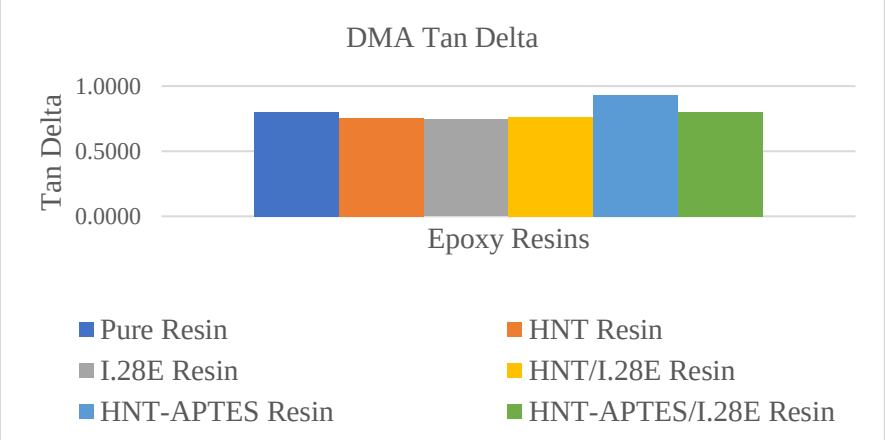

Figure 4.16: DMA Average Tan Delta Graphs

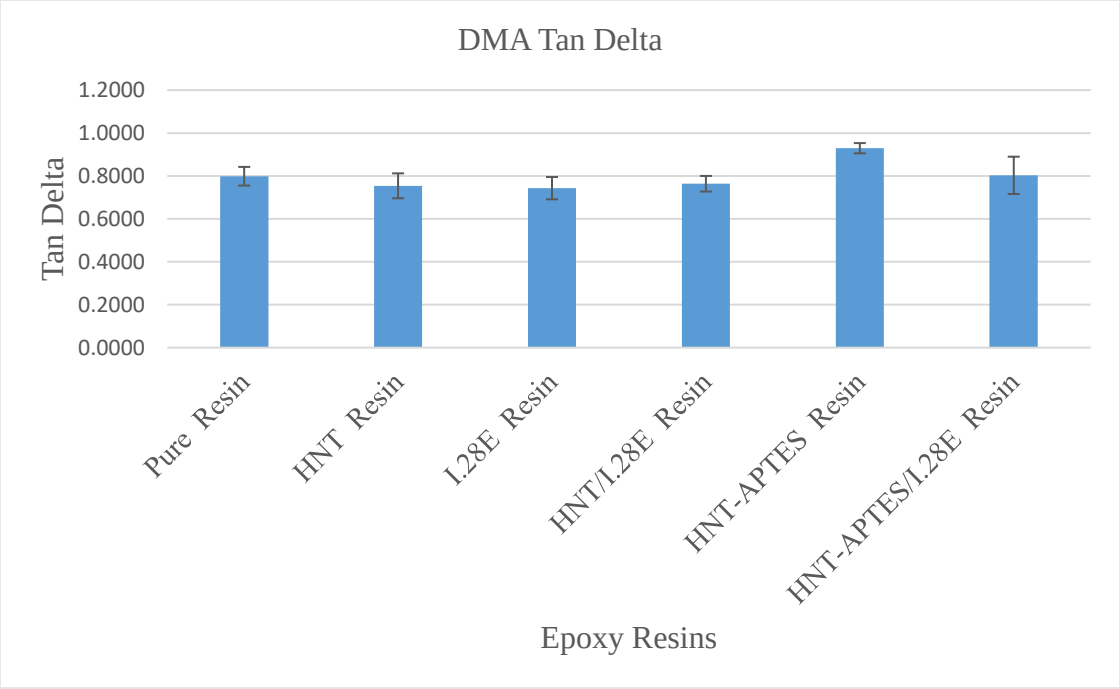

Figure 4.17: DMA Epoxy Resins Tan Delta Graphs

4.3.3 DMA Epoxy Resins Storage Modulus

Storage modulus refers to the ability of the sample to store or return energy. In this study, storage modulus at 60 °C and 70 °C temperatures were analyzed using DMA. As seen in Table 4.8 and the corresponding Figure 4.18, functionalized halloysite showed the highest storage modulus, followed by pure epoxy, and the third being HNT-APTES/I.28E hybrid epoxy resin.

The presence of the nanomer I.28E in the hybrid samples have shown a reduction in the storage modulus. Incorporation of HNT-APTES to the epoxy resin led to improved storage modulus by 18-22%. Nanomer I.28E significantly reduced the storage modulus of the epoxy polymer by 42-44%, whereas pure halloysite by 23-25%. The hybrid nanocomposites showed decreased storage modulus by 29-30% and 11-14%, i.e., HNT/I.28E and HNT-APTES/I.28E, respectively. The DMA results did prove that the larger particles nanomer I.28E tend to form agglomerates, and also the longer chains were sliding to each other and as well with the incorporated filler.

The surface modification of the halloysite provided proper dispersion in the matrix. This was evident in the HNT-APTES/I.28E hybrid, whereby storage modulus was reduced by a small degree compared to the pure HNT, I.28E, and HNT/I.28E hybrid epoxy resin samples.

Table 4.8: DMA Epoxy Resins Storage Modulus

DMA - Storage Modulus				
Epoxy Resin	@60 °C	% Difference	@70 °C	% Difference
Pure Resin	755.9	-	724.7	-
Pure HNT Resin	570.2	-24.57%	552.3	-23.79%
Nanomer I.28E Resin	426.3	-43.60%	413.3	-42.97%
HNT/I.28E Resin	529.7	-29.92%	513.7	-29.12%
HNT-APTES Resin	898.2	18.83%	882.7	21.80%
HNT-APTES/I.28E Resin	655.8	-13.24%	642.5	-11.34%

$$DMA_{Storage_{modulus}}\%\,Diff = \left(\frac{DMA\_Storage_{modulus\_nano} - DMA\_Storage_{modulus\_pristine}}{DMA\_Storage_{modulus\_pristine}}\right) x100 \quad \text{.....4.7}$$

Where, $DMA\_Storage_{modulus\_nano}$ is the storage modulus for nano enriched sample, and $DMA\_Storage_{modulus\_pristine}$ is the storage modulus for pure epoxy resin obtained from the DMA analysis.

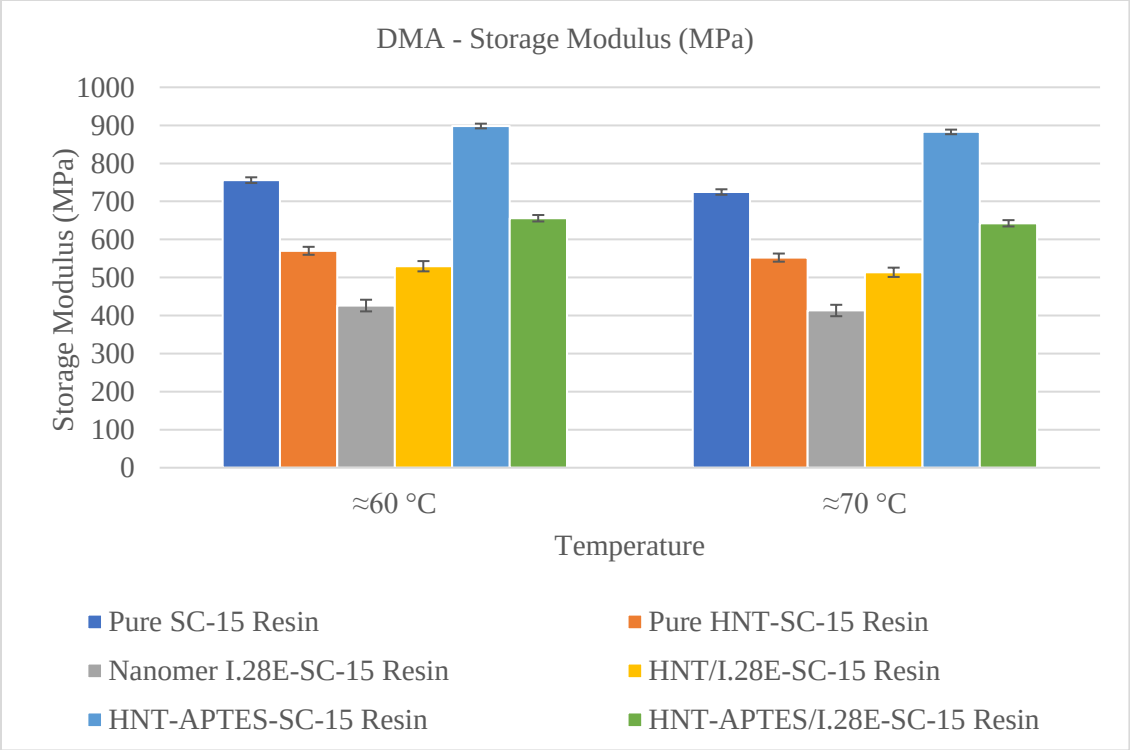

Figure 4.18: DMA Epoxy Resins Storage Modulus

4.4 Mode I Fracture Toughness

4.4.1 Crack Initiation and Propagation Force

Mode I interlaminar force-displacement curves for the GFRP materials exhibited the three distinctive regions. The regions comprised the linear elastic region, non-linear region, and multiple peak load plateaus region as reported in various works of literature, including Zeinedini et al. (2020). The illustrative force versus displacement curve for the randomly picked sample, as seen in Figure 4.19, shows the three regions (I, II, III). In region I, the load is linearly increased with displacement. In contrast, in region II, the curve becomes non-linear, and this region is related to the crack initiation. In region III, several descending peaks are observed until complete failure. For most of the material configuration, the linearity behavior did occur between 60% - 90% of the maximum load of the corresponding material configurations.

The crack initiation for each material configuration was observed at different load levels, and the average values were computed accordingly. Pristine, pure HNT, nanomer I.28E, HNT/I.28E hybrid, HNT-APTES, and HNT-APTES/I.28E hybrid GFRPs, crack initiated at 25.9N, 34.3N, 34.7N, 39.9N, 35.7N, and 42.8N, respectively. The hybrid nanocomposite composites showed the most remarkable improvement on neat GFRP in the force needed to initiate the crack, i.e., 54.05% and 65.25% for pure HNT/I.28E and HNT-APTES/I.28E hybrids, respectively. The required force for crack propagation was considerably increased in nanomodified hybrid to even higher than those of crack initiation force, which is essential to maintain the structural integrity of the GFRP even after crack initiation. The combined hybrid filler materials have improved toughened capabilities, increasing the surface roughness of the hybrid nanocomposites, hence the preserved strength after the crack initiation.

As seen in Figure 4.20, the hybrid GFRP composites exhibited the lowest magnitude of load rate compared to the GFRP materials modified with the individual filler materials and the neat GFRP. The phenomenon implied that the load required to grow the crack for the hybrid configurations was insignificantly reduced compared to the corresponding peak load.

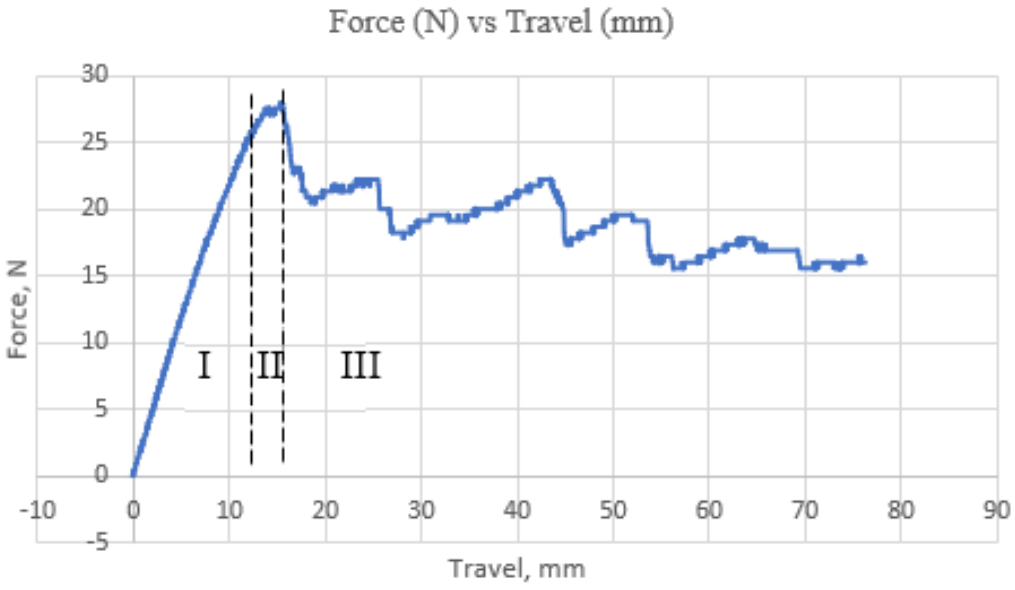

Figure 4.19: Illustrative Mode-I Fracture Toughness Force versus Displacement Phases

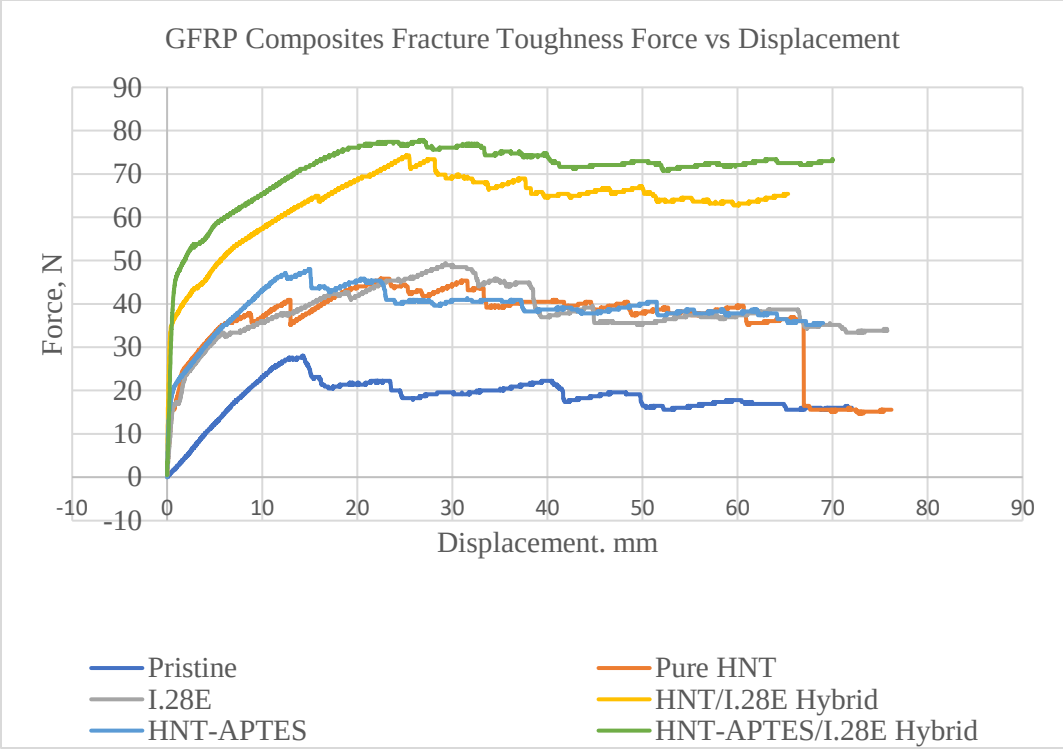

Figure 4.20: Illustrative Mode-I Fracture Toughness Force versus Displacement Curves

Table 4.9: Crack Initiation Force

GFRP Materials	Crack initiation Force (N)	$Fracture_{force\_initiation}\ \%\ Diff$
Pristine GFRP	25.9	-
Pure HNT	34.3	32.43%
Nanomer I.28E	34.7	33.98%
Pure HNT/I.28E Hybrid	39.9	54.05%
HNT APTES	35.7	37.84%
HNT APTES/I.28E Hybrid	42.8	65.25%

$$Fracture_{force\_initiation}\ \%\ Diff =$$

$$\left(\frac{Fracture_{force\_initiation\_nano} - Fracture_{force\_initiation\_pristine}}{Fracture_{force\_initiation\_pristine}}\right) x100 \quad \text{.....4.8}$$

Where $Fracture_{force\_initiation\_nano}$ is the initiation crack force for the nanomodified GFRP, and $Fracture_{force\_initiation\_pristine}$ is the initiation crack force for the pristine GFRP.

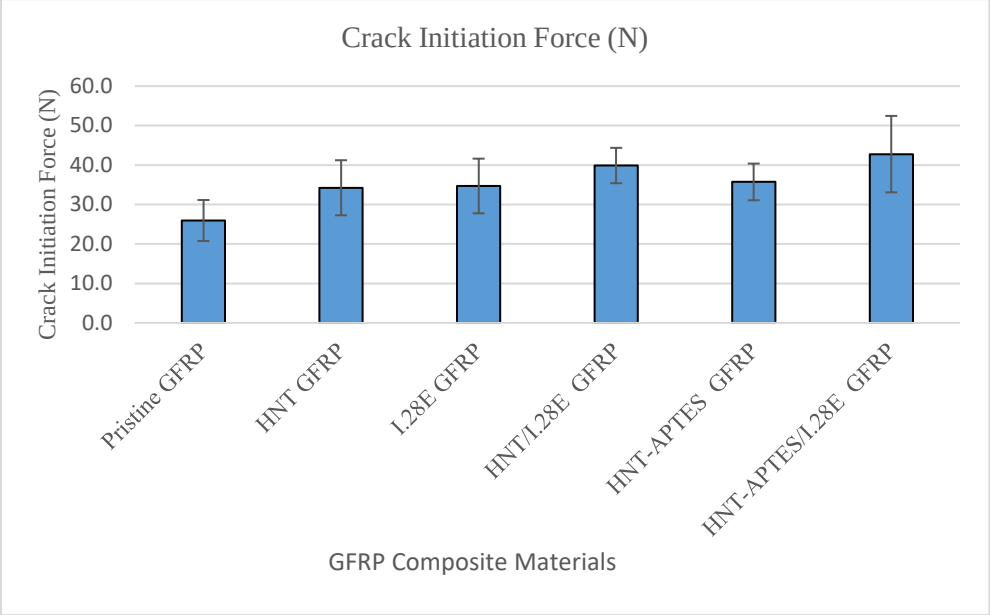

Figure 4.21: Crack Initiation Force Graphs

4.4.2 Interlaminar Fracture Toughness

Table 4.10 and the corresponding Figure 4.22 show the mode I interlaminar fracture toughness for pristine and nanomodified specimens. The morphological synergy for the hybrid nanofillers integrated with the glass fiber reinforcement and polymer matrix was shown. HNT APTES/I.28E hybrid showed improvement of fracture toughness of pristine GFRP by ≈ 3.51 times, whereas the hybrid with non-functionalized halloysite showed ≈ 2.16 times improvement to the neat GFRP. The individual nanomodified material configurations showed 60.53%, 63.16%, and 84.21% improvement in fracture toughness, i.e., for pure halloysite, nanomer I.28E, and functionalized halloysite, respectively, compared to the neat GFRP composite.

Tubular halloysite clay modification with APTES effectively achieved an excellent bonding between the epoxy and the clay. Thus the fracture toughness was significantly improved when incorporated with the surface-modified nanomer I.28E clay nanoplatelets in GFRP reinforcement configuration. The morphological synergy of the platelet nanomer I.28E clay combined with pure halloysite clay, epoxy matrix, and glass fiber reinforcement provided a higher crack propagation resistance and hence higher fracture toughness than the individual clay particles configurations.

Table 4.10: Interlaminar Fracture Toughness

Material	G_{IC} (N-mm/mm^2)	G_{IC} Strength_Nano	$Fracture_{toughness}$ % Diff
Pristine GFRP	0.76	-	-
Pure HNT	1.22	1.61	60.53%
Nanomer I.28E	1.24	1.63	63.16%
Pure HNT/I.28E Hybrid	1.64	2.16	115.79%
HNT APTES	1.40	1.84	84.21%
HNT APTES/I.28E Hybrid	2.67	3.51	251.32%

$$G_{IC}\ \text{Strength\_Nano} = \frac{Fracture_{toughness\_nano}}{Fracture_{toughness\_pristine}} \quad \text{.....4.9}$$

and

$$Fracture_{toughness}\ \%\ Diff = \left(\frac{Fracture_{toughness\_nano} - Fracture_{toughness\_pristine}}{Fracture_{toughness\_pristine}}\right) x100 \quad \text{.....4.10}$$

Where $Fracture_{toughness\_nano}$ is the interlaminar fracture toughness for the nanomodified GFRP, and $Fracture_{toughness\_pristine}$ is the interlaminar fracture toughness for the pristine GFRP.

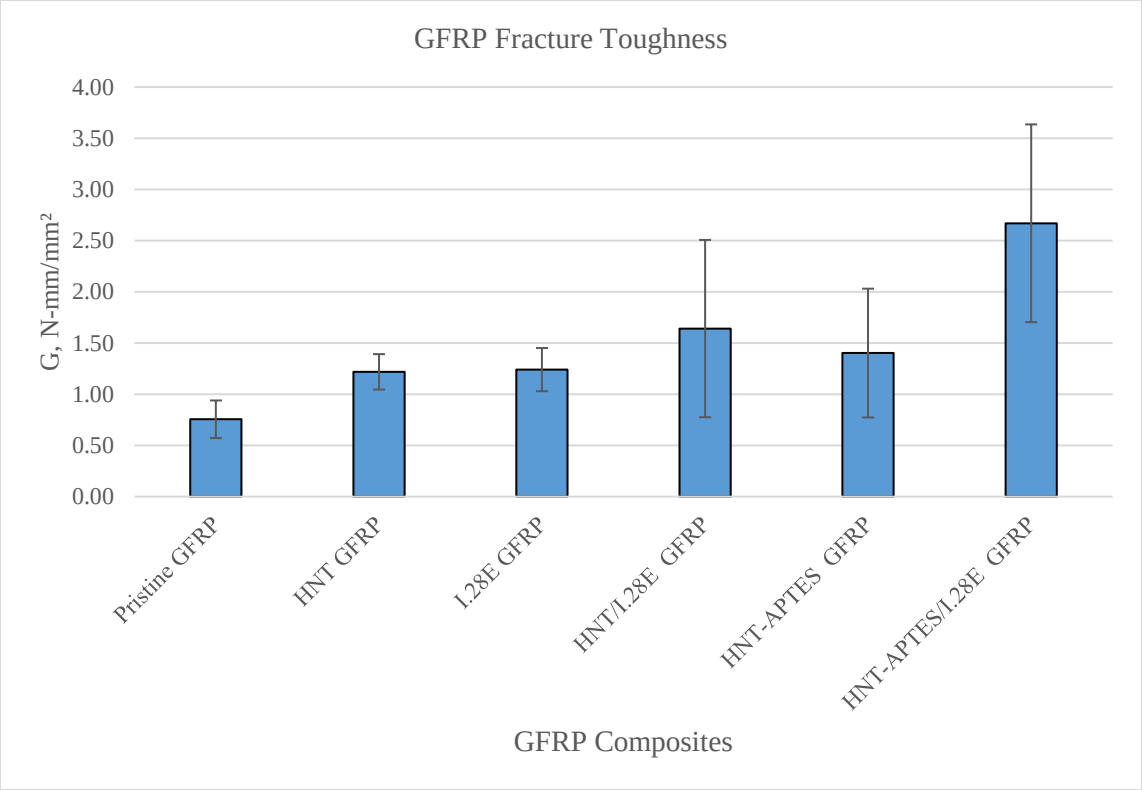

Figure 4.22: GFRP Fracture Toughness Graphs

4.5 Tensile Test

In this study, the tensile strength and modulus were analyzed. The results showed some improvement on the tensile properties of the GFRP composites, i.e., up to 12% and 7% for the tensile strength and modulus, respectively. (Vahedi and Pasbakhsh 2014) in their study on epoxy/HNT nanocomposites, they noted that no reasonable trend in the tensile strength and modulus was observed. In this study, some improvements have been noted in incorporating nano-modified HNT (HNT-APTES) epoxy resin into the GFRP reinforcement.

Figure 4.23 shows illustrative force versus displacement for randomly picked samples from each type of GFRP material. From the data results, average strength and modulus were determined accordingly.

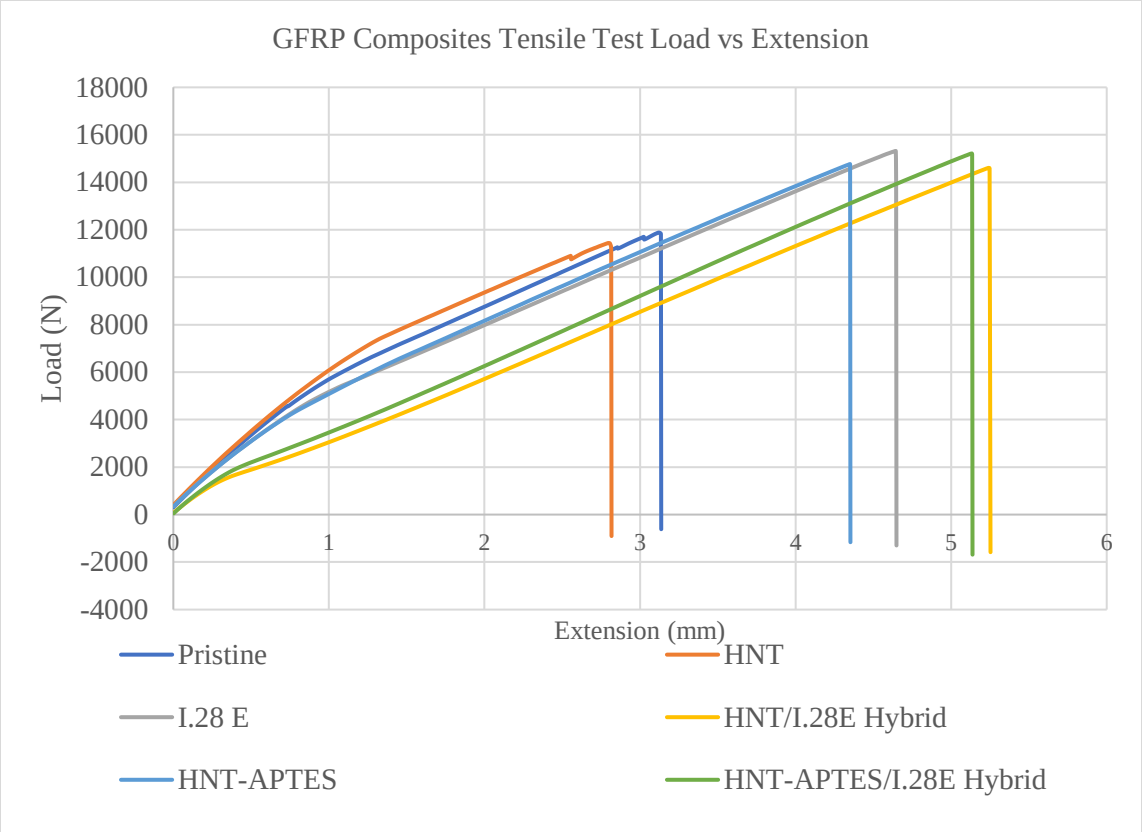

Figure 4.23: Illustrative Force versus Displacement Curves for the Tensile Test

4.5.1 Tensile Strength

Table 4.11 and the corresponding Figure 4.24 show the tensile strength properties of the composite materials. The tensile strength of pure GFRP was ≈ 170 MPa, while the nanomodified and hybrid enriched samples ranged from ≈ 180 MPa to ≈ 190 MPa. No significant change was noted when comparing the nanomodified and their hybrid GFRP nanocomposites configurations. Pure halloysite, nanomer I.28E, HNT/I.28E hybrid, HNT-APTES, and HNT-APTES/I.28E hybrid improved tensile strength by 7.63%, 11.54%, 9.17%, 11.05%, and 11.89%, respectively. In general, incorporating the nanofillers and the hybrid configurations to glass fiber-matrix showed improved tensile strength compared to the neat GFRP composite.

Table 4.11: Tensile Strength for the GFRP Composites

GFRP Material	Tensile Strength (MPA)	$Tensile_{strength}$ % Difference
Pristine GFRP	170.09	-
Pure Halloysite	183.07	7.63%
I.28E	189.71	11.54%
Halloysite_I.28E Hybrid	185.69	9.17%
Halloysite-APTES	188.88	11.05%
Halloysite-APTES_I.28E Hybrid	190.32	11.89%

$$Tensile_{strength}\,\%\,Difference = \left(\frac{Tensile_{stregth\_nano} - Tensile_{stregth\_pristine}}{Tensile_{stregth\_pristine}}\right) x100 \quad \text{.....4.11}$$

Where, $Tensile_{stregth\_nano}$ is the tensile strength for nano enriched sample, and $Tensile_{stregth\_pristine}$ is the tensile strength for pure epoxy resin obtained from the tensile test.

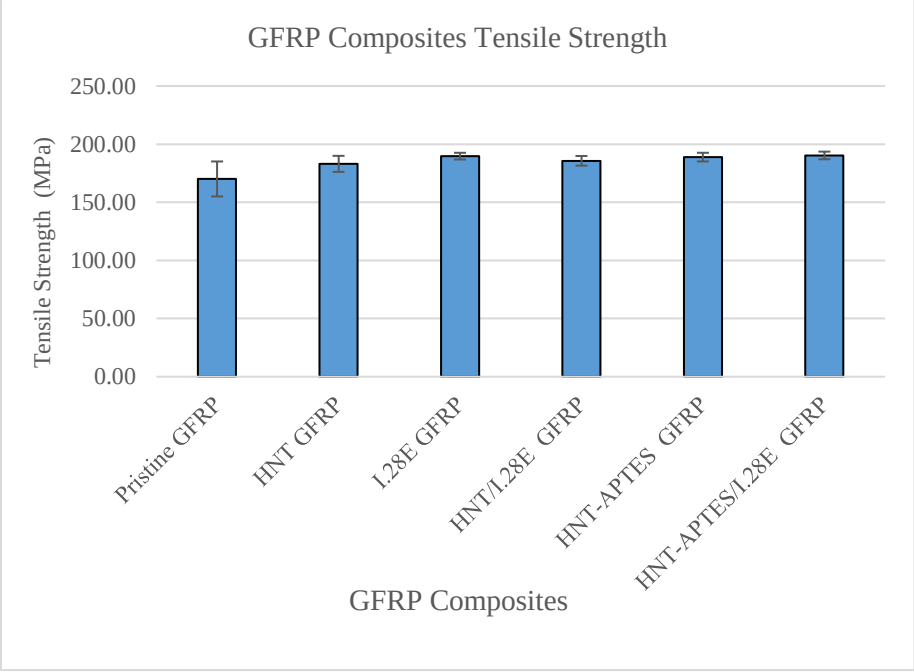

Figure 4.24: Tensile Strength Graphs for the GFRP Composites

4.5.2 Tensile Modulus

Table 4.12 and the corresponding Figure 4.25 show tensile modulus properties of the composite materials. Pure halloysite and as received surface-modified nanomer I.28E GFRP materials showed no significant change (0.49% and 0.78%, respectively) in the tensile modulus. Halloysite modified with APTES showed the highest improvement (≈ 6.81%), followed by HNT-APTES/I.28E hybrid (≈ 4.69%) and HNT/I.28E hybrid (≈ 3.68%). The existence of silane groups in the functionalized HNT provided good dispersive adhesion and substantial capacitance on the glass fiber reinforcement matrix providing stiffer properties that resisted elongation. This was extended when the material was incorporated in the HNT-APTES/I.28E hybrid GFRP composite. The synergy between the pure halloysite and the nanomer I.28E fillers on the GFRP composite hybrid did show better adhesion within the reinforcement matrix environment than would individual nanofillers exhibit. The better adhesion provided constraint on the puling/extending forces during the tensile test.

Table 4.12: Tensile Modulus for the GFRP Composites

GRFP Material	Tensile Modulus (MPa)	$Tensile_{modulus}$ % Difference
Pristine	3747.47	-
HNT	3765.91	0.49%
I.28E	3776.87	0.78%
HNT/I.28E Hybrid	3885.55	3.68%
HNT-APTES	4002.55	6.81%
HNT-APTES/I.28E Hybrid	3923.26	4.69%

$$Tensile_{modulus}\ \%\ Difference = \left(\frac{Tensile_{modulus\_nano} - Tensile_{modulus\_pristine}}{Tensile_{modulus\_pristine}}\right) x100 \text{…...……} 4.12$$

Where, $Tensile_{modulus\_nano}$ is the tensile modulus for nano enriched sample, and $Tensile_{modulus\_pristine}$ is the tensile modulus for pure epoxy resin obtained from the tensile test.

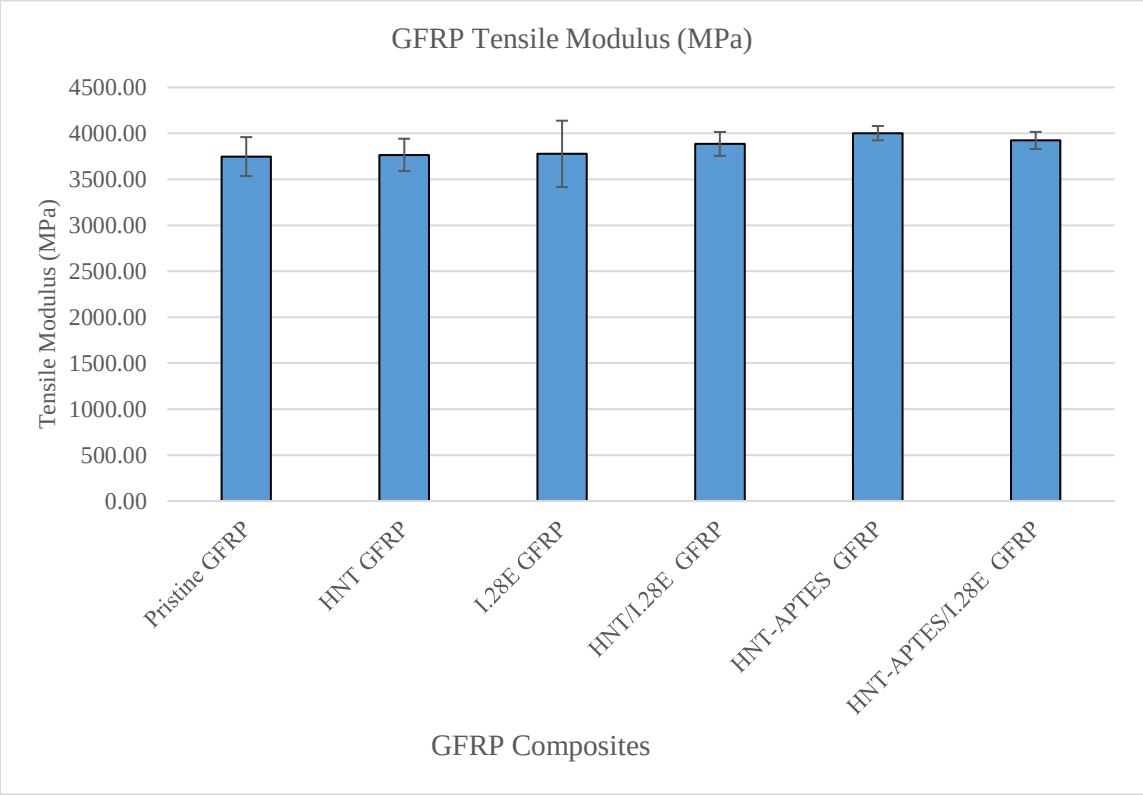

Figure 4.25: Tensile Modulus Graphs for the GFRP Composites

4.6 Vibration Analysis

Obtained Fast Fourier transform (FFT) response of different samples showed consistency in vibration properties of the manufactured GFRPs as shown in Figure 4.26. Vibration analysis done on several repetitive tests at different times showed that the nanomodified composites have better damping properties than the neat GFRP.

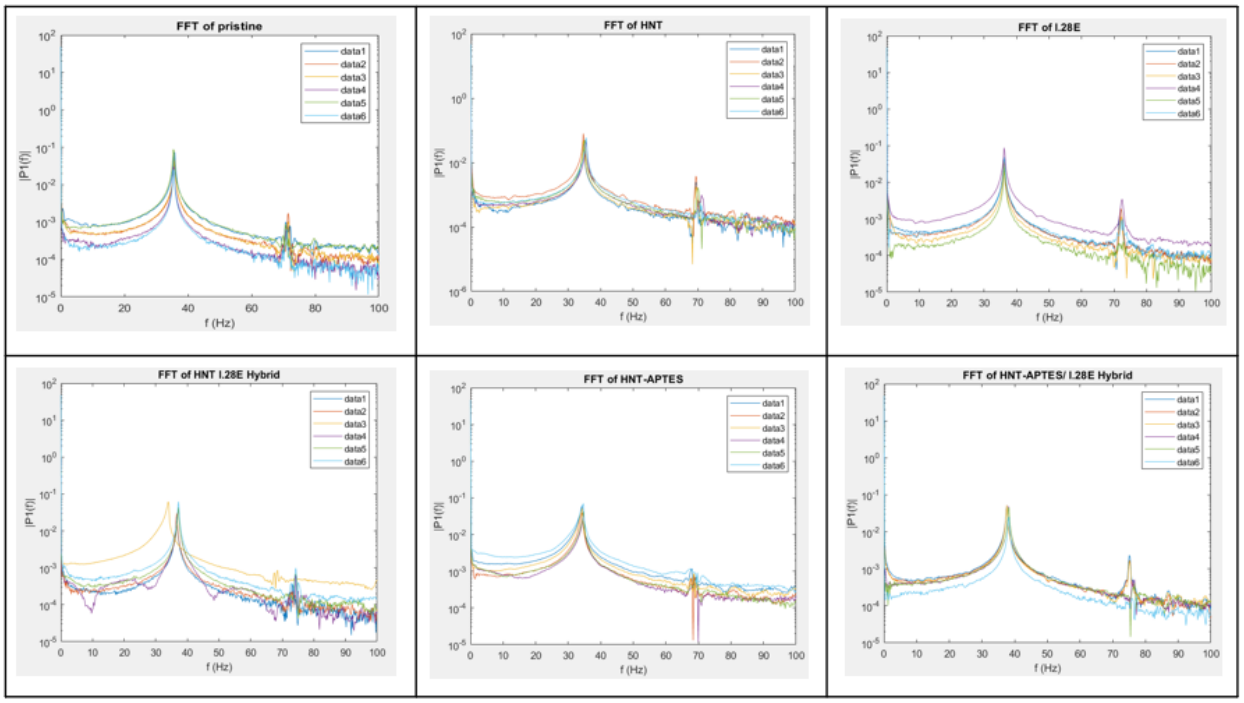

Figure 4.26: FFT Responses for the GFRP Composite Materials

4.7 Scanning Electron Microscope (SEM) Morphology

4.7.1 Clay Samples Sem

Scanned powder samples at X30,000 confirmed that the shape for pure halloysite is tubular and nanomer I.28E plate-like structure. Halloysite-APTES shape was also tubular, confirming that the functionalization did not alter the shape of the successfully functionalized clay, as shown in Figure 4.27. The tubular halloysite has a length ranging from 1-3 microns with a diameter of 30-70 nanometers. In contrast, the average particle size for the plate-like nanomer I.28E is approximately 20 microns.

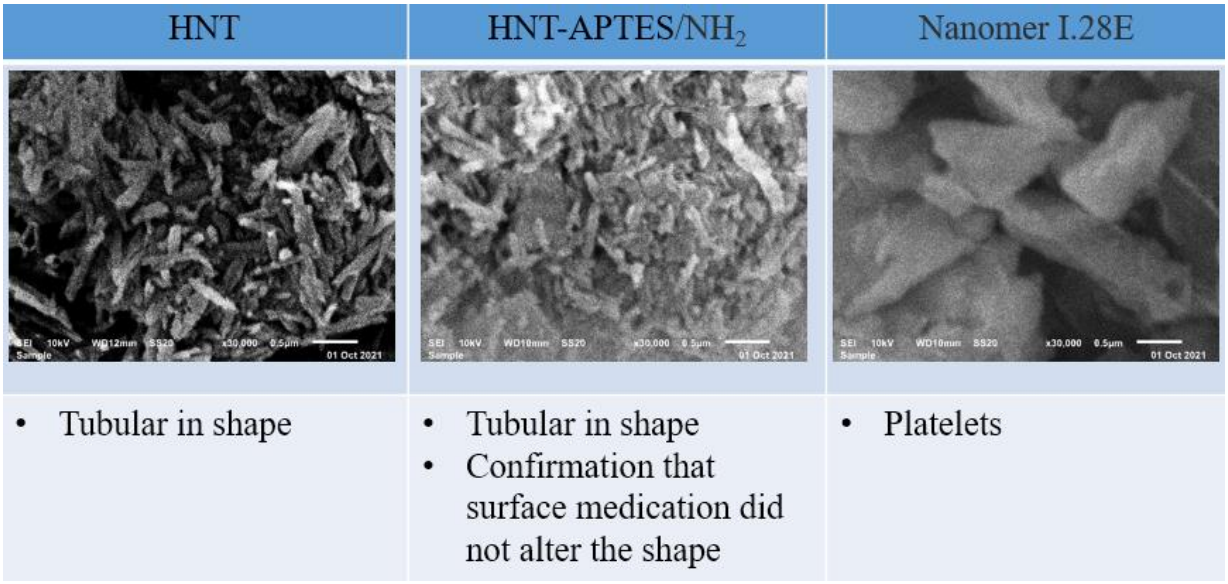

Figure 4.27: SEM Images for the Clay Samples

4.7.2 Mode I And Tensile Fractured Surfaces SEM

SEM was carried out to evaluate the state of dispersion and adhesion of the different clay configurations and the glass fiber epoxy resin matrix. Mode I fractured surfaces were scanned at X1000, X500, and X100 magnifications, whereases tensile fractured surfaces were taken at X1500, X1000, and X500 magnifications.

In general, the Mode I delaminated surfaces of the GFRPs observed showed the failure mechanism for all specimens consisting of matrix crazing, cracking, fiber-matrix debonding, and fiber pullout. Interfacial interaction between the nanomodified hybrid fillers and the resin enabled the GFRP to be more resilient to breakage, evident from the SEM results as shown in Figures 4.28, 4.29, and 4.30.

Micrographs of the fractured surfaces of the tensile specimens are shown in Figures 4.31, 4.32, and 4.33. Images of tensile fractured surfaces showed uncoated fibers in the absence of filler materials. In addition, many cavities surrounded the fiber and detached fibers from fiber withdrawal. However , there were few detached fibers with the filler materials and evidence of the nanomodified epoxy polymer on the GFRP surfaces supporting the tensile test results.

4.7.2.1 Mode Fractured Surfaces SEM

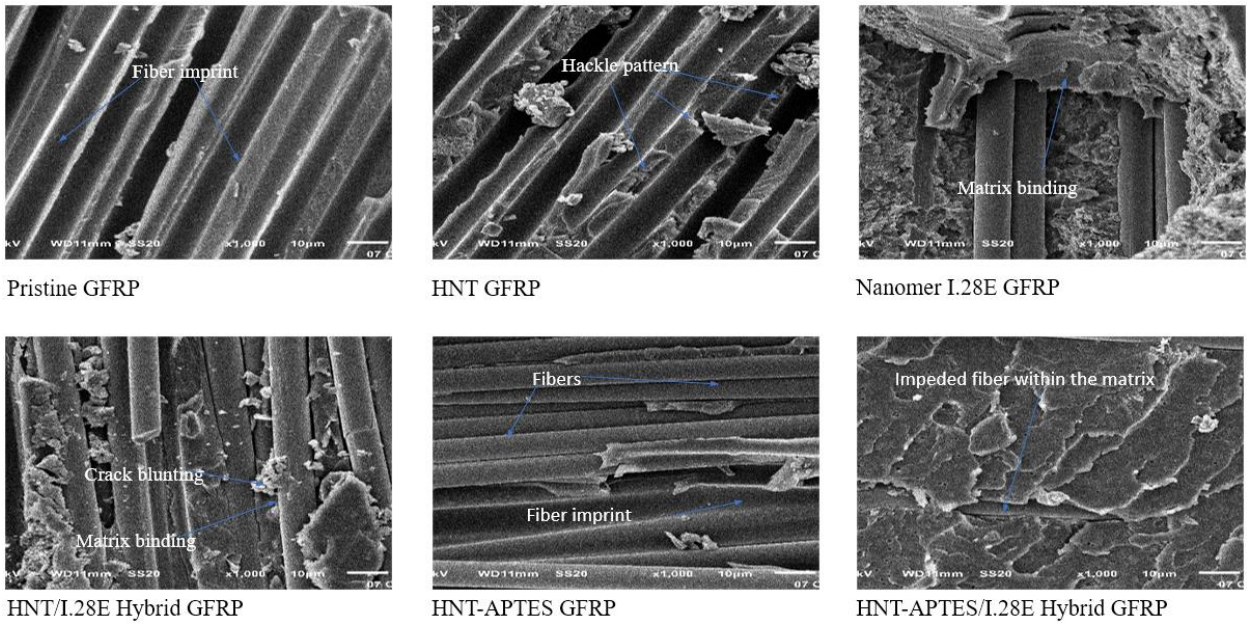

Figure 4.28: SEM for the Mode I Fractured Surfaces X1000

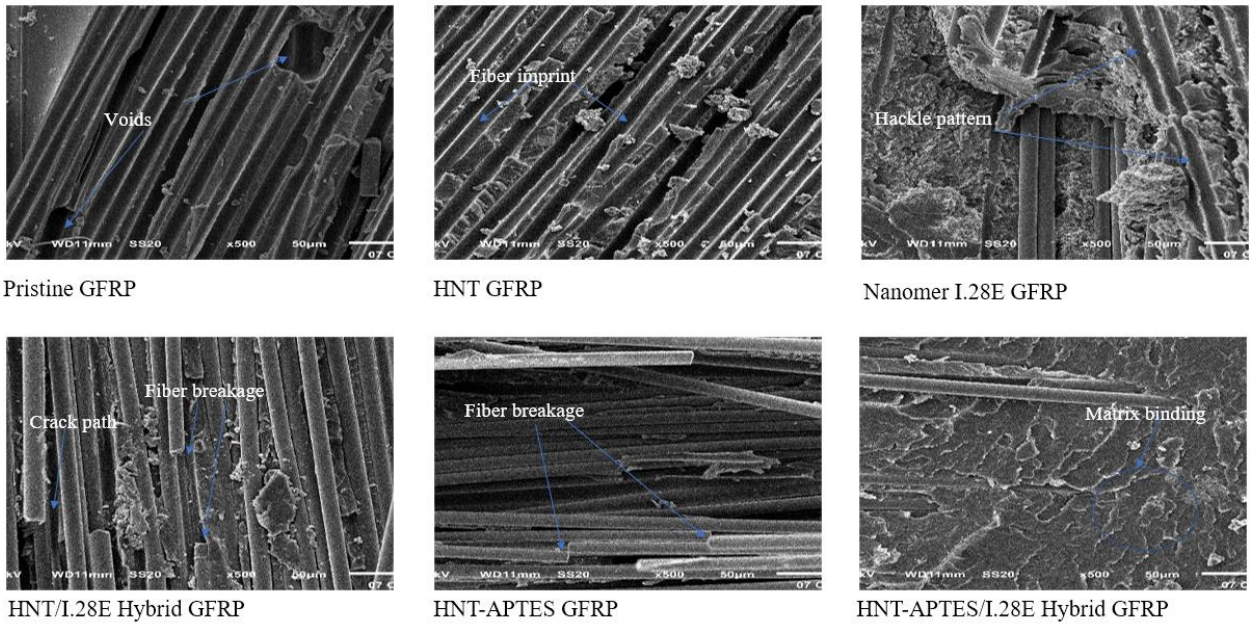

Figure 4.29: SEM for the Mode I Fractured Surfaces X500

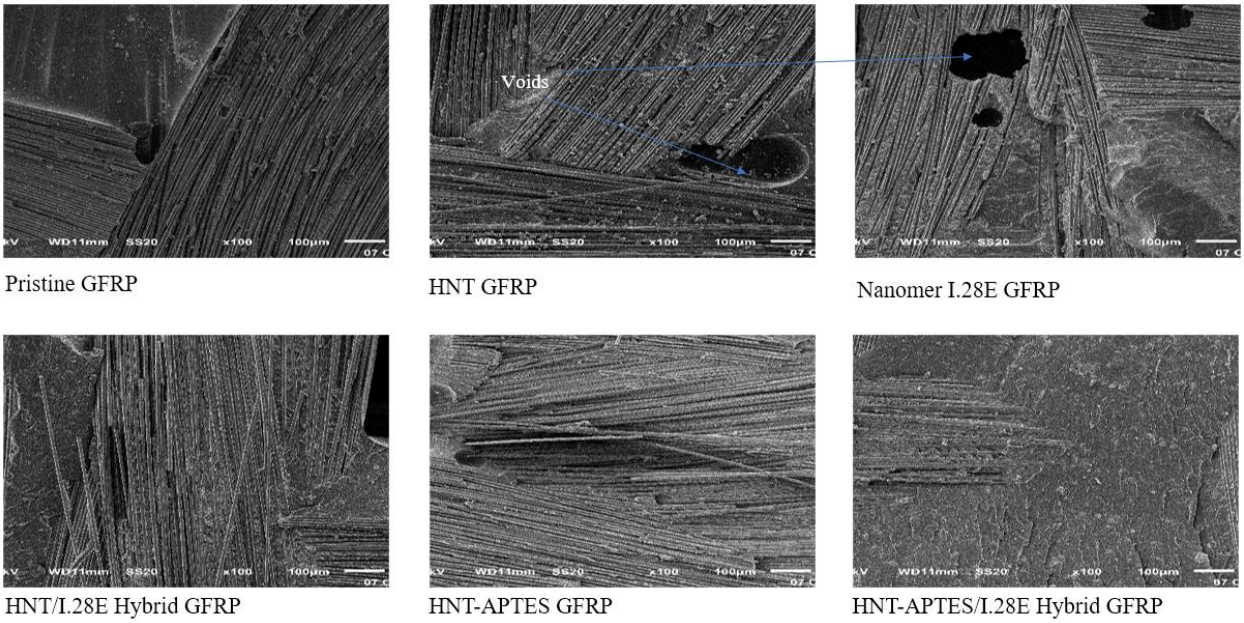

Figure 4.30: SEM for the Mode I Fractured Surfaces X100

4.7.2.2 Tensile Fractured Surfaces SEM

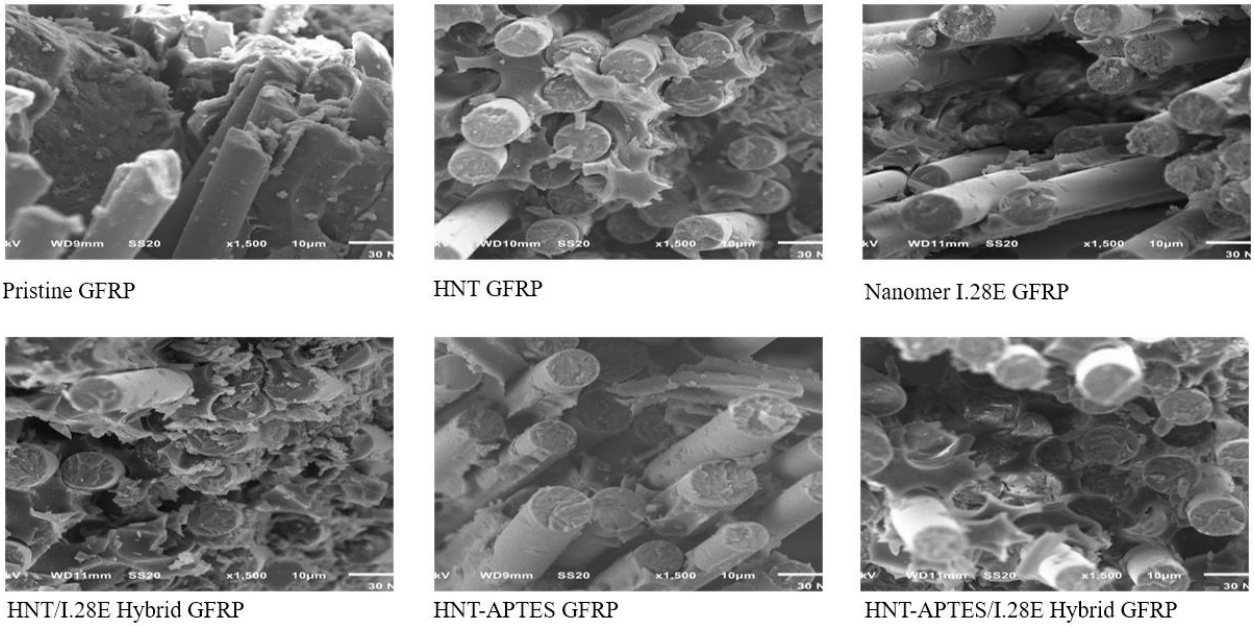

Figure 4.31: SEM for the Tensile Fractured Surfaces X1500

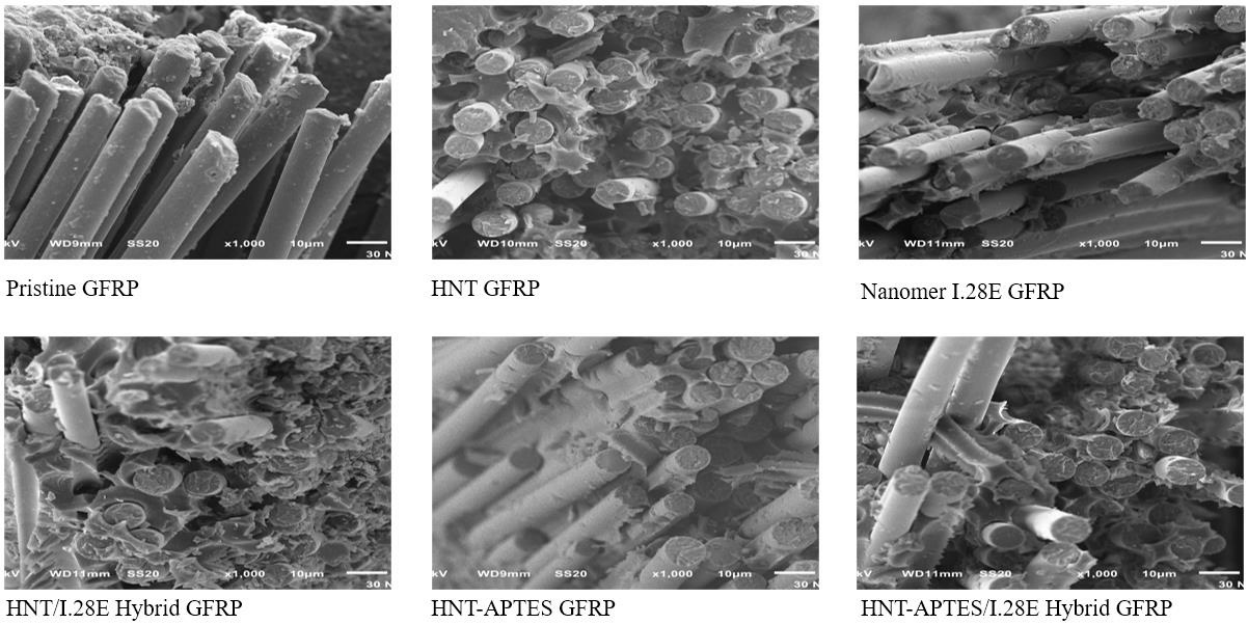

Figure 4.32: SEM for the Tensile Fractured Surfaces X1000

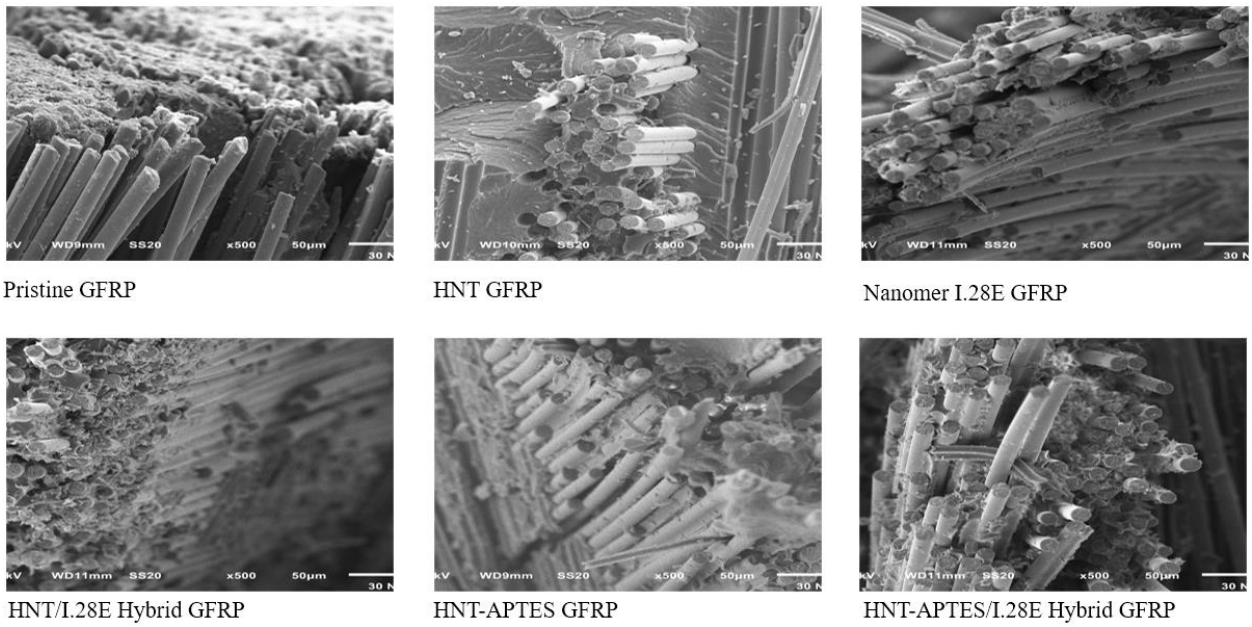

Figure 4.33: SEM for the Tensile Fractured Surfaces X500

CHAPTER 5

5. CONCLUSION

5.1 Summary

This work presents an ongoing investigation of the effect of nano-modified hybrid fillers on the properties of GFRP composites. Application of GFRP composites in aerospace, civil, automotive, and military are continually subjected to stresses in different directions. Hence, studying the materials' thermal stability, storage modulus, fracture toughness, tensile properties, and vibration properties was important.

In this study, GFRP composites nanomodified with as received tubular halloysite and platelet nanomer I.28E clays, HNT modified with APTES, and the hybrid combination of the two HNTs with the nanomer were successfully fabricated and their properties investigated. The existence of silane groups on HNT-APTES were investigated using TGA, and the clay shapes were confirmed with SEM. The shape of the HNT-APTES was not changed during the surface modification, i.e., the tubular of the as-received halloysite was maintained.

To evaluate the effects and morphological characteristics of the hybrid fillers on the epoxy resin matrix, TGA, DSC, and DMA were analyzed. Thermal stability analyzed using TGA showed good interaction between the fillers and the matrix. DSC results proved the purity of clay samples. DSC analysis of the pure and nano-enriched epoxy resin samples showed interfacial interaction of the configurations. The enthalpies of the epoxy resin showed improvement of 41.58%, 60.93%, and 30.49% for pure HNT, HNT-APTES, and HNT-APTES/I.28E hybrid resins, respectively, in comparison to pure epoxy resin.

The average DMA and DSC T_g values ranged from 95 °C to 110 °C and 85 °C to 100 °C, respectively. The nanomodified resin samples T_g % difference (compared to pure/unfilled epoxy resin) for both the DMA and DSC analysis were less than 10%; the nanocomposites are considered within the range of service life of composite materials. DMA tan δ results for HNT-APTES, HNT-APTES/I.28E hybrid, and pure SC-15 were 0.9293, 0.8028, and 0.7987, respectively. The functionalized halloysite epoxy resin did show the highest tan δ value compared to the other filler materials. More chain segments moved uniformly

at that temperature within the matrix, increasing the internal friction, i.e., the loss modulus. The analyzed storage modulus at 60 °C and 70 °C showed functionalized halloysite having the highest storage modulus, followed by pure resin epoxy and the third HNT-APTES/I.28E hybrid epoxy resin. Incorporation of HNT-APTES to the epoxy resin led to improved storage modulus by 18-22%. Nanomer I.28E significantly reduced the storage modulus of the epoxy polymer by 42-44%, whereas pure halloysite by 23-25%. The hybrid nanocomposites showed decreased storage modulus by 29-30% and 11-14%, i.e., HNT/I.28E and HNT-APTES/I.28E, respectively.

The DMA results did prove that the larger particles nanomer I.28E tend to form agglomerates, and as well the longer chains were sliding to each other and the incorporated filler. The surface modification of the halloysite provided proper dispersion in the matrix. This was evident in the HNT-APTES/I.28E hybrid, whereby storage modulus was reduced by a small degree compared to the HNT, I.28E, and HNT/I.28E epoxy resin samples. In general, in combination with other analytical techniques, DMA results can provide helpful information about the filler-matrix interaction and filler-filler interaction within the polymer. Hence the interfacial interactions and thermal stability of nanocomposites are essential in determining the useful service life of the material.

Delamination is one of the major phenomena that leads to composite laminate failure. It continually grows internally, hence the need to be mitigated to increase the materials service life. Mode-I fracture toughness test, showed that the crack initiation for each material configuration was observed at different load levels, i.e., 25.9N, 34.3N, 34.7N, 39.9N, 35.7N, and 42.8N for the pristine, HNT, nanomer I.28E, HNT/I.28E hybrid, HNT-APTES, and HNT-APTES/I.28E hybrid respectively. The hybrid nanocomposite composites showed the most significant improvement compared to neat GFRP in the force needed to initiate the crack, i.e., 54.05% and 65.25% for pure HNT/I.28E and HNT-APTES/I.28E hybrids, respectively. The required force for crack propagation was considerably increased in nanomodified hybrid to even higher than those of crack initiation force, which is essential to maintain the structural integrity of the GFRP even after crack initiation.

HNT APTES/I.28E hybrid showed improvement of fracture toughness of pristine GFRP by ≈ 3.51 times, whereas the hybrid with non-functionalized halloysite showed ≈ 2.16 times improvement to the neat GFRP. The individual nanofiller material configurations showed 60.53%, 63.16%, and 84.21% improvement in fracture toughness, i.e., pure halloysite, nanomer I.28E, and functionalized halloysite, respectively. The morphological synergy of the larger platelet size of the nanomer I.28E clay incorporated with the halloysite clays, glass fiber, and epoxy matrix provided a higher crack propagation resistance and hence higher fracture toughness than the individual clay particles. Though the failure mechanism for all specimens consists of matrix crazing, cracking, fiber-matrix debonding, and fiber pullout, SEM did show well dispersed and proper matrix binding for the hybrid nanocomposites.

Incorporating the nanofillers and the hybrid configurations to glass fiber-matrix improved tensile strength compared to the neat GFRP composite. Pure halloysite, nanomer I.28E, HNT/I.28E hybrid, HNT-APTES, and HNT-APTES/I.28E hybrid improved tensile strength by 7.63%, 11.54%, 9.17%, 11.05%, and 11.89%, respectively. Pure halloysite and as received surface-modified nanomer I.28E GFRP materials showed no significant change (i.e., 0.49% and 0.78%, respectively) in the tensile modulus. Halloysite modified with APTES showed the highest improvement (≈ 6.81%), followed by HNT-APTES/I.28E hybrid (≈ 4.69%) and HNT/I.28E hybrid (≈ 3.68%). The existence of silane groups in the functionalized HNT provided good dispersive adhesion and substantial capacitance on the glass fiber reinforcement matrix, hence the stiffer properties resisting elongation, which was extended when the material was incorporated in the HNT-APTES/I.28E hybrid GFRP composite.

Vibration analysis done on several repetitive tests at different times showed that the nanomodified composites have better damping properties than the neat GFRP. Through vibration analysis, a high damping ratio of nano enriched composites configurations will respond quickly to unwanted disturbances compared to neat GFRP material with a lower damping ratio.

The data suggest that toughening epoxy with nanomodified filler is instrumental to various applications by improving and maintaining the overall integrity of structures, such as in the automotive and aerospace industry. Nano enriched GFRP with HNT-APTES and I.28E hybrid showed the highest overall integrity. Electron microscopy testing techniques were used to support the results and conclusions.

5.2 Future Works

Composite materials play a significant role in the current and future vehicle, aerospace, and military components. The present work demonstrated the possibility of introducing hybrid surface-modified filler materials that can significantly improve GFRP composite materials' properties. Proper selection of the hybrid filler materials is critical in optimizing the matrix properties. Depending on the selected filler materials, the correct content of each filler material to be incorporated in the hybrid configuration is vital in determining the final GFRP composite materials' properties. Effective dispersion and proper interfacial relationships played an important role in demonstrating how nanocomposites are affected when selecting the hybrid configuration. In that regard, a cap for optimized hybrid nanocomposites in terms of the mechanical properties of glass fiber reinforcement and all aspects of the materials' properties, such as the improved storage modulus, glass transition temperatures, thermal stability, etc., needs to be addressed.

REFERENCES

Bashir, Muhammad Ahsan. 2021. “Use of Dynamic Mechanical Analysis (DMA) for Characterizing Interfacial Interactions in Filled Polymers.” *Solids* 2 (1). MDPI AG: 108–20. doi:10.3390/solids2010006.

Battistella, M., M. Cascione, B. Fiedler, M. H.G. Wichmann, M. Quaresimin, and K. Schulte. 2008. “Fracture Behaviour of Fumed Silica/Epoxy Nanocomposites.” *Composites Part A: Applied Science and Manufacturing* 39 (12). Elsevier Ltd: 1851–58. doi:10.1016/j.compositesa.2008.09.010.

Bazli, Milad, Hamed Ashrafi, Armin Jafari, Xiao Ling Zhao, Hamed Gholipour, and Asghar Vatani Oskouei. 2019. “Effect of Thickness and Reinforcement Configuration on Flexural and Impact Behaviour of GFRP Laminates after Exposure to Elevated Temperatures.” *Composites Part B: Engineering* 157 (August 2018): 76–99. doi:10.1016/j.compositesb.2018.08.054.

Bazli, Milad, Hamed Ashrafi, Armin Jafari, Xiao Ling Zhao, R. K. Singh Raman, and Yu Bai. 2019. “Effect of Fibers Configuration and Thickness on Tensile Behavior of GFRP Laminates Exposed to Harsh Environment.” *Polymers* 11 (9): 1–23. doi:10.3390/polym11091401.

Behera, Rohit Pratyush, Prashant Rawat, K. K. Singh, Sung Kyu Ha, Anand Gaurav, and Santosh K. Tiwari. 2019. “Fracture Analysis and Mechanical Properties of Three Phased Glass/Epoxy Laminates Reinforced with Multiwalled Carbon Nanotubes.” *Journal of Science: Advanced Materials and Devices* 4 (2). Elsevier Ltd: 299–309. doi:10.1016/j.jsamd.2019.03.003.

Behera, Rohit Pratyush, Prashant Rawat, and Kalyan Kumar Singh. 2018. “Tensile Behavior of Three Phased Glass/Epoxy Laminate Embedded with MWCNTs: An Experimental Approach.” *Materials Today: Proceedings* 5 (2). Elsevier Ltd: 8176–83. doi:10.1016/j.matpr.2017.11.506.

Bindu, P., and Sabu Thomas. 2013. “Viscoelastic Behavior and Reinforcement Mechanism in Rubber Nanocomposites in the Vicinity of Spherical Nanoparticles.” *Journal of Physical Chemistry B* 117 (41): 12632–48. doi:10.1021/jp4039489.

Binu, P.P., K.E. George, and M.N. Vinodkumar. 2016. “Effect of Nanoclay, Cloisite15A on the

Mechanical Properties and Thermal Behavior of Glass Fiber Reinforced Polyester." *Procedia Technology* 25 (Raerest). The Author(s): 846–53. doi:10.1016/j.protcy.2016.08.191.

Bourchak, Mostefa, Abdullah Algarni, Adnan Khan, and Usama Khashaba. 2018. "Effect of SWCNTs and Graphene on the Fatigue Behavior of Antisymmetric GFRP Laminate." *Composites Science and Technology* 167 (July). Elsevier: 164–73. doi:10.1016/j.compscitech.2018.07.047.

Chavhan, Ganesh R., and Lalit N. Wankhade. 2020. "Improvement of the Mechanical Properties of Hybrid Composites Prepared by Fibers, Fiber-Metals, and Nano-Filler Particles-A Review." *Materials Today: Proceedings* 27. Elsevier Ltd.: 72–82. doi:10.1016/j.matpr.2019.08.240.

Chawla, K., S. Ray-Chaudhuri, and R. Kitey. 2019. "Interlaminar Fracture Toughness of Short Fibre Reinforced GFRP Laminates." *Procedia Structural Integrity* 14 (2018). Elsevier B.V.: 571–76. doi:10.1016/j.prostr.2019.05.070.

Chen, Zixuan, Tao Tianyu Yu, Yun Hae Kim, Zetian Yang, Yan Li, and Tao Tianyu Yu. 2021. "Different-Structured Nanoclays Incorporated Composites: Computational and Experimental Analysis on Mechanical Properties." *Composites Science and Technology* 203 (August 2020). Elsevier Ltd: 108612. doi:10.1016/j.compscitech.2020.108612.

Daitx, Tales S., Larissa N. Carli, Janaina S. Crespo, and Raquel S. Mauler. 2015. "Effects of the Organic Modification of Different Clay Minerals and Their Application in Biodegradable Polymer Nanocomposites of PHBV." *Applied Clay Science* 115. Elsevier B.V.: 157–64. doi:10.1016/j.clay.2015.07.038.

Das, Subhankar, Sudipta Halder, Nazrul Islam Khan, Bappi Paul, and M. S. Goyat. 2020. "Assessing Damage Mitigation by Silanized Milled Graphite Nanoparticles in Hybrid GFRP Laminated Composites." *Composites Part A: Applied Science and Manufacturing* 132 (December 2019). Elsevier: 105784. doi:10.1016/j.compositesa.2020.105784.

Davis, J.R. 2004. "Introduction to Tensile Testing." *Tensile Testing*, 1–13.

Domun, Nadiim, Cihan Kaboglu, Keith R. Paton, John P. Dear, Jun Liu, Bamber R.K. Blackman, Gholamhossein Liaghat, and Homayoun Hadavinia. 2019. "Ballistic Impact Behaviour of Glass

Fibre Reinforced Polymer Composite with 1D/2D Nanomodified Epoxy Matrices." *Composites Part B: Engineering* 167 (February). Elsevier: 497–506. doi:10.1016/j.compositesb.2019.03.024.

Enamul Hossain, M. 2011. "The Current and Future Trends of Composite Materials: An Experimental Study." *Journal of Composite Materials* 45 (20): 2133–44. doi:10.1177/0021998311401066.

Eslami, Shiva, Fathollah Taheri-Behrooz, and Farid Taheri. 2012. "Effects of Aging Temperature on Moisture Absorption of Perforated GFRP." *Advances in Materials Science and Engineering* 2012. doi:10.1155/2012/303014.

Fereidoon, Abdolhossein, Farzaneh Memarian, and Zahra Ehsani. 2013. "Effect of CNT on the Delamination Resistance of Composites." *Fullerenes Nanotubes and Carbon Nanostructures* 21 (8): 712–24. doi:10.1080/1536383X.2012.654541.

Fleischer, Jürgen, Roberto Teti, Gisela Lanza, Paul Mativenga, Hans Christian Möhring, and Alessandra Caggiano. 2018. "Composite Materials Parts Manufacturing." *CIRP Annals* 67 (2). CIRP: 603–26. doi:10.1016/j.cirp.2018.05.005.

Gaaz, Tayser Sumer, Abu Bakar Sulong, Abdul Amir H. Kadhum, Ahmed A. Al-Amiery, Mohamed H. Nassir, and Ahed Hameed Jaaz. 2017. "The Impact of Halloysite on the Thermo-Mechanical Properties of Polymer Composites." *Molecules* 22 (5): 13–15. doi:10.3390/molecules22050838.

Garcia, Cristobal, Jodi Wilson, Irina Trendafilova, and Liu Yang. 2017. "Vibratory Behaviour of Glass Fibre Reinforced Polymer (GFRP) Interleaved with Nylon Nanofibers." *Composite Structures* 176. Elsevier Ltd: 923–32. doi:10.1016/j.compstruct.2017.06.018.

Gaurav, Anand, and K. K. Singh. 2019. "Effect of Pristine MWCNTs on the Fatigue Life of GFRP Laminates-an Experimental and Statistical Evaluation." *Composites Part B: Engineering* 172 (May). Elsevier Ltd: 83–96. doi:10.1016/j.compositesb.2019.05.069.

Guru Mahesh, G., and K. Jayakrishna. 2019. "Evaluation of Mechanical Properties of Nano Filled Glass Fiber Reinforced Composites." *Materials Today: Proceedings* 22. Elsevier Ltd.: 3305–11. doi:10.1016/j.matpr.2020.03.293.

Hassan, Mohamadou Al, Zhicheng Wang, Wen bin Liu, Jun Wang, Yuan Zhigang, Muhammad Khan,

Mohsen M.M. Ali, Rejep Geldiyev, Mahamady Diaby, and Mehdi Derradji. 2021. “Thermal Stability and Gamma Ray Shielding Properties of Tungsten Borides/Epoxy Micro-Composites.” *Radiation Physics and Chemistry* 189 (May). Elsevier Ltd: 109769. doi:10.1016/j.radphyschem.2021.109769.

Jafari, Armin, Milad Bazli, Hamed Ashrafi, Asghar Vatani Oskouei, Samira Azhari, Xiao Ling Zhao, and Hamed Gholipour. 2019. “Effect of Fibers Configuration and Thickness on Tensile Behavior of GFRP Laminates Subjected to Elevated Temperatures.” *Construction and Building Materials* 202. Elsevier Ltd: 189–207. doi:10.1016/j.conbuildmat.2019.01.003.

Jagadish Chandra Bose, K., A. Thiagarajan, D. NagaVenkatesh, and K. Velmurugan. 2019. “Effects of ZnO Nano Reinforcements in the Polymer Matrix on the GFRP Composites Fabricated through VARTM.” *Materials Today: Proceedings* 19. Elsevier Ltd.: 721–25. doi:10.1016/j.matpr.2019.08.081.

Kara, Memduh, Muhammed Kırıcı, Ahmet Caner Tatar, and Ahmet Avcı. 2018. “Impact Behavior of Carbon Fiber/Epoxy Composite Tubes Reinforced with Multi-Walled Carbon Nanotubes at Cryogenic Environment.” *Composites Part B: Engineering* 145 (January): 145–54. doi:10.1016/j.compositesb.2018.03.027.

Kim, Yun Hae, Soo Jeong Park, Jin Woo Lee, and Kyung Man Moon. 2015. “A Study on the Effect of Halloysite Nanoparticle Addition on the Strength of Glass Fiber Reinforced Plastic.” *Modern Physics Letters B* 29 (6–7): 1–5. doi:10.1142/S0217984915400035.

Koricho, Ermias G., Anton Khomenko, Mahmoodul Haq, Lawrence T. Drzal, Giovanni Belingardi, and Brunetto Martorana. 2015. “Effect of Hybrid (Micro- and Nano-) Fillers on Impact Response of GFRP Composite.” *Composite Structures* 134 (December). Elsevier Ltd: 789–98. doi:10.1016/j.compstruct.2015.08.106.

Kosmann, N, J M Karsten, M Schuett, K Schulte, and B Fiedler. 2015. “Composites : Part B Determining the Effect of Voids in GFRP on the Damage Behaviour under Compression Loading Using Acoustic Emission.” *Composites Part B* 70. Elsevier Ltd: 184–88. doi:10.1016/j.compositesb.2014.11.010.

Kostagiannakopoulou, C., T. H. Loutas, G. Sotiriadis, A. Markou, and V. Kostopoulos. 2015. “On the Interlaminar Fracture Toughness of Carbon Fiber Composites Enhanced with Graphene Nano-Species.” *Composites Science and Technology* 118. Elsevier Ltd: 217–25. doi:10.1016/j.compscitech.2015.08.017.

Kostagiannakopoulou, C., X. Tsilimigkra, G. Sotiriadis, and V. Kostopoulos. 2017. “Synergy Effect of Carbon Nano-Fillers on the Fracture Toughness of Structural Composites.” *Composites Part B: Engineering* 129. Elsevier Ltd: 18–25. doi:10.1016/j.compositesb.2017.07.012.

Krishnaiah, Prakash, Sivakumar Manickam, Chantara Thevy Ratnam, M. S. Raghu, L. Parashuram, S. Prasanna Kumar, and Byong Hun Jeon. 2021. “Mechanical, Thermal and Dynamic-Mechanical Studies of Functionalized Halloysite Nanotubes Reinforced Polypropylene Composites.” *Polymers and Polymer Composites* 29 (8): 1212–21. doi:10.1177/0967391120965115.

Kumar, Sandeep, Brian G. Falzon, Jeffery Kun, Emma Wilson, Georg Graninger, and Stephen C. Hawkins. 2020. “High Performance Multiscale Glass Fibre Epoxy Composites Integrated with Cellulose Nanocrystals for Advanced Structural Applications.” *Composites Part A: Applied Science and Manufacturing* 131 (July 2019). doi:10.1016/j.compositesa.2020.105801.

Leong, Y. W., M. B. Abu Bakar, Z. A.Mohd Ishak, A. Ariffin, and B. Pukanszky. 2004. “Comparison of the Mechanical Properties and Interfacial Interactions between Talc, Kaolin, and Calcium Carbonate Filled Polypropylene Composites.” *Journal of Applied Polymer Science* 91 (5): 3315–26. doi:10.1002/app.13542.

Maharana, Sunil Manohar, Mihir Kumar Pandit, and Arun Kumar Pradhan. 2021. “Influence of Fumed Silica Nanofiller and Stacking Sequence on Interlaminar Fracture Behaviour of Bidirectional Jute-Kevlar Hybrid Nanocomposite.” *Polymer Testing* 93 (October 2020). Elsevier Ltd: 106898. doi:10.1016/j.polymertesting.2020.106898.

Mahato, Kishore Kumar, Krishna Dutta, and Bankim Chandra Ray. 2019. “Assessment of Mechanical, Thermal and Morphological Behavior of Nano-Al 2 O 3 Embedded Glass Fiber/Epoxy Composites at in-Situ Elevated Temperatures.” *Composites Part B: Engineering* 166 (February). Elsevier: 688–

700. doi:10.1016/j.compositesb.2019.03.009.

Mahato, Kishore Kumar, Dinesh Kumar Rathore, Krishna Dutta, Rajesh Kumar Prusty, and Bankim Chandra Ray. 2020. “Effect of Severely Thermal Shocked Nano-Al2O3 Filled Glass Fiber Reinforced Polymeric Composites: An Assessment on Tensile, Thermal and Morphological Behaviour.” *Materials Today: Proceedings* 33. Elsevier Ltd.: 5521–25. doi:10.1016/j.matpr.2020.03.334.

Marichelvam, M.K. 2020. “Investigation on Mechanical Properties of Automobile Strut Made by GFRP Composites.” *Materials Today: Proceedings*, no. xxxx. Elsevier Ltd. doi:10.1016/j.matpr.2020.06.026.

McAninch, Ian M., Giuseppe R. Palmese, Joseph L. Lenhart, and John J. La Scala. 2015. “DMA Testing of Epoxy Resins: The Importance of Dimensions.” *Polymer Engineering and Science* 55 (12). John Wiley and Sons Inc.: 2761–74. doi:10.1002/pen.24167.

Mia, Xiaoqian, Liuyue Zhonga, Fang Wei, Liang Zeng, Junheng Zhang, Daohong Zhang, and Tiwen Xu. 2019. “Fabrication of Halloysite Nanotubes/Reduced Graphene Oxide Hybrids for Epoxy Composites with Improved Thermal and Mechanical Properties.” *Polymer Testing* 76 (April). Elsevier: 473–80. doi:10.1016/j.polymertesting.2019.04.007.

Mishra, B. P., D. Mishra, P. Panda, and A. Maharana. 2020. “An Experimental Investigation of the Effects of Reinforcement of Graphene Fillers on Mechanical Properties of Bi-Directional Glass/Epoxy Composite.” *Materials Today: Proceedings* 33. Elsevier Ltd.: 5429–41. doi:10.1016/j.matpr.2020.03.154.

Mohammady, Sayed Z., and Khalid S. Khairou. 2021. “Impact of Filler on the Soft Phase Molecular Dynamics of PP/EPDM/SiO2 Thermoplastic Elastomeric Nano-Composites.” *Egyptian Journal of Petroleum* 2 (xxxx). Egyptian Petroleum Research Institute: 1–5. doi:10.1016/j.ejpe.2021.01.004.

Mourad, Abdel Hamid I., Amir Hussain Idrisi, Nizar Zaaroura, Muhammad M. Sherif, and Hasan Fouad. 2020. “Damage Assessment of Nanofiller-Reinforced Woven Kevlar KM2plus/Epoxy Resin Laminated Composites.” *Polymer Testing* 86 (December 2019). Elsevier Ltd: 106501.

doi:10.1016/j.polymertesting.2020.106501.

Murphy, Zachary, Malachi Kent, Christian Freeman, Shainaz Landge, and Ermias Koricho. 2020. "Halloysite Nanotubes Functionalized with Epoxy and Thiol Organosilane Groups to Improve Fracture Toughness in Nanocomposites." *SN Applied Sciences* 2 (12). Springer Nature. doi:10.1007/s42452-020-03909-2.

Nagavally, Rahul Reddy. 2017. "Composite Materials - History, Types, Fabrication Techniques, Advantages, and Applications." *International Journal of Mechanical And Production Engineering* 5 (9): 82–87.

Nayak, Smaranika, R. K. Nayak, I. Panigrahi, and A. K. Sahoo. 2019. "Tribo-Mechanical Responses of Glass Fiber Reinforced Polymer Hybrid Nanocomposites." *Materials Today: Proceedings* 18. Elsevier Ltd.: 4042–47. doi:10.1016/j.matpr.2019.07.347.

Ng, H. M., Norshahirah M. Saidi, Fatin Saiha Omar, K. Ramesh, S. Ramesh, and Shahid Bashir. 2018. "Thermogravimetric Analysis of Polymers." *Encyclopedia of Polymer Science and Technology*, no. 13: 1–29. doi:10.1002/0471440264.pst667.

Ning, Huiming, Jinhua Li, Ning Hu, Cheng Yan, Yaolu Liu, Liangke Wu, Feng Liu, and Jianyu Zhang. 2015. "Interlaminar Mechanical Properties of Carbon Fiber Reinforced Plastic Laminates Modified with Graphene Oxide Interleaf." *Carbon* 91. Elsevier Ltd: 224–33. doi:10.1016/j.carbon.2015.04.054.

Panchagnula, Kishore Kumar, and Palaniyandi Kuppan. 2019. "Improvement in the Mechanical Properties of Neat GFRPs with Multi-Walled CNTs." *Journal of Materials Research and Technology* 8 (1). Brazilian Metallurgical, Materials and Mining Association: 366–76. doi:10.1016/j.jmrt.2018.02.009.

Ruban Rajasekar, B., R. Asokan, V. Jamin Daniel Selvakumar, P. Fathima, and A. G. Bala Akash. 2018. "Fracture Toughness on GFRP with Multi Fillers." *Materials Today: Proceedings* 5 (11). Elsevier Ltd: 24486–96. doi:10.1016/j.matpr.2018.10.245.

Saurabh, Sushant, Srinivasu Dasari, Bankim Chandra Ray, and Rajesh Kumar Prusty. 2020. "Mode I

Interlaminar Fracture Toughness Improvement of the Glass/Epoxy Composite by Using Multiscale Composite Approach." *Materials Today: Proceedings* 33. Elsevier Ltd.: 5328–33. doi:10.1016/j.matpr.2020.03.023.

Sela, N., and O. Ishai. 1989. "Interlaminar Fracture Toughness and Toughening of Laminated Composite Materials: A Review." *Composites* 20 (5): 423–35. doi:10.1016/0010-4361(89)90211-5.

Senthil Kumar, M. S., N. Mohana Sundara Raju, P. S. Sampath, and M. Chithirai Pon Selvan. 2018. "Influence of Nanoclay on Mechanical and Thermal Properties of Glass Fiber Reinforced Polymer Nanocomposites." *Polymer Composites* 39 (6): 1861–68. doi:10.1002/pc.24139.

Sharma, B., S. Mahajan, R. Chhibber, and R. Mehta. 2012. "Glass Fiber Reinforced Polymer-Clay Nanocomposites: Processing, Structure and Hygrothermal Effects on Mechanical Properties." *Procedia Chemistry* 4: 39–46. doi:10.1016/j.proche.2012.06.006.

Sravanthi, K., V. Mahesh, B Nageswara Rao, and B. Nageswara Rao. 2020. "Influence of Micro and Nano Carbon Fillers on Impact Behavior of GFRP Composite Materials." *Materials Today: Proceedings* 37 (Part 2). Elsevier Ltd.: 1075–78. doi:10.1016/j.matpr.2020.06.298.

Srivastava, Shakun, and Anjaney Pandey. 2019. "Mechanical Behavior and Thermal Stability of Ultrasonically Synthesized Halloysite-Epoxy Composite." *Composites Communications* 11 (November 2018). Elsevier: 39–44. doi:10.1016/j.coco.2018.11.003.

Sundareswaran, Santhosh Kumar, Balaji Rajendran, and P.K. Dinesh Kumar. 2021. "Experimental Evaluation of Glass Fiber Composite Reinforced with Cellulose Nanoparticles." *Materials Today: Proceedings* 39. Elsevier Ltd.: 1221–27. doi:10.1016/j.matpr.2020.04.002.

Tang, Youhong, Shiqiang Deng, Lin Ye, Cheng Yang, Qiang Yuan, Jianing Zhang, and Chengbi Zhao. 2011. "Effects of Unfolded and Intercalated Halloysites on Mechanical Properties of Halloysite-Epoxy Nanocomposites." *Composites Part A: Applied Science and Manufacturing* 42 (4). Elsevier Ltd: 345–54. doi:10.1016/j.compositesa.2010.12.003.

Tcherbi-Narteh, Alfred, Mahesh Hosur, Eldon Triggs, and Shaik Jeelani. 2013. "Thermal Stability and Degradation of Diglycidyl Ether of Bisphenol A Epoxy Modified with Different Nanoclays Exposed

to UV Radiation." *Polymer Degradation and Stability* 98 (3). Elsevier Ltd: 759–70. doi:10.1016/j.polymdegradstab.2012.12.013.

Truong, Gia Toai, and Kyoung Kyu Choi. 2020. "Effect of Short Multi-Walled Carbon Nanotubes on the Mode I Fracture Toughness of Woven Carbon Fiber Reinforced Polymer Composites." *Construction and Building Materials* 259. Elsevier Ltd: 119696. doi:10.1016/j.conbuildmat.2020.119696.

Ulus, Hasan, Halil Burak Kaybal, Volkan Eskizeybek, and Ahmet Avc. 2020. "Halloysite Nanotube Reinforcement Endows Ameliorated Fracture Resistance of Seawater Aged Basalt / Epoxy Composites," no. 409. doi:10.1177/0021998320902821.

Vahedi, Vahdat, and Pooria Pasbakhsh. 2014. "Instrumented Impact Properties and Fracture Behaviour of Epoxy/Modified Halloysite Nanocomposites." *Polymer Testing* 39. Elsevier Ltd: 101–14. doi:10.1016/j.polymertesting.2014.07.017.

Vardhan, D. Harsha, A. Ramesh, and B. Chandra Mohana Reddy. 2020. "Effect of Ceramic Fillers on Flexural Strength of the GFRP Composite Material." *Materials Today: Proceedings* 37 (Part 2). Elsevier Ltd.: 1739–42. doi:10.1016/j.matpr.2020.07.356.

Venkatesan, M., K. Palanikumar, and S. Rajendra Boopathy. 2018. "Experimental Investigation and Analysis on the Wear Properties of Glass Fiber and CNT Reinforced Hybrid Polymer Composites." *IEEE Journal of Selected Topics in Quantum Electronics* 25 (5): 963–74. doi:10.1515/secm-2017-0068.

Viets, Christian, Simon Kaysser, and Karl Schulte. 2014. "Damage Mapping of GFRP via Electrical Resistance Measurements Using Nanocomposite Epoxy Matrix Systems." *Composites Part B: Engineering* 65. Elsevier Ltd: 80–88. doi:10.1016/j.compositesb.2013.09.049.

Vishal Kumar Rao, M., B. Sai Krishna Patro, Kanchan Kumari, M. Srivatsava, Duryodhan Sahu, and Nilesh Dalai. 2021. "Study of Thermo Mechanical Properties of Surface Modified Graphene on E-Glass Composite." *Materials Today: Proceedings*, no. xxxx. Elsevier Ltd.: 3–8. doi:10.1016/j.matpr.2021.01.701.

Wang, Pengfei, Wanshuang Liu, Xin Zhang, Xuehong Lu, and Jinglei Yang. 2015. "Enhanced Fracture

Toughness of Carbon Fabric/Epoxy Laminates with Pristine and Functionalized Stacked-Cup Carbon Nanofibers." *Engineering Fracture Mechanics* 148. Elsevier Ltd: 73–81. doi:10.1016/j.engfracmech.2015.09.010.

Wei, Minghai, Li Sun, and Jie Zhu. 2020. "Effects of Parameters Controlling the Impact Resistance Behavior of the GFRP Fabric Impregnated with a Shear Thickening Fluid." *Materials and Design* 196. The Authors: 109078. doi:10.1016/j.matdes.2020.109078.

Withers, G. J., Y. Yu, V. N. Khabashesku, L. Cercone, V. G. Hadjiev, J. M. Souza, and D. C. Davis. 2015. "Improved Mechanical Properties of an Epoxy Glass-Fiber Composite Reinforced with Surface Organomodified Nanoclays." *Composites Part B: Engineering*. doi:10.1016/j.compositesb.2014.12.008.

Yuan, Peng, Peter D. Southon, Zongwen Liu, Malcolm E.R. Green, James M. Hook, Sarah J. Antill, and Cameron J. Kepert. 2008. "Functionalization of Halloysite Clay Nanotubes by Grafting with γ-Aminopropyltriethoxysilane." *Journal of Physical Chemistry C* 112 (40): 15742–51. doi:10.1021/jp805657t.

Zeinedini, A., M. H. Moradi, H. Taghibeigi, and J. Jamali. 2020. "On the Mixed Mode I/II/III Translaminar Fracture Toughness of Cotton/Epoxy Laminated Composites." *Theoretical and Applied Fracture Mechanics* 109 (August). Elsevier: 102760. doi:10.1016/j.tafmec.2020.102760.

Zhang, B., P. Yuan, H. Guo, L. Deng, Y. Li, L. Li, Q. Wang, and D. Liu. 2020. "Effect of Curing Conditions on the Microstructure and Mechanical Performance of Geopolymers Derived from Nanosized Tubular Halloysite." *Construction and Building Materials*, no. xxxx. doi:10.1016/j.conbuildmat.2020.121186.